AD-A031 109 CALIFORNIA UNIV SANTA BARBARA DEPT OF PHYSICS F/G 7/4
PHOTOLUMINESCENCE SPECTROSCOPY OF DIATOMIC MOLECULES.(U)
JUL 76 H P BROIDA N00014-69-A-0200-8013
UNCLASSIFIED NL

1 OF 1
AD A031109

END

DATE FILMED
11-76

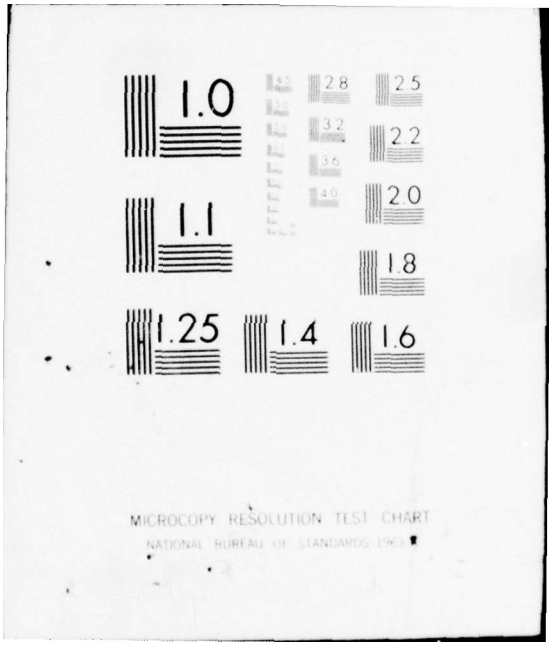
1.0
2.8
2.5
3.2
2.2
3.6
4.0
2.0
1.1
1.8
1.25
1.4
1.6
MICROCOPY RESOLUTION TEST CHART
NATIONAL BUREAU OF STANDARDS 1963

395-007

FC

6

FC

FINAL REPORT

Organization: Office of Naval Research
Contract No.: N00014-75-C-0829

Period: June 1, ~~1975~~ 1974 through May 31, 1976

Title: Photoluminescence Spectroscopy of Diatomic Molecules
(Unclassified)

Herbert P. Broida
Principal Investigator
Department of Physics and Quantum Institute
University of California
Santa Barbara, California 93106

22 July 1976

(Ref 1473
Reverse

Unclassified

SECURITY CLASSIFICATION OF THIS PAGE (When Data Entered)

REPORT DOCUMENTATION PAGE		READ INSTRUCTIONS BEFORE COMPLETING FORM
1. REPORT NUMBER	2. GOVT ACCESSION NO.	3. RECIPIENT'S CATALOG NUMBER
4. TITLE (and Subtitle) PHOTOLUMINESCENCE SPECTROSCOPY OF DIATOMIC MOLECULES		5. TYPE OF REPORT & PERIOD COVERED Final, June 1, 1974 through May 31, 1976 6. PERFORMING ORG. REPORT NUMBER 2
7. AUTHOR(s) Herbert P. Broida		8. CONTRACT OR GRANT NUMBER(s) N00014-69-A-0200-8013 N00014-75-C-0829
9. PERFORMING ORGANIZATION NAME AND ADDRESS University of California, Department of Physics Santa Barbara, CA 93106		10. PROGRAM ELEMENT, PROJECT, TASK AREA & WORK UNIT NUMBERS
11. CONTROLLING OFFICE NAME AND ADDRESS Office of Naval Research Physics Program Office Arlington, Virginia 22217		12. REPORT DATE 22 July 1976 13. NUMBER OF PAGES 53
14. MONITORING AGENCY NAME & ADDRESS (if different from Controlling Office) Final rept. 1 Jun 74 - 31 May 76,		15. SECURITY CLASS. (of this report) Unclassified 15a. DECLASSIFICATION/DOWNGRADING SCHEDULE

16. DISTRIBUTION STATEMENT (of this Report)

"Approved for Public Release; distribution unlimited."

17. DISTRIBUTION STATEMENT (of the abstract entered in Block 20, if different from Report)

"Approved for Public Release; distribution unlimited."

18. SUPPLEMENTARY NOTES

19. KEY WORDS (Continue on reverse side if necessary and identify by block number)

Laser Photochemistry, Photoluminescence, Electronic States, Constants

20. ABSTRACT (Continue on reverse side if necessary and identify by block number)

Unclassified

Optical spectroscopy has been used to study laser spectrochemistry of Bi_2 molecules. Molecular constants and new electronic states of Bi_2, energy exchange between Bi_2 and foreign gases, lifetimes of excited states, and chemical reactions between bismuth vapor and several oxidants have been measured. Two different types of apparatus, a flow furnace system and a heat pipe system were used for bismuth sources. Special attention has been given to reactions

DD FORM 1 JAN 73 1473 EDITION OF 1 NOV 65 IS OBSOLETE S/N 0102-014-6601 |

Unclassified

SECURITY CLASSIFICATION OF THIS PAGE (When Data Entered)

400 628

of bismuth with various oxidants in heat-pipe reactors. Preliminary surveys of reactions of aluminum and calcium with hydrogen containing molecules were made.

A "photon correlator" which is a delayed coincidence device, has been constructed to measure lifetimes and time resolved spectra of a very weak signal. Capabilities of this device were successfully demonstrated by measurements of lifetimes of I_2 in single rotational transitions.

Some interesting new results were obtinaed in the laser photoluminescence of Ca_2 in the heat-pipe.

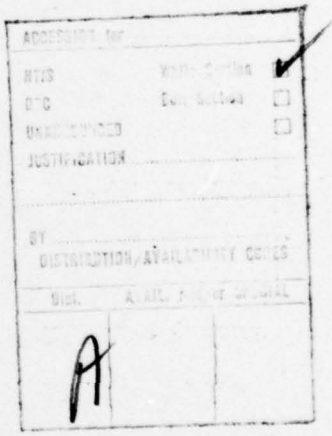

Abstract

Optical spectroscopy has been used to study laser spectrochemistry of Bi_2 molecules. Molecular constants and new electronic states of Bi_2, energy exchange between Bi_2 and foreign gases, lifetimes of excited states, and chemical reactions between bismuth vapor and several oxidants have been measured. Two different types of apparatus, a flow furnace system and a heat pipe system were used for bismuth sources. Special attention has been given to reactions of bismuth with various oxidants in heat-pipe reactors. Preliminary surveys of reactions of aluminum and calcium with hydrogen containing molecules were made.

A "photon correlator" which is a delayed coincidence device, has been constructed to measure lifetimes and time resolved spectra of a very weak signal. Capabilities of this device were successfully demonstrated by measurements of lifetimes of I_2 in single rotational transitions.

Some interesting new results were obtained in the laser photoluminescence of Ca_2 in the heat-pipe.

Table of Contents

I. General Discussion

A. Laser Photoluminescence of Bi_2 and Electronic States and Molecular Constants of Bi_2

There have been relatively few spectroscopic investigations of the diatomic molecule bismuth, Bi_2; therefore spectroscopic data was incomplete and possibly unreliable. Several electornic states of Bi_2 had been observed and are labeled as A to H states. New measurements combined with a critical evaluation of previous measurements and assignments were needed to construct realistic potential energy curves and to calculate accurate Franck-Condon factors.

A problem in studying heavy molecules such as Bi_2 is that rotational and vibrational constants are usually very small making correct numbering difficult. Vibrational bands of such molecules are heavily overlapped and difficult to analyze. Laser-excited photoluminescence spectroscopy has proved to be a very useful tool for analyzing complicated spectra. The bandwidth of the laser oscillation can be made sufficiently small so that a single rotational-vibrational line of a heavy molecule like Bi_2 can be excited. From the analysis of photoluminescence bands in the usual manner coupled with a comparison of measured intensities with Franck-Condon factors, we can definitely assign the transitions and obtain molecular constants. Franck-Condon factors are an excellent test for vibrational numbering and vibrational and rotational constants. Excited state radiative lifetimes also are very important in determining the nature of excited states including possible predissociations and energy exchange between various species. In Sections, IIA and B, results of measurements and analyses of laser and white light photoluminescence of Bi_2 with resulting new information on several low-lying electronic states are presented.

Two different types of apparatus were used to produce Bi_2 molecules. In one apparatus using a furnace immersed in flowing inert gas, Bi_2 molecules were produced by heating a sample of bismuth metal in an Al_2O crucible. The pressure of the inert carrier gas was varied from less than 0.1 to 20 torr. The bismuth partial pressure in this system was at least one order of magnitude less than that of the lowest carrier gas pressure. In order to study the Bi_2 at high bismuth pressure (0.1 to 5 torr), bismuth metal was contained in a cross-shaped heat pipe oven. The heat pipe was stainless steel with a 4.5 mil wire, #100 mesh stainless steel screen used as a wick for returning condensed liquid metal to the heated zone.

For the excitation of Bi photoluminescence, several laser sources He-Ne, He-Cd, Ar^+ and a tunable CW rhodamine 6G laser (570-630 nm) and a 500 W Xe arc lamp were used. Photoluminescence spectra were recorded photoelectrically with 3/4 m Fastie-Ebert scanning monochromator from 400-900 nm, with various resolutions from 0.02 to 10 nm. For better wavelength measurement, a 2 m McPherson spectrograph was used.

Wavelength measurements were carried out by comparing photoluminescence spectra with spectra of an Fe-Ne hollow-cathode lamp. For lifetime measurements, a N_2-laser-pumped dye-laser (450-570 nm) was used. Peak power, spectral width, and time pulse width of this laser were typically 1 kW, 0.5 nm and 10 nsec respectively. Fluorescence intensity decays after the pulsed-laser excitation were measured by means of a fast transient recorder (Biomation 8100).

Radiative lifetimes and quenching cross-sections were measured directly by pulse laser excitation from 450.0 to 520.0 nm. At 514.5 nm excitation, the lifetime was 0.7 μsec and the quenching cross-section was 30 $\AA^2$. With 488.0 nm excitation two lifetimes were found to be 0.1 and 0.7 μsec. The longer lifetimes correspond to the lifetime of A state, the shorter one to the lifetime of upper state of the K series. From the two measurements of spectra and lifetime, we conclude that there is at least one other low-lying state X' about 5000 cm^{-1} above the X state and one other higher excited state A' about 20,000 cm^{-1} above the X' state.

B. Chemical Reactions in a Heat Pipe Oven

We made two types of heat pipe ovens for chemical reactions. One consisted of a simple cross-shaped (+) stainless steel pipe with a 5 cm diameter and an arm length of 15 cm. Four heater sets of 250 W capacity were used to heat the pipe, 1150 K was the maximum available temperature. A #100 stainless steel mesh was used to return liquid metal to the heating zone. The other heat pipe was more complicated. Its shape was a double cross, consisting of 5 cm stainless steel tubes, eight sets of 250 W heater elements, and an additional cooling system. The eight sets of heaters were in three groups, controlled by three variac transformers. By combinations of heating currents of the various groups and flow of cooling water, temperatures to 1150 K with a variety of temperature gradients can be realized. This heat pipe used vertical arms so that gravitational flow, as well as mesh capillary action, was used to return the liquid metal to the heating zone. Since in heat pipe action, capillary action of the mesh is very important for returning liquid metal to the heating zone, it is necessary that the metal wet the stainless steel mesh. Most of the alkaline and alkaline earth metals are known to wet stainless steel mesh. Bismuth will not wet oxidized stainless steel mesh but clean, new stainless mesh does work. However liquid metal bismuth itself can play a role in returning the metal to the heating zone. We thought that with this mode without wick action might be used for heat pipe action for metals which do not wet stainless steel mesh. Insertion of quartz inlet tubing for introducing reactant gases did not affect the heat pipe action since the heat leak was small. Nor was deposition of metal observed at the end of the inlet tubing. When the heat pipe is properly working, the temperature and pressure of the system is in equilibirum determined by the vapor pressure of the metal. The vapor pressure was measured directly by a pressure gauge and the temperature directly obtained from vapor pressure vs. temperature tables.

Laser induced photoluminescence of Bi_2 molecules was used to determine the distribution of metal vapor along the pipe. Metal vapor only existed in the middle heating zone and a very sharp boundary was observed between the metal and carrier gas zones. About 4 cm outside the sharp boundary, particles of bismuth were observed. The metallic particle region was about 4 cm long. Scattered light from these particles was completely plane polarized, indicating particle sizes much smaller than the wavelength of light. Even when the carrier gas pressure was higher than the equilibrium vapor pressure, and there was no heat pipe action, there was a separation of the metal zone from the carrier gas zone. We believe that the operation of this kind, without heat pipe action but with a separation of the metal rich zone from the carrier gas zone, will be useful for chemical reaction studies as well as for spectroscopic measurements.

For determining the optimum conditions for studying chemical reactions in the heat pipe, many inlets for oxidant and observation windows have been made. A 12.5 mm diameter quartz tubing was used to introduce microwave discharge products into the center of the metal vapor region and 3 mm stainless steel tubing was used to introduce other reactants. We tried chemical reactions between bismuth and several oxidants such as O_2, discharged O_2, N_2O, NO_2. During the chemical reaction, laser photoluminescence was used to detect the concentration of Bi_2 as well as reactant products in the reaction zone. A brief discussion of these measurements is reported in Section IIC.

We would like to remark on some particular experiences observed during the reaction of bismuth and oxidant. Some observations are connected only to the bismuth and oxidant system, while others are more general and pertain to chemical reactions in heat pipe ovens. In one manner of operation, during the reaction, metal is supplied by evaporation while oxidant is supplied from outside the metal vapor region. Metal oxides and other reactant products condense in the pipe and a steady state condition can take place so that the heat pipe is used as a stable reactor. The reaction of Ba + N_2O corresponds to this case.[4] Unfortunately the bismuth and oxidant reaction does not fit this mode of operation; it is necessary to pump out excess oxidant and products to maintain a stable pressure. By pumping, a steady-state condition is established in which the pumping just balances the evaporation of metal and supply of oxidant. Also when the reaction is small, the oxidant reacts with the hot stainless mesh and the gas inlets.

During the reaction of discharged O_2, the stainless steel mesh and gas inlets were ruined. Even the quartz tubing for the gas inlet was "eaten" by some chemical reaction in the hot heat pipe in the presence of bismuth. About 1 cm length of quartz tubing disappeared in each 5 hours of operation. Deposition of bismuth oxide was observed on the end of the quartz tubing. Possibly at high temperatures bismuth oxide corrodes the quartz tubing. At excess pressures (15 to 30 torr) of N_2O, soot-like small particles were observed. These may come from the oxidant of small metallic particles. We believe that we need a special structure for the

gas inlet tube with a cooling mechanism inside and a heating mechanism outside. In our present system, the metal tube itself and the contained oxide are heated to the oven temperature. The reacting oxidant molecules were vibrationally excited, since kT is nearly 1000 cm^{-1}. In addition some fraction of the oxidant, especially in the case of N_2O, is decomposed before entering the reaction zone. Quantitative studies of chemical reaction rates, photon yield, etc. probably will be difficult with the pumping mode, since the calibration of the quantity of oxidant used will be difficult. Another difficulty of the present system is the strong background thermal emission from the walls and from the metal vapor itself.

Small particulate formation of bismuth metal was observed between the hot and cold transient region in the heat pipe as well as in the flow system at very slow gas-flow rate. Spectra of scattered light from these small particles were taken by a Xe arc lamp. The scattered light is completely polarized and its spectrum has a maximum at 400 nm with a width of 50 nm and some oscillatory structures. This resonance is due to the plasma resonance scattering from very fine bismuth particles. A related study on homogeneously nucleated particles of PbI_2 is discussed in Section IID.

In order to test the heat pipe as a general tool for studying chemical reactions of metal vapors, we attempted to make metal hydrides. Weak chemiluminescence was observed in the reactions of Al and of Ca with formaldehyde (Section IIE).

Although our preliminary experiments indicated versatile and wide range uses for heat pipes in studies of chemically reacting systems, our experience has not borne out this optimism. Because of the many problems connected with temperature and mixture stabilization, the time to reach true steady-state conditions, the changing effects due to product contamination, the large effects of impurities, and the condensation of both reactants and products in cooler regions, we believe that the heat pipe has only limited use in the study of chemical reactions.

C. Laser Photoluminescence of Calcium Molecules

In the course of using photoluminescence as a tool in the chemically reacting systems, many impurity molecules were found including CaCl, BaCl, BaBr, and Ca_2. Some interesting results on this latter molecule are reported in Section IIF.

D. Lifetime Measurements of I_2

In the course of developing suitable equipment for measuring lifetimes, we developed a photon correlator. This instrument was first tested on I_2 (Section IIG).

Laser photoluminescence of Bi_2*

G. Gerber,† K. Sakurai,‡ and H. P. Broida

Quantum Institute and Department of Physics, University of California, Santa Barbara, California 93106
(Received 1 December 1975)

Bismuth diatomic molecules are produced in an inert gas flow system and in a heat-pipe oven at pressures from 10^{-4} to 10 torr. Photoluminescence of Bi_2 has been studied with various laser sources and with white light. Strong photoluminescence is due to different vibrational–rotational transitions of the $A-X$ system. Observed weaker photoluminescence series are due to vibrational–rotational transitions of four previously unknown electronic systems of Bi_2 with $\omega_e = 154.29 \pm 0.45$ cm^{-1}; $\omega_e = 141.23 \pm 0.35$ cm^{-1}; $\omega_e = 127.05 \pm 0.1$ cm^{-1} and $\omega_e = 105.68 \pm 0.25$ cm^{-1}. Long v'' progressions extending over the whole Franck–Condon distribution (including both maxima) are measured for several electronic transitions. Molecular constants for the lower electronic states involved are obtained from spectroscopic analysis. The laser-excited photoluminescence experiments suggest that A is not the first excited state in Bi_2 and that X is not the ground state of Bi_2 but that the X' state is probably the lowest energy state. Photoluminescence with white light excitation consists of emission from Bi_2 and atomic Bi. In addition to discrete line photoluminescence, continuum spectra arising from an unbound upper state are observed with 514.5 nm laser excitation and with white light excitation.

I. INTRODUCTION

Spectra of the homonuclear diatomic molecules N_2, P_2 and As_2 of the lighter elements of the fifth group have been extensively studied both in emission and absorption. However, few spectroscopic investigations have been made of the heavier diatomic molecules, Sb_2 and Bi_2, of the same group.

Almy and Sparks[1] photographed the absorption spectrum of Bi_2 in the spectral region 211–790 nm at temperatures from 1120 to 1770 K. The spectrum was analyzed into four discrete band systems: (1) the visible system from 450–790 nm consisting of over 300 bands due to $A \leftarrow X$ transitions; (2) the ultraviolet system from 260–290 nm assigned to $C \leftarrow X$ transitions; (3) the far ultraviolet system below 225 nm ($F \leftarrow X$), which shows diffuse band heads; and (4) the violet system which appears only at temperatures greater than 1270 K. The violet system consists of three parts: (a) a group of sharp-edged bands extending from 405 to 420 nm ($D \leftarrow A$), (b) a series of diffuse "continuous bands" from 420 to 450 nm, and (c) a group of diffuse and closely spaced bands from 400 to 405 nm. In addition there is strong continuous absorption in the neighborhood of 310 nm. From the close agreement between vibrational constants of the lower state of the $D \leftarrow A$ system and constants of the upper state of the visible system $A \leftarrow X$, they concluded that the lower state of the $D \leftarrow A$ system is the A state.

Results of absorption spectroscopy on Bi_2 by Nakamura and Shidei[2] are in general agreement with those of Almy and Sparks.[1] Åslund *et al.*[3] have derived molecular constants for the $A-X$ system from analysis of partially resolved bands obtained by absorption measurements.

Emission spectra of the Bi_2 molecule excited in a microwave discharge were studied more recently by Reddy and Ali.[4] Their investigations revealed the existence of three new band systems: (1) $G \rightarrow A$ in the wavelength region 803–882 nm, (2) $H \rightarrow A$ consisting of a single progression in the region 673–705 nm, and (3) $I \rightarrow A$ between 629–657 nm. The three new band systems are found to have a common lower electronic state, which probably is the upper state of the $A-X$ system.

A problem in studying heavy molecules, such as Bi_2, is that rotational constants are very small and correct numbering of rotational lines therefore is difficult. In addition, most metal diatomic molecules are weakly bound with fairly small vibrational frequencies. Vibrational bands of such molecules are heavily overlapped and thus are difficult to analyze. In the last few years, laser-excited photoluminescence spectroscopy[5] has proved to be a very useful tool for analyzing complicated spectra because the band width of the laser oscillation can be sufficiently narrow so that only a single vibrational–rotational transition is excited even in a heavy molecule like Bi_2.

In this paper we report results of laser-excited photoluminescence of Bi_2 as well as white light photoluminescence. The results of our investigations lead to the conclusion that the X state, previously considered[1–4] to be the ground state of Bi_2, is probably not the ground state. Our experiments indicate that there is another electronic state X' with $\omega_e = 154.29$ cm^{-1} which lies about 1500 cm^{-1} below the X state.[6] Also we find three other low-lying electronic states (one of them is a repulsive state) below the A state and two electronic states which are higher in energy than the A state. In addition to these well characterized electronic states we observe four more states which are upper states of photoluminescence series.

The new observations are in good agreement with previous data[1–4] for the $A-X$ system. However, there is partial disagreement with assignments of the earlier data[1,2,4] but, a re-evaluation[6] removes most of the discrepancies.

In most laser-excited photoluminescence studies, the laser excites one or more different vibrational–rotational transitions within one electronic system. However, in the experiments carried out with Bi_2, several Ar^+ laser lines excite transitions of more than one

electronic system. For instance the 488.0 nm Ar^+ laser line simultaneously excites vibrational–rotational transitions of four different electronic systems—$K-X'$, $A-X$, $E-B$, and $N-G$. Calculated Franck–Condon factors[6] based on RKR-potential curves are used to confirm the spectroscopic assignments, which in some cases are unambiguous because of long observed progressions ($v''=0$ up to $v''=49$). A second paper[6] examines these photoluminescence observations in more detail in terms of potential curves and Franck–Condon factors. In addition the published data of Bi_2[1-4] are reevaluated and a potential energy diagram for Bi_2 is derived from all available data.

II. EXPERIMENTAL

Two types of apparatus are used to produce Bi_2 molecules. In one apparatus Bi_2 is produced by heating a sample of metal bismuth in an Al_2O_3 crucible. The Bi_2 vapor then is cooled and carried by an inert gas flow (Ar, He or N_2) to the observation region.[7] The pressure of the inert carrier gas is varied from less than 0.1 torr to 20 torr. Partial pressures[8] of Bi_2 are at least one order of magnitude lower than the lowest carrier gas pressure used. Under these nonequilibrium conditions the pressure of Bi_2 in the observation region is not well known but is considerably less than the equilibrium pressure. Therefore, in order to achieve a controlled and measurable vapor pressure of Bi_2, two different heat-pipe ovens[9] are used. One was a cross-shaped heat pipe and the other consists of two vertical arms in addition to the horizontal cross (Fig. 1). The heat pipes are made of stainless steel with a 4.5 mil, # 100 mesh stainless steel wire screen for wicks. Both Ar and He are used as buffer gases. Bi metal is placed on the bottom of the vertical arm (Fig. 1). The laser beam comes through the upper vertical arm and the photoluminescence is observed perpendicular to the laser beam.

Usually heat-pipe action[9] is achieved at equilibrium of metal vapor and buffer gas pressures. Heat-pipe action means that metal vapor condenses in the cooler region and returns to the hot region due to the capillary action of the mesh. With constant pressure, an increase in heating does not result in increasing temperature after reaching equilibrium, but rather in an elongation of the vapor region.

It is possible to operate the heat pipe in a somewhat different manner. By keeping the pressure inside the heat pipe constant while continuously supplying and pumping the buffer gas at very low flow rates, an increase in temperature is obtained. Maintaining a buffer gas (Ar) pressure near 0.1 torr, we are able to reach a gas temperature of 1450 K even though the Bi_2 vapor pressure[8] of 0.1 torr corresponds to a temperature of only 1170 K. The temperature reached by the heat pipe is approximately measured with a thermocouple attached to the outside wall of the heated cross. Spectra serve as a second and calibrating thermometer. From a thermal emission spectrum of Bi_2 ($A \rightarrow X$) as well as from white light photoluminescence spectra, the gas temperature inside the heat pipe is measured from vi-

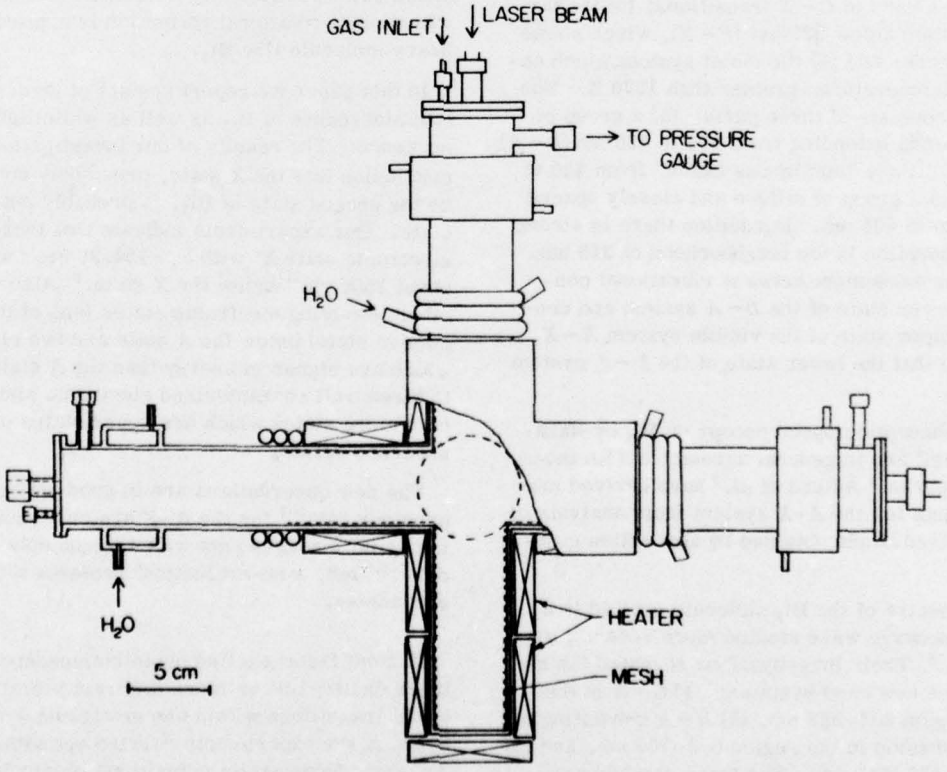

FIG. 1. Heat-pipe oven used for production of Bi_2.

brational populations. These two spectroscopically measured temperatures are consistent with each other and with the thermocouple measurements to within 10%.

In addition to production of gaseous Bi_2, small particle formation[10] is observed between the hot and cold transient region in the heat pipe at buffer gas pressures greater than 0.5 torr.

Several laser photoluminescence sources—He–Ne, He–Cd, Ar^+, and a cw Ar^+ pumped tunable rhodamine 6 G dye—are used. Most investigations use multimode laser excitation, but a few experiments are made with the Ar^+ laser operating single mode with an intracavity etalon. Multimode excitation mainly is used with a frequency spread of 5 GHz (~ 0.15 cm^{-1}), while the bandwidth of single mode operation was about 20 MHz. At higher currents, our Ar^+ laser simultaneously oscillates at 488.0 and 488.9 nm[11] with an intensity ratio 488.9/488.0 of $10^{-1} - 10^{-2}$ depending on the discharge current. The cw dye laser was tunable in the range 580–615 nm with output power varying from 100–400 mW. The light of a 150 W Xe arc lamp is used for white light excitation of Bi_2 photoluminescence.

Spectra are recorded both photoelectrically and photographically. For the photoelectric measurements a $\frac{3}{4}$ m grating monochromator was used with various photomultipliers. Relative line intensities are obtained by comparison with a calibrated lamp. Spectra are measured with various resolutions from 0.02–2 nm. Photographic measurements are obtained using a two meter grating spectrograph with linear dispersion of 0.378 nm/mm and an achieved resolution of 0.003 and 0.007 nm with 15 and 50 μ slits, respectively. Exposure times run from 30 min to several hours. Wavelengths are determined by comparison with a Fe spectrum produced by a 30 mA Fe–Ne hollow cathode lamp and by interpolation using Fe–Ne hollow cathode wavelength standard lines.[12] The achieved accuracy is ± 0.004 nm (0.2 cm^{-1}).

III. METHODS OF DATA ANALYSIS

The line positions $\nu(v'J';v''J'')$ of a photoluminescence series may be represented by the energy difference between the $(v'J')$ and $(v''J'')$ vibrational–rotational levels of the excited and ground states[13]

$$\nu(v'J';v''J'') = \nu_e + [G(v') - G(v'')] + [F_{v'}(J') - F_{v''}(J'')] , \tag{1}$$

where the vibrational energy

$$G(v) = \omega_e(v+\tfrac{1}{2}) - \omega_e x_e(v+\tfrac{1}{2})^2 + \omega_e y_e(v+\tfrac{1}{2})^3 + \omega_e z_e(v+\tfrac{1}{2})^4 + \cdots \tag{2}$$

and the rotational energy in the v level

$$F_v(J) = B_v[J(J+1) - \Lambda^2] - D_v[J(J+1) - \Lambda^2]^2 + \cdots . \tag{3}$$

The rotational constants B_v and D_v depend upon the vibrational level v as[13]

$$B_v = B_e - \alpha_e(v+\tfrac{1}{2}) + \gamma_e(v+\tfrac{1}{2})^2 + \cdots , \tag{4}$$

$$D_v = D_e + \beta_e(v+\tfrac{1}{2}) + \delta_e(v+\tfrac{1}{2})^2 + \cdots , \tag{5}$$

and Λ is the absolute value of the projection of the angular momentum upon the internuclear axis. $\nu_e = T_e' - T_e''$ is the difference in electronic energy of the two states. The vibrational spacing of the lower electronic state or the spacing between pairs of lines (v'', J'') and $(v''+1, J'')$ of the same photoluminescence series, $\Delta\nu_{\text{vib}}$, is obtained from Eqs. (1)–(5):

$$\Delta\nu_{\text{vib}}(v) = a_0 - a_1 v + a_2 v^2 + a_3 v^3 + \cdots , \tag{6}$$

where[5]

$$\begin{aligned} a_0 &= \omega_e - 2\omega_e x_e + 3.25\,\omega_e y_e + 5\,\omega_e z_e + (-\alpha_e + 2\gamma_e)J(J+1) \\ &\quad - (\beta_e + 2\delta_e)[J(J+1)]^2 , \\ a_1 &= 2\omega_e x_e - 6\,\omega_e y_e - 13\,\omega_e z_e - \gamma_e J(J+1) + 2\delta_e[J(J+1)]^2 , \\ a_2 &= 3\omega_e y_e + 12\,\omega_e z_e , \\ a_3 &= 4\,\omega_e z_e . \end{aligned} \tag{7}$$

From a plot of $\Delta\nu_{\text{vib}}$ as a function of v'' or from a weighted nonlinear least-squares fit, the coefficients a_i are obtained, determining the vibrational constants ω_e, $\omega_e x_e$, $\omega_e y_e$, and $\omega_e z_e$ of the lower electronic state. The accuracy of the molecular constants derived from such a plot depends, of course, upon the correct vibrational assignment v''. However, if the constants are determined by a weighted nonlinear least-squares fit the absolute values of the constants also depend upon the number of constants to be determined. Even with as much data as given for the A–X photoluminescence series (Fig. 7), the constants ω_e and $\omega_e x_e$ have different values depending on whether two, three, or four constants (including $\omega_e y_e$ and $\omega_e z_e$) are included in the fit. The fact that different sets of constants describe the experimental data equally well (the RMS deviation being almost the same) is due to the strong correlation of the constants and the limited number of experimental data, but does not much depend on the accuracy of the experimental data.

From the same Eqs. (1)–(5), the spacing between the doublet lines $(v'', J'+1)$ and $(v'', J'-1)$ of a P, R photoluminescence series is given by

$$\Delta\nu_{\text{rot}}(v) = b_0 - b_1 v + b_2 v^2 , \tag{8}$$

where[5]

$$\begin{aligned} b_0 &= (4B_e - 2\alpha_e + \gamma_e)(J'+\tfrac{1}{2}) + \cdots , \\ b_1 &= (4\alpha_e - 4\gamma_e)(J'+\tfrac{1}{2}) + \cdots , \\ b_2 &= 4\gamma_e(J'+\tfrac{1}{2}) + \cdots , \end{aligned} \tag{9}$$

neglecting higher orders of J' and small contributions from D_e, β_e and δ_e. The coefficients b_i may be obtained either from a plot of $\Delta\nu_{\text{rot}}$ versus v'', or from a nonlinear least-squares fit, thus giving the rotational constants B_e, α_e, and γ_e.

The emission intensity of a $(v'J') \rightarrow (v''J'')$ line is approximately given by

$$\begin{aligned} I(v'J', v''J'') &= \alpha[N_{v'J'}/(2J'+1)] \\ &\quad \times \nu^4(v'J', v''J'')R_e^2 Q_{v'v''} S_{J'}^{J''} , \end{aligned} \tag{10}$$

where $N_{v'J'}$ is the population of the $(v'J')$ level, $\nu(v'J', v''J'')$ is the transition frequency, R_e^2 is the electronic transition moment, $Q_{v'v''}$ is the Franck–Condon factor of the $(v'J', v''J'')$ transition and α is a proportionality

constant. Carrying out the summation over all J' lines of a band gives the emission intensity of a vibrational band and makes the Hönl–London factor $S_{J'}^{J''}$ equal to unity. Assuming that the electronic transition moment R_e^2 varies slowly with v, the relative population of the vibrational levels v' may be found from

$$N_{v'} \propto \frac{I(v', v'')}{\nu^4(v', v'')Q_{v'v''}} . \tag{11}$$

From the measurement of emission intensities, Franck–Condon factors, and transition frequencies, the relative vibrational populations are obtained.

Using white light excitation with nearly constant intensity over the absorbing wavelength region, the vibrational population $N_{v'}$ is proportional to the sum of $N_{v''}$. In this case $N_{v''}$ refers to the population of the initial vibrational level of the lower electronic state.

$$N_{v'} \propto \sum_{v''=0}^{v''_{max}} N_{v''} Q_{v'v''} \nu(v', v'') . \tag{12}$$

The summation extends usually over all vibrational levels $v''=0$ to v''_{max}. However, in some favorable cases[14] this summation can be restricted to only a few v'' levels. White light photoluminescence of Bi_2 (Fig. 9) can be treated in this way because the spectrum consists mainly of three progressions $v''=0$, 1, 2. The second maximum of the Franck–Condon distribution does not contribute to the spectrum. From the values of $N_{v'}$ obtained according to Eq. (11), values of $N_{v''}$ are determined by inverting the set of equations given by Eq. (12). Once values of $N_{v''}$ are found, the temperature connected with these populations may be obtained from

$$N_{v''} \propto e^{-G(v'')/kT_{vib}} , \tag{13}$$

assuming a Boltzmann distribution for the vibrational populations.

IV. RESULTS

The various observed photoluminescence transitions of Bi_2 are given in Table I. Molecular transitions excited by different light sources are listed in this table together with a rough classification of observed intensities of both photoluminescence lines and relaxation band heads. The assignment of a transition is made in the following way. The number of measured anti-Stokes lines (i.e., photoluminescence lines with wavelengths shorter than the exciting laser line) gives, in a first approximation, the vibrational level of the lower electronic state. Either with known molecular constants or with constants derived from vibrational and doublet spacings [Eqs. (6) and (8)], potential curves for the electronic states involved are calculated[6] using the RKR method. Once potential curves $V(r)$ are constructed, Franck–Condon intensity factors can be calculated for vibrational–rotational transitions. A comparison of measured intensities of a photoluminescence series with Franck–Condon factors for this series provides a sensitive test for the accuracy of the assignment, especially for long vibrational progressions. In the case of one observed transition which involves previously unknown electronic states, an assignment of the transition was not made because of lack of information about the upper state available from laser photoluminescence data containing only one vibrational–rotational excitation. Therefore only the multiplet character and the number of anti-Stokes lines of the photoluminescence series has been given with the values for the molecular constants of the lower electronic state.

A typical photoluminescence spectrum in which the 528.7 nm Ar^+ laser excites both the $v'=11$ and 12 levels of the A state is shown in Fig. 2. This spectrum consists of two doublet photoluminescence series and of some weak bands indicating that rotational and vibrational relaxation occurs. These relaxation bands are observed even at inert gas pressures as low as 0.1 torr, but they become stronger with increasing pressure. The laser line excites both a P and an R transition. Emission to the vibrational–rotational levels of the lower electronic state forms the two resonance doublet series. Measured wavelengths of the P, R doublets of the photoluminescence are used to determine the molecular constants of the lower electronic state. In this way we assign the two transitions excited by the 528.7 nm Ar^+ laser as due to the A–X system of Bi_2. The laser line coincides with $R=45$ of the $v''=2 \rightarrow v'=12$ transition and with a high rotationally excited state such as $P=290$ of the $v''=0 \rightarrow v'=11$ transitions. Both photoluminescence series are observed from $v''=0$ to $v''=37$ between 520 and 750 nm.

A more complex photoluminescence spectrum is obtained from 514.5 nm laser excitation with a number of rotational transitions overlapped within the bandwidth (5 GHz) of the 514.5 nm line. The 514.5 nm photoluminescence was observed in the heat-pipe at temperatures as low as 790 K (corresponding to Bi_2 vapor pressure[8] of approximately 10^{-4} torr). Observed line intensities increase linearly with increasing vapor pressure and laser intensity. Relaxed bands are observed at Bi_2 pressures as low as 10^{-2} torr. An analysis based on photographic measurements such as illustrated in Fig. 3(a) shows that four vibrational–rotational transitions of the A–X system are excited (Table I). The upper part of Fig. 3(a) clearly shows rotational and vibrational relaxation in a number of bands. It is interesting to note that strong photoluminescence is observed from the $v'=18$ level, even though it is not directly populated by a laser transition. From the measured line positions of the photoluminescence series vibrational and rotational constants of the X state are determined according to Eqs. (6) and (8) by a weighted nonlinear least-squares fit. These constants are given in Table II together with previously published constants,[3,4] and show agreement within the given uncertainties of one standard deviation. Observed band heads are used to determine the vibrational constants for both the X and A states and ν_e. The derived constants also are given in Table II and show agreement with published constants[3,4] and constants obtained from line photoluminescence. Figure 3(b) shows, for comparison, a portion of the photoelectrically measured photoluminescence spectrum of Bi_2 excited by the 514.5 nm line. Photoelectrically recorded spectra are easier to use for relative intensities, whereas photographic spectra provide more accurate wavelength data.

TABLE I. Bi_2 photoluminescence excited by different light sources.

Laser wavelength nm (air)[a]	Molecular transition excited v' v''	J[b]	System[c]	Photoluminescence intensity[d]	Relaxation[d] vib	rot
Ar^+ 528.690	12 2	R290	$A-X$	m	m	m
	11 0	P45	$A-X$	m	s	s
Ar^+ 514.532	17 1	R270	$A-X$	s	s	s
	19 4	R10	$A-X$	m	s	
	20 4	R170	$A-X$	s	m	s
	21 5	R120		m	s	s
	continuous photoluminescence (approximately 10^{-5} of line photoluminescence)					
Ar^+ 501.716	19 1	R60	$A-X$	m	s	s
Ar^+ 496.507	30 7	R130	$A-X$	w	none	
	unidentified $A-X$ transition with 12 anti-Stokes lines		$A-X$	vw	none	
	doublet photoluminescence series with $\omega_e = 127.7\ cm^{-1}$ and 7 anti-Stokes lines			vw	none	
Ar^+ 488.903	22 0	P80	$A-X$	m	none	w
Ar^+ 487.986	26 2	R160	$A-X$	m	none	
	1 8	R105	$E-B$	m	none	
	$\omega_e = 105.68\ cm^{-1}$, 2 anti-Stokes lines	P245	$N-G$	w	none	
	$\omega_e = 154.29\ cm^{-1}$, 20 anti-Stokes lines		$K-X'$	vw	none	
Ar^+ 476.486	31 3	R40	$A-X$	w	none	
	33 4	R20	$A-X$	w	none	
	doublet photoluminescence series with $\omega_e = 141.23\ cm^{-1}$, 6 anti-Stokes lines		$L-A'$	vw	none	
	$\omega_e = 154.9\ cm^{-1}$, 20 anti-Stokes lines		$K-X'$	vw	none	
He–Cd 421.5	no photoluminescence observed at $T = 1100$ K					
He–Ne 632.8	no photoluminescence observed at $T = 1100$ K					
Rhodamine 6G dye 580–615	weak photoluminescence observed color of photoluminescence changes from deep red to green blue with various excitation lines					
White-light Xe arc lamp	strong discrete photoluminescence (490–765 nm, mainly $A-X$) and very weak continuous photoluminescence from Bi_2 and discrete photoluminescence from atomic Bi.					

[a] As given by Ref. 11.

[b] Approximate J values only because of the small B_e values. Even with high resolution photographic measurements, the rotational numbering is still not unambiguous.

[c] Assignments of electronic systems are taken from Ref. 6.

[d] s, strong; m, medium; w, weak; vw, very weak.

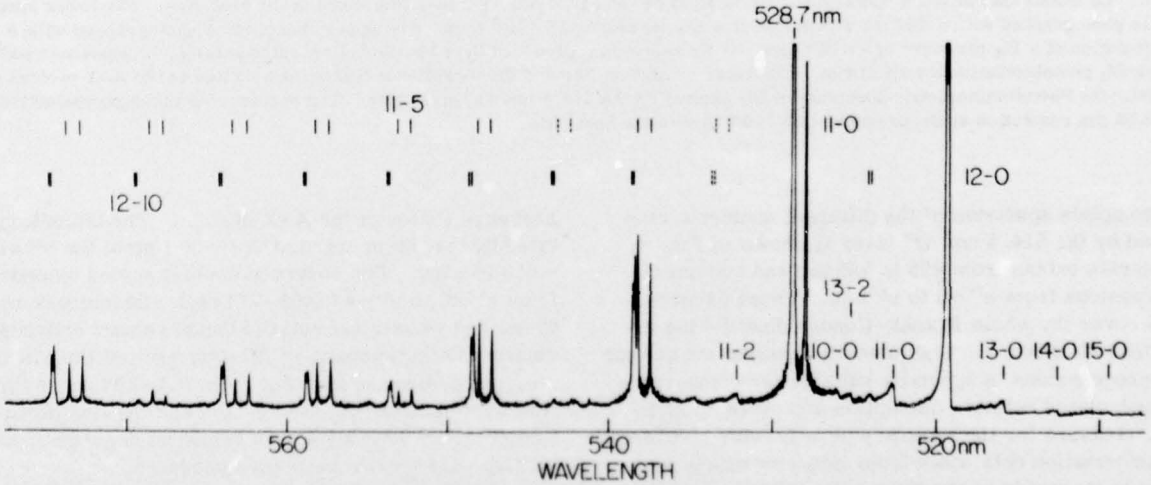

FIG. 2. Photoluminescence spectrum of Bi_2 excited by the 528.7 nm Ar^+ laser line. The spectrum is taken with 0.06 nm resolution in the flow system at an Ar-carrier gas pressure of 1 torr and is not corrected for instrumental response. The two observed doublet series as well as some rotational and vibrational relaxation can be seen.

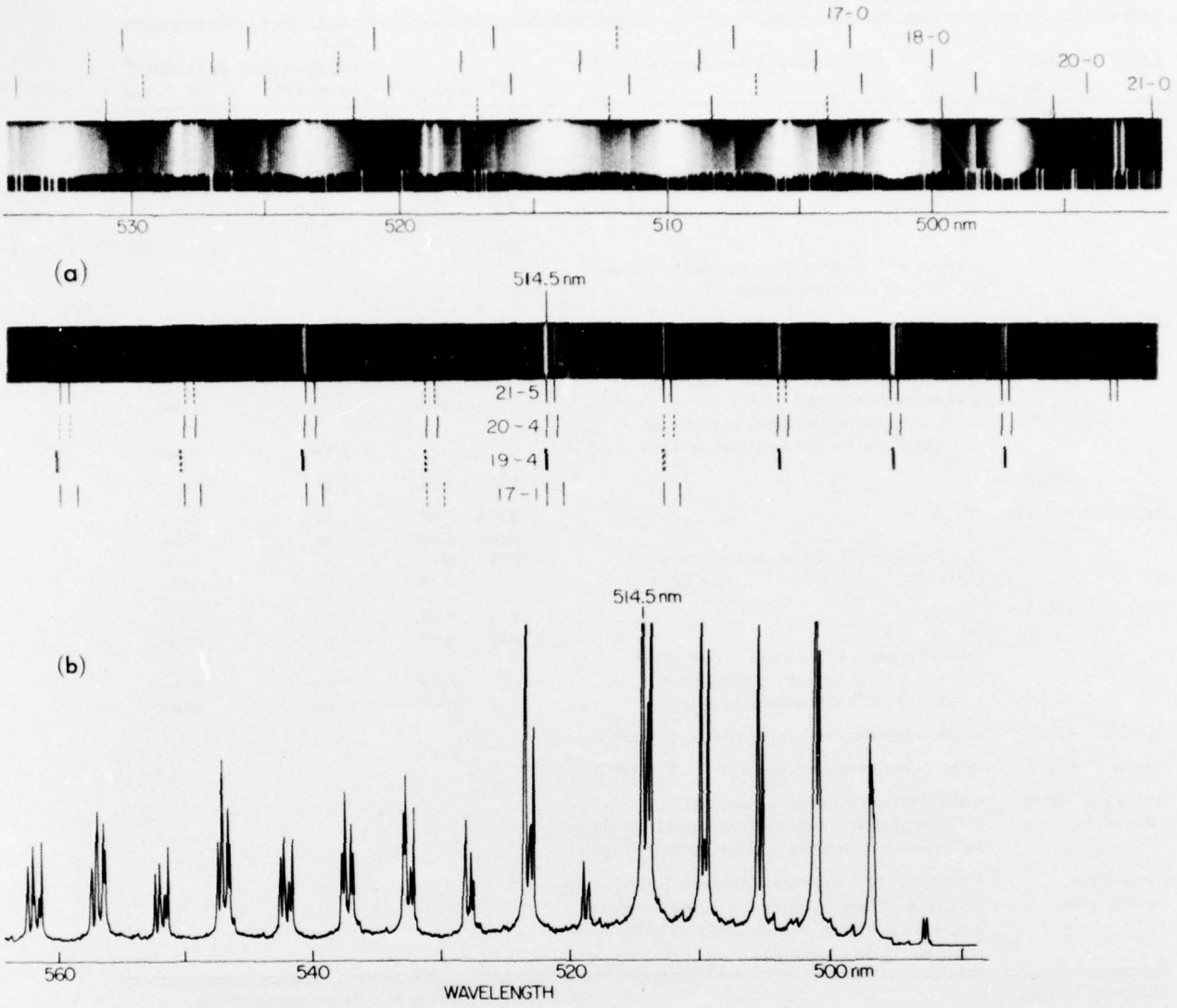

FIG. 3. (a) Photoluminescence spectrum of Bi_2 excited by the 514.5 nm Ar^+ laser line taken in the heat pipe. The lower spectrum is photographed with 0.007 nm resolution at a Bi_2 pressure of 5×10^{-2} torr. The upper spectrum is photographed with 0.02 nm resolution at a Bi_2 pressure of 5×10^{-1} torr. A Fe spectrum, produced by a Fe–Ne hollow cathode lamp, is superimposed below the Bi_2 photoluminescence spectrum. The laser excitation line and the vibrational transitions excited in the $A-X$ system are marked. (b) Photoluminescence spectrum of Bi_2 excited by the 514.5 nm Ar^+ laser line. The spectrum is taken photoelectrically with 0.02 nm resolution at Bi_2 pressure of 5×10^{-1} torr in the heat pipe.

A complete spectrum of the different doublet series excited by the 514.5 nm Ar^+ laser is shown in Fig. 4. The series extend from 495 to 785 nm and consist of progressions from $v''=0$ to $v''=49$. These progressions cover the whole Franck–Condon distribution including both maxima. The intensity distribution of such long progressions is specially suitable for comparison with calculated relative intensities and gives an additional measure for the accuracy of molecular constants. The information obtainable from intensity measurements is discussed in the following paper.[6]

Photoluminescence resulting from excitation of Bi_2 with the 501.7 nm Ar^+ laser consists of one photoluminescence series of the $A-X$ system. The transition excited by that laser line is the $P=60$ line of the $v''=1 \rightarrow v'=19$ band. The observed doublet series extends from $v''=0$ to $v''=47$ (498–775 nm). Intensity of rotational and vibrational relaxed bands remain constant relative to the intensity of directly excited lines at carrier gas pressures (Ar, N_2) from 0.1–20 torr in the flow system, but both the relaxed and the line photoluminescence intensities are pressure dependent, becoming weaker with increased pressure.

Excitation of Bi_2 by the 496.5 nm laser line produces a photoluminescence spectrum (lower part of Fig. 5) consisting of a doublet series due to the $A-X$ transi-

TABLE II. Molecular constants for the $A-X$ system.

State	ν_e[a]	ω_e	$\omega_e x_e$	$\omega_e y_e$	$\omega_e z_e$	B_e	α_e	D_v	
A	1500	132.56	0.319						This work[b]
	17739.0(±0.7)	±0.13	±0.005						
	17739.3	132.49	0.302	-2.1×10^{-3}	5.5×10^{-5}	0.01968	5.3×10^{-5}	1.71×10^{-9}	Ref. 3, 4
		±0.22	±0.036	$\pm2\times10^{-3}$	$\pm3.8\times10^{-5}$	$\pm2\times10^{-5}$	$\pm0.2\times10^{-5}$	$\pm0.08\times10^{-9}$	
X	1500[d]	173.22	0.392						This work[b]
		±0.22	±0.009						
	1500[d]	172.98	0.385	-6.3×10^{-4}			5.5×10^{-5}		This work[c]
		±0.2	±0.005	$\pm1\times10^{-4}$			$\pm5\times10^{-7}$		
	0	172.71	0.341	-1.8×10^{-3}	1.0×10^{-5}	0.022806	5.0×10^{-5}	1.50×10^{-9}	Ref. 3, 4
		±0.27	±0.023	$\pm0.7\times10^{-3}$	$\pm0.6\times10^{-5}$	$\pm4\times10^{-6}$	$\pm0.2\times10^{-5}$	$\pm0.07\times10^{-9}$	

[a]All molecular constants are given in cm^{-1}. For a definition of ν_e, ω_e, $\omega_e x_e$... see Eqs. (1)–(5).
[b]From band heads.
[c]From spacings of doublet photoluminescence series according to Eqs. (6)–(9).
[d]From Ref. 6.

tions and a weaker series with vibrational spacings which do not fit the X state spacing. A plot of $\Delta\nu_{vib}$ as a function of v'' leads to $\omega_e = 127.7 \pm 0.4$ cm^{-1} for the lower electronic state which is probably the same state B seen with 488.0 nm excitation. However, the observed $\omega_e x_e = 0.44 \pm 0.04$ cm^{-1} does not agree with $\omega_e x_e = 0.29 \pm 0.01$ cm^{-1} for the 488.0 nm photoluminescence series. From the measured spectrum it is not clear if this photoluminescence series consists of triplets or of two overlapping doublets of the same electronic system. This photoluminescence appears at a temperature of about 1230 K, but the intensity even at higher temperatures was too weak to be seen on a photographic plate. The photoluminescence of the $A-X$ system does not show vibrational or rotational relaxation, indicating that the lifetime of the Bi_2 molecules in high vibrational levels of the A state is shortened by some mechanism.

The upper part of Fig. 5 shows a portion of the photoluminescence spectrum excited by the 476.5 nm laser line. Besides the $A-X$ series which again show no vibrational relaxation, there is a weak doublet series with a vibrational spacing of $\omega_e = 141.23 \pm 0.35$ cm^{-1} and 6 anti-Stokes components; this transition is observed only at temperatures above 1300 K. In addition there is a photoluminescence series with many anti-Stokes lines extending to shorter wavelengths (425 nm) with $\omega_e = 154.9$ cm^{-1}, probably having the same lower state as observed with 488.0 nm excitation. The strong single peaks which form the $A-X$ photoluminescence series are actually produced by overlap of two different vibrational–rotational transitions of the $A-X$ systems. Both series involve low J-values, so that the doublet separations are resolved only by high resolution photographic measurements.

In most laser-induced fluorescence experiments different vibrational–rotational transitions are excited within one electronic system. However in Bi_2 some Ar^+ laser lines excite vibrational–rotational transitions from different low lying thermally populated electronic states. The photoluminescence spectrum of Bi_2 at a temperature of 1370 K excited by the 488.0 nm Ar^+ laser line consists of transitions between as many as four different electronic systems. Part of the spectrum excited by the 488.0 nm line is shown in Fig. 6. The

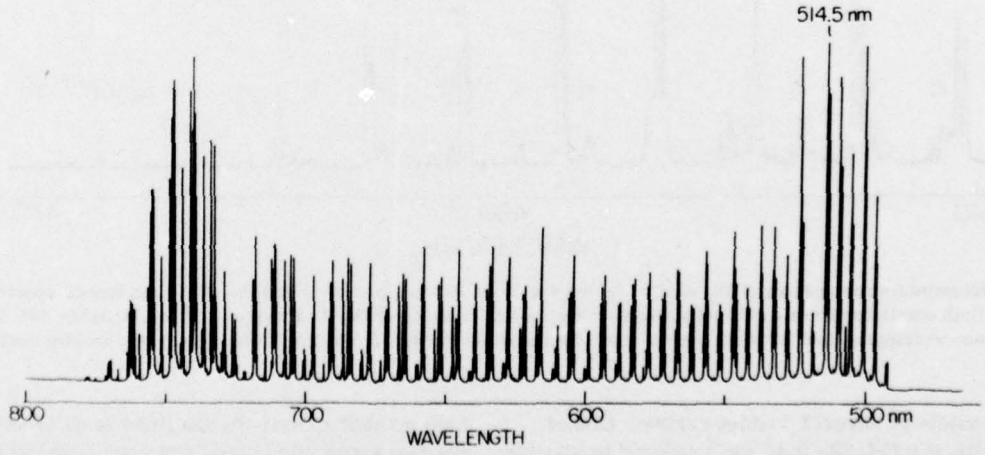

FIG. 4. Photoluminescence spectrum of Bi_2 excited by the 514.5 nm Ar^+ laser line obtained with 0.02 nm resolution. This spectrum extends over the whole Franck–Condon distribution including both maxima; it is not corrected for instrumental response.

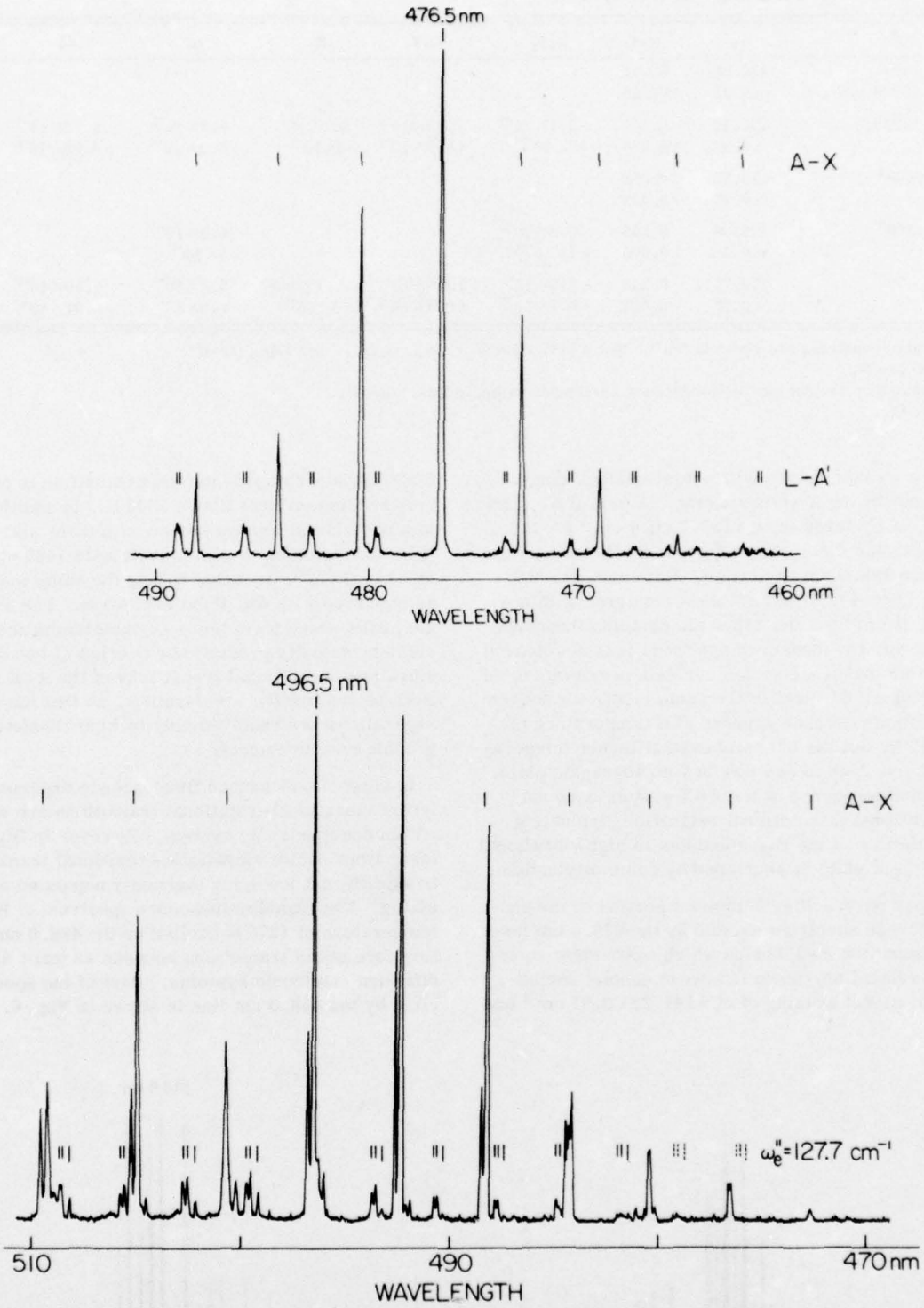

FIG. 5. Photoluminescence spectra of Bi_2 excited by the 496.5 nm (lower spectrum) and the 476.5 nm (upper spectrum) Ar^+ laser lines. Both excitation lines excite vibrational–rotational transitions of the $A-X$ system. In addition the 496.5 nm laser lines excite two overlapping doublet photoluminescence series while the 476.5 nm laser line excites one doublet series.

spectrum consists of several doublet series. One of the series with $\omega_e = 154.29 \pm 0.45$ cm^{-1} extends to shorter wavelengths and consists of 24 anti-Stokes components in addition to a number of Stokes components. Such a high number of anti-Stokes lines is quite unusual. From the measured vibrational spacings (Fig. 7) and the calculated Franck–Condon factors of the $A-X$ system,[6] it is clear that this series is not due to an excitation of

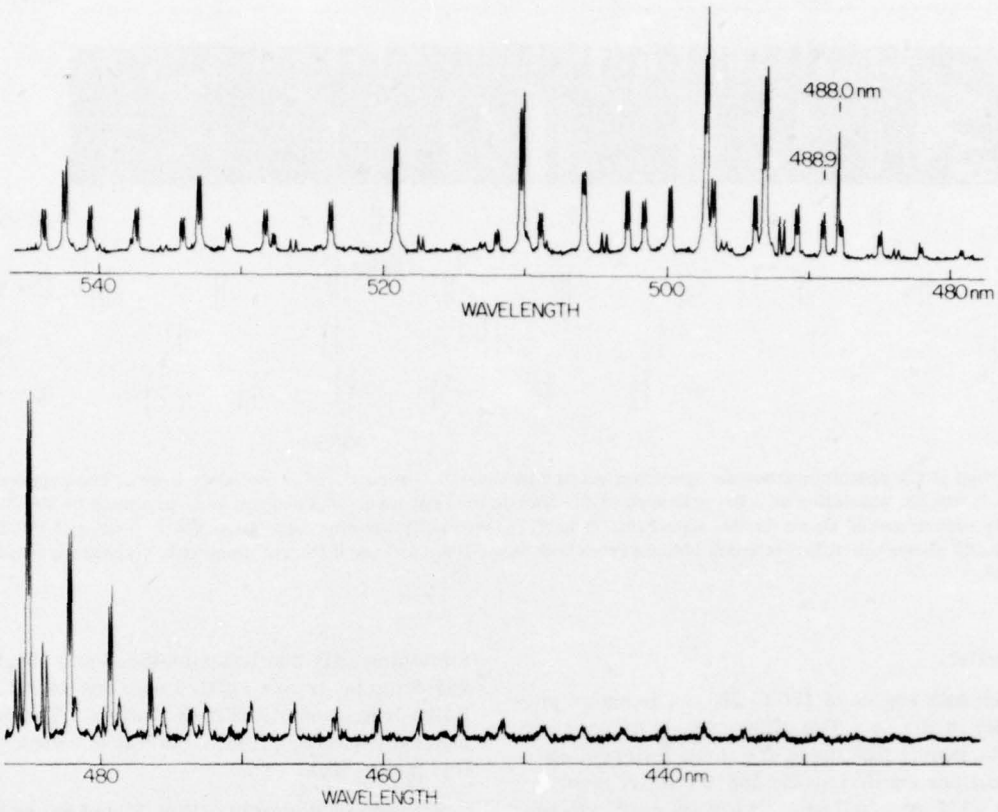

FIG. 6. Photoluminescence spectrum of Bi_2 in the heat pipe excited by 488.0 nm and 488.9 nm Ar^+ laser lines. The 488.0 nm laser line excites four different electronic transitions, one of them consists of a high number of anti-Stokes lines extending to shorter wavelengths.

high vibrational levels of the X state. Photoluminescence of the series with $\omega_e = 154.29$ cm^{-1} was observed at temperatures as low as 1120 K and originates from an unknown low-lying electronic system. The dependence of line intensities with increasing pressure (for Bi_2 pressures < 0.5 torr) is linear. At Bi_2 pressures greater than 0.5 torr the line intensities increase less than linearly with increased pressure, probably due to

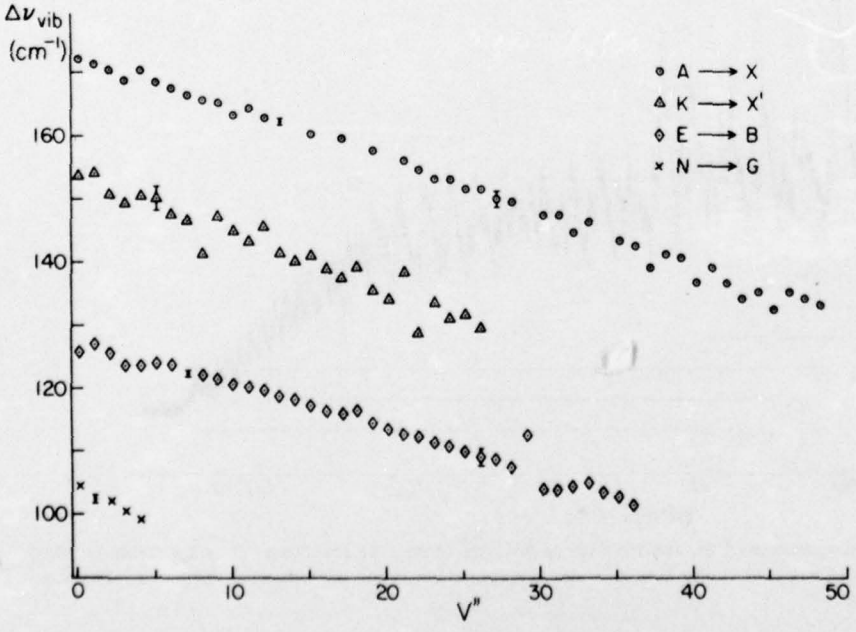

FIG. 7. Plots of $\Delta\nu_{vib}$ as a function of v'' for the four different electronic transitions of Bi_2 excited by the 488.0 nm laser line. The values $\Delta\nu_{vib}(v'')$ are taken from photographic (small error bars) and from photoelectric (bigger error bars) measurements.

14

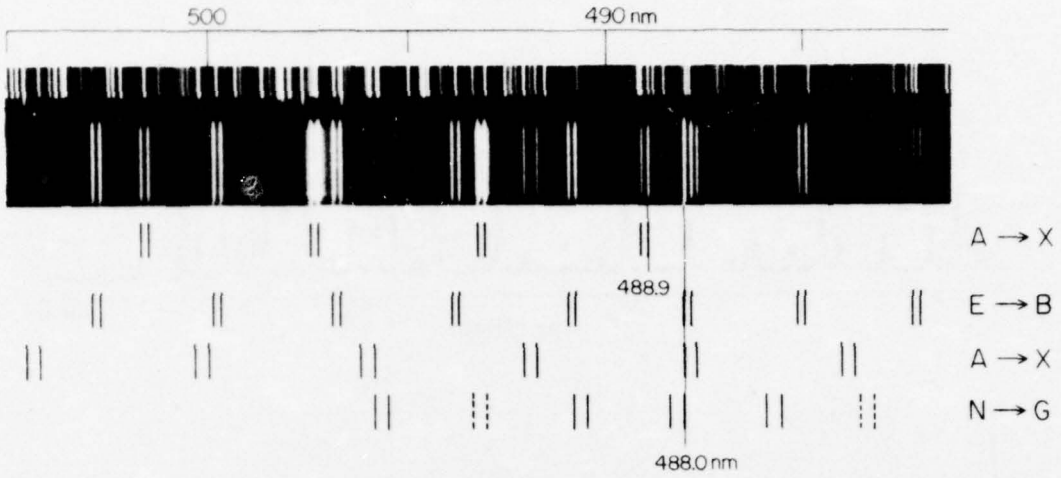

FIG. 8. Portion of the photoluminescence spectrum excited by the 488.0 nm and 488.9 nm laser lines. The spectrum is photographed with 0.015 nm resolution at a Bi_2 pressure of 0.1 torr in the heat pipe. A Fe-spectrum, produced by Fe–Ne hollow cathode lamp, is superimposed above the Bi_2 spectrum. The Ar^+ laser oscillates simultaneously at 488.0 nm and 488.9 nm. The spectrum clearly shows the different contributions from both laser lines and the different electronic transitions excited by the 488.0 nm line.

energy transfer.

The wavelength region of 480 to 505 nm is shown photographically in Fig. 8. The different doublet spacings show unambiguously that there are three different electronic transitions excited by the 488.0 nm Ar^+ laser line with $\omega_e = 127.05$, 105.68, and 172.98 cm^{-1}. In addition the measurement also shows that the Ar^+ laser simultaneously oscillates at 488.0 and 488.9 nm. The 488.9 nm laser line excited only one vibrational–rotational transition of the A–X system. The photoluminescence with $\omega_e = 154.29$ cm^{-1} is too weak to be seen on this photograph.

Both the photographic (Fig. 8) and the photoelectric (Fig. 6) measurements show that the excited transitions

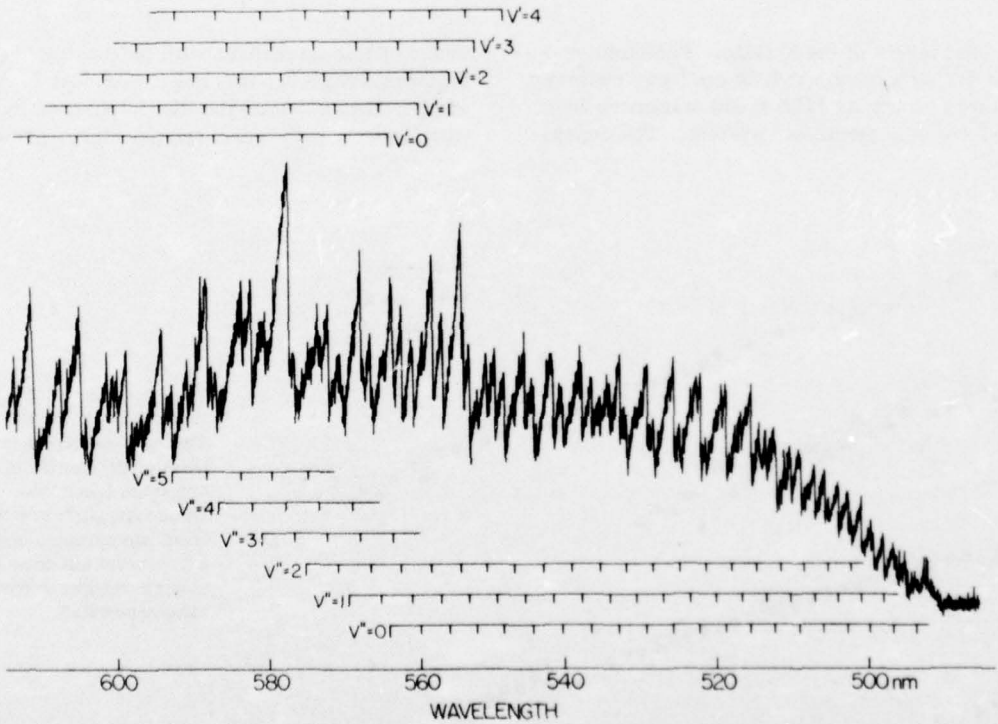

FIG. 9. Portion of the photoluminescence spectrum of Bi_2 excited with white-light from a Xe arc lamp. The spectrum is taken with 0.02 nm resolution at a Bi_2 pressure of 0.1 torr in the heat pipe and is not corrected for instrumental response. The spectrum consists of bands of the A–X system.

TABLE III. Molecular constants[a] of systems excited by the Ar^+ laser.

ω_e	$\omega_e x_e$	$\omega_e y_e$	B_e	α_e
154.29 ± 0.45	0.42 ± 0.05		0.0219[b]	6.5×10^{-5}[d]
172.98 ± 0.2	0.385 ± 0.005	-6.3×10^{-4} $\pm1\times10^{-4}$	0.022806[c] $\pm4\times10^{-6}$	5.5×10^{-5} $\pm5\times10^{-7}$
127.05 ± 0.1	0.29 ± 0.01	$\pm1\times10^{-3}$ $\pm2\times10^{-4}$	0.0179[b]	4.6×10^{-5} $\pm1\times10^{-6}$
141.23 ± 0.35	0.37 ± 0.04	-1.9×10^{-3} $\pm2\times10^{-4}$	0.0199[b]	5.6×10^{-5} $\pm2\times10^{-6}$
132.56 ± 0.13	0.319 ± 0.005		0.01968[c] $\pm2\times10^{-5}$	5.3×10^{-5}[d]
105.68 ± 0.25	0.63 ± 0.03		0.0149[b]	1.4×10^{-4} $\pm5\times10^{-6}$
127.7 ± 0.4	0.44 ± 0.04			

[a]All constants are given in cm^{-1}. For a definition of ω_e, $\omega_e x_e$, ... see Eqs. (1)–(5).

[b]These B_e values are estimated according to $r_e^2\omega_e = \text{const}$[13], where the constant value is taken from Refs. 3, 4.

[c]These values are taken from Ref. 3.

[d]These α_e values are calculated using the Pekeris relation.

of the A–X system have no vibrational relaxation and in the case of 488.0 nm excitation ($v''=2$, $v'=26$) have no rotational relaxation. However with 488.9 nm excitation ($v''=0$, $v'=22$) weak rotational relaxation occurs. By comparison with the photoluminescence excited by 528.7 nm (Fig. 2) and by 514.5 nm [Figs. 3(a), 3(b)], both consisting of strong vibrationally and rotationally relaxed bands of the A–X system, the absence of vibrational relaxation in the 488.0 and 488.9 nm spectra indicates that at approximately $v'=22$ there is strong perturbation of the A state. The line intensities of the 488.9 nm A–X photoluminescence show a very strong dependence on buffer gas pressure. The intensities are down by a factor of 5 when the buffer gas pressure is increased from 0.1 to 5 torr, whereas the line intensities of the 488.0 nm A–X photoluminescence are slightly increased.

The assignments for the A–X transitions excited by 488.0 nm and 488.9 nm are made by counting the number of anti-Stokes lines and confirming the assignment by the calculated Franck–Condon factors. In the case of vibrational–rotational transitions between previously unknown electronic states the accuracy of an assignment depends on how many transitions are actually measured. The more vibrational–rotational transitions measured, the more accurate are the constants obtained from $\Delta\nu_{vib}=f(v'')$ and $\Delta\nu_{rot}=f(v'')$. Plots of $\Delta\nu_{vib}$ as a function of v'' for all observed transitions of the 488.0 nm excitation of Bi_2 are shown in Fig. 7. These plots also show vibrational levels in the lower electronic states which are perturbed. The molecular constants for the lower states of these four electronic systems are obtained according to Eqs. (6)–(9) by a weighted nonlinear least-squares fit and are given in Table III.

The doublet photoluminescence series with $\omega_e=127.05$ cm^{-1} excited by the 488.0 nm laser consists of 39 vibrational transitions which form a unique intensity pattern. This photoluminescence, extending from 465 to 585 nm and covering the complete Franck–Condon distribution, is investigated in more detail in the following paper.[6]

In this case both Franck–Condon maxima are close together and not as well separated as with the 514.5 nm photoluminescence (Fig. 4). The intensities of the observed photoluminescence lines increase strongly with higher temperatures but show almost no buffer gas pressure dependence.

The photoluminescence spectrum, shown in Fig. 6, consists of various doublet series excited by the Ar^+ laser, simultaneously oscillating at 488.9 and 488.0 nm. One of them which is excited by the 488.0 nm line (Fig. 8) involves a lower state with $\omega_e=105.68$ cm^{-1}. This transition is weak and observed only at temperatures above 1270 K. At buffer gas pressures below 0.5 torr the intensities of the photoluminescence lines increase approximately quadratically with increasing pressure whereas at higher pressures no simple dependence exists.

Very weak photoluminescence is produced by the 472.7, 465.8, 457.9, and 454.4 nm Ar^+ laser lines. With the 421.6 nm line of the He–Cd laser and the 632.8 nm line of the He–Ne laser, there was no detectable photoluminescence of Bi_2 at temperatures below 1120 K. During photoluminescence studies by laser excitation, no emission of the Bi atom was detected in the wavelength region from 180 to 980 nm.

Preliminary photoluminescence spectra also have been observed by excitation with a cw tunable dye laser. The dye laser excites photoluminescence over its entire tuning range from 580–615 nm. With the dye laser locked on the 589.6 nm atomic resonance line of sodium

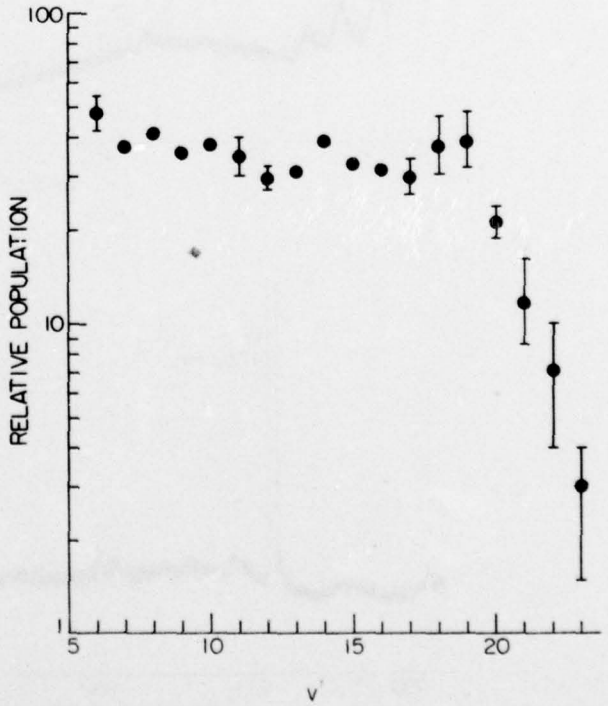

FIG. 10. Plot of the relative population N_v, of the vibrational levels of the upper state A, as given by white light photoluminescence, versus v'. The rapid falloff near $v'=20$ indicates a strong interaction with another electronic state.

16

Bi_2 photoluminescence has been successfully observed.

A portion of the discrete photoluminescence spectrum obtained with white light excitation using the incoherent light of a 150 W Xe arc lamp is shown in Fig. 9. This discrete spectrum begins near 490 nm and extends to longer wavelengths near 765 nm. At shorter wavelengths the spectrum is made up of $v'' = 0, 1, 2$ progressions of the $A-X$ system, which are observed up to $v' = 23$. At longer wavelengths, transitions occur mainly between different v' and v'' levels of the $A-X$ system and no long progressions are formed. The intensity distribution seen in Fig. 9 is similar to that of the $A-X$ emission spectrum of Bi_2 obtained using a microwave discharge.[4] The shape of the spectrum at short wavelengths and the break off at $v' \approx 20$ of the $v'' = 0, 1, 2$ progressions indicates that there is a process which removes Bi_2 molecules in high vibrational levels ($v' \gtrsim 20$) of the A state. For example the Franck–Condon factors[6] for the $v'' = 2$ progressions indicate equal intensities for the 28–2 and 14–2 transitions but the 28–2 band is not observed whereas the 14–2 band is reasonably strong. Similar patterns hold for the $v'' = 0$ and 1 progressions. A combination of higher population of the lower state vibrational levels and more favorable Franck–Condon factors is the reason that the white light photoluminescence spectrum at short wavelengths is mainly due to the $v'' = 0, 1, 2$ progressions.

From the knowledge of the emission intensity, the Franck–Condon factors and the transition frequency, relative vibrational populations $N_{v'}$ are obtained from Eq. (11) (Fig. 10). Populations of the upper vibrational levels v' are almost the same from $v' = 0$ to 19 and then decrease rapidly, indicating a quenching mechanism effective at higher v'. Populations of lower v' levels ($v' \lesssim 5$) cannot be determined accurately because of small Franck–Condon factors and strong overlapping transitions of higher vibrational levels (v', v'').

Photoluminescence spectra obtained with white-light excitation provide a means to determine vibrational temperatures. Spectra such as shown in Fig. 9, allow evaluation in a straightforward manner. Neglecting that portion of the spectrum at short wavelengths which is perturbed in some way, the structure between 495 and

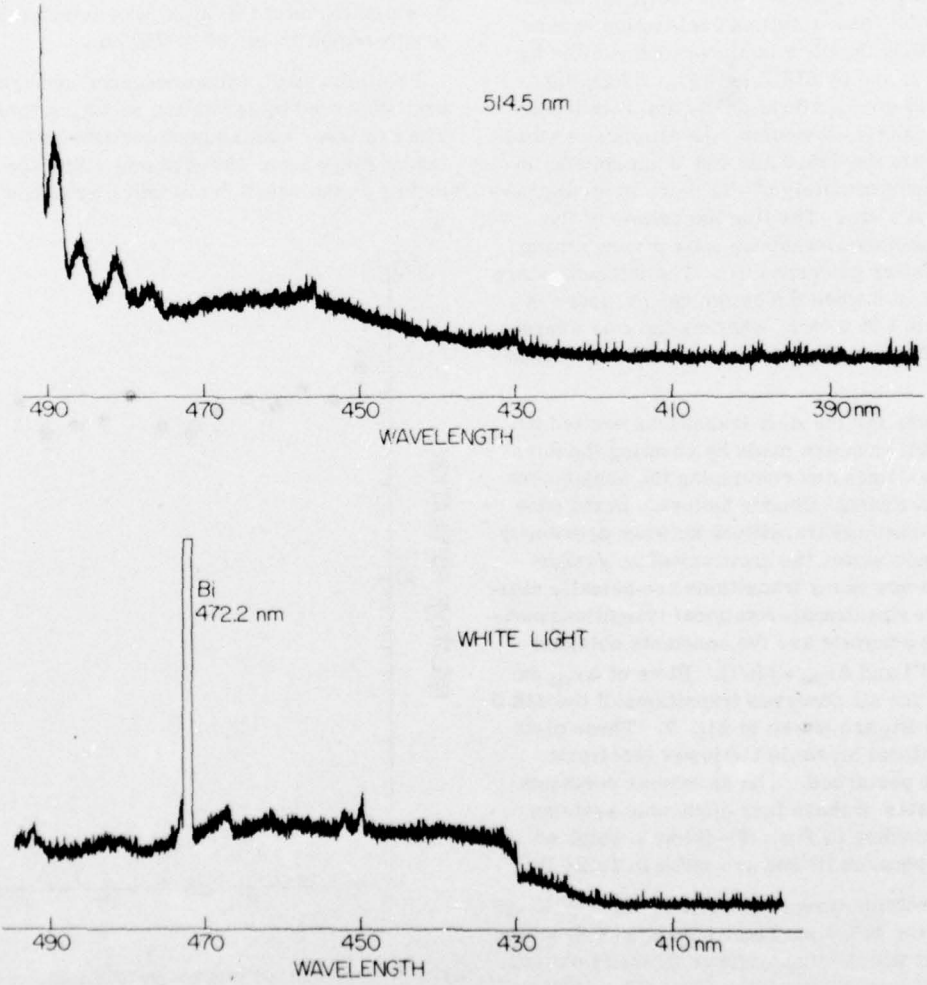

FIG. 11. Continuous spectra are obtained with white light excitation (lower spectrum) and with 514.5 nm Ar^+ laser excitation (upper spectrum) of Bi_2 at a pressure of 0.1 torr and temperature of 1090 K in the heat pipe.

570 nm reflects the population $N_{v'}$ of the upper vibrational levels. Since this portion of the spectrum mainly consists of only three v'' progression the $N_{v'}$ populations can be inverted to $N_{v''}$ populations, thus obtaining an approximate vibrational temperature of the Bi_2 molecules. A similar procedure has been used by Sinha *et al.*[14] for the determination of the vibrational temperature of Na_2 molecules in a nozzle beam.

Values of $N_{v''}$ found from the measured values of $N_{v'}$ of the white light photoluminescence spectrum (Fig. 9) lead to a vibrational temperature of $T_{v1b} = 980$ K according to Eq. (13). This measured vibrational temperature represents the gas temperature inside the heat-pipe. A comparison between the measured wall temperature and this gas temperature shows agreement within 10%.

Another portion of the photoluminescence spectrum obtained with white light excitation is shown on the lower part of Fig. 11. This spectrum shows a continuous distribution and several lines due to atomic bismuth, where the 472.2 nm line $[6s^26p^27s(^4P_{1/2}) - 6s^26p^3(^2D_{3/2})]$ is the strongest. During the experiments with white light excitation several atomic Bi transitions are observed. For instance a group of forbidden lines 459.7 nm ($^2P_{3/2} \rightarrow {}^2D_{3/2}$), 461.5 nm ($^2P_{1/2} \rightarrow {}^4S_{3/2}$), 564.0 nm ($^2P_{3/2} \rightarrow {}^2D_{5/2}$) and 647.6 nm ($^2D_{3/2} \rightarrow {}^4S_{3/2}$) all belonging to transitions between levels of the configuration $6p^3$ is observed. Forbidden lines of different configurations 472.2 nm ($^4P_{1/2} \rightarrow {}^2D_{3/2}$) and 652.3 nm ($^4P_{5/2} \rightarrow {}^2P_{3/2}$) are observed; three unidentified lines at 450.4, 453.2 and 474.0 nm also are seen. The very weak continuum begins gradually near 420 nm but shows a sharp onset at 430 nm and extends to longer wavelengths where it is masked by the stronger discrete spectrum. This continuum does not arise at temperatures below 1020 K. We believe that this continuous distribution is due to transitions from a repulsive state to the X state. The sharp wavelength onset of the continuum is possibly caused by the crossing of this repulsive state with the repulsive part of the A state potential curve. The crossing region is therefore approximately determined by the wavelength of the onset.[6]

The upper part in Fig. 11 shows the shorter wavelength region of photoluminescence excited by the 514.5 nm laser line. The same onset of a continuous distribution is observed at 430 nm, probably due to the same repulsive state seen with white light photoluminescence. From the 514.5 nm photoluminescence spectrum it is not quite clear if the structure near 457 nm is due to another weak continuum or to a broad atomic Bi emission.

It should be mentioned that white light photoluminescence spectroscopy is very useful for measuring band heads and determining different possible transitions. White light photoluminescence spectroscopy gives the same wavelength information that can be obtained from absorption measurements but often it is much easier to observe.

V. ACKNOWLEDGMENTS

We would like to thank Dr. Robert W. Field for suggesting these experiments and Dr. Joseph M. Brom for many valuable discussions. Dr. G. Gerber wants to thank the Deutsche Forschungsgemeinschaft for a fellowship.

*Work supported in part by Office of Naval Research, Contract No. N00014-69-A-0200-8013.

†Present address: Fakultät für Physik, University of Freiburg, D78 Freiburg, West Germany.

‡Present address: Department of Pure and Applied Physics, University of Tokyo, Komaba, Meguro-Ku, Tokyo, Japan.

[1] G. M. Almy and F. M. Sparks, Phys. Rev. 44, 365 (1933); G. M. Almy, J. Phys. Chem. 41, 47 (1937).

[2] G. Nakamura and T. Shidei, Jpn, J. Phys. 10, 11 (1934).

[3] N. Åslund, R. F. Barrow, W. G. Richards, and D. N. Travis, Ark. Fys. 30, 171 (1965).

[4] S. P. Reddy and M. K. Ali, J. Mol. Spectrosc. 35, 285 (1970).

[5] W. Demtröder, M. McClintock, and R. N. Zare, J. Chem. Phys. 51, 5495 (1969); K. Sakurai, S. E. Johnson, and H. P. Broida, J. Chem. Phys. 52, 1625 (1970).

[6] G. Gerber and H. P. Broida, J. Chem. Phys. 64, 3423 (1976) following paper.

[7] J. B. West, R. S. Bradford, Jr., J. D. Eversole, and C. R. Jones, Rev. Sci. Instrum. 46, 164 (1975).

[8] R. E. Honig, "Vapor Pressure Data for the Elements," in *The Characterization of High Temperature Vapors*, edited by J. L. Hargrave (Wiley, New York, 1967).

[9] C. R. Vidal and J. Cooper, J. Appl. Phys. 40, 3370 (1968); C. R. Vidal and F. B. Haller, Rev. Sci. Instrum. 42, 1779 (1971).

[10] D. M. Mann and H. P. Broida, J. Appl. Phys. 44, 4950 (1973); J. D. Eversole and H. P. Broida, J. Appl. Phys. 45, 596 (1974).

[11] *Handbook of Lasers* (Chemical Rubber, Cleveland, 1971), p. 251.

[12] *American Institute of Physics Handbook*, edited by D. E. Gray (McGraw-Hill, New York, second edition, 1963), p. 7/90–121; H. M. Crosswhite, Johns Hopkins Spectroscopic Report No. 13, 1958.

[13] G. Herzberg, *Spectra of Diatomic Molecules* (Van Nostrand, Princeton, 1950).

[14] M. P. Sinha, A. Schultz, and R. N. Zare, J. Chem. Phys. 58, 549 (1973).

Electronic states and molecular constants of Bi_2*

G. Gerber† and H. P. Broida

Quantum Institute and Department of Physics, University of California, Santa Barbara, California 93106
(Received 1 December 1975)

Potential energy curves of several electronic states of Bi_2 have been calculated by the Rydberg–Klein–Rees method using molecular constants obtained from laser-excited photoluminescence of Bi_2. These potential curves are used to compute Franck–Condon factors. Franck–Condon factors for the $A-X$ system are compared with measured intensities of photoluminescence series extending over 50 vibrational levels ($v''=0$–49) and including both Franck–Condon maxima. It is shown that more accurate molecular constants can be derived by using the information contained in these intensity data. Another important result is achieved by deriving previously unknown vibrational and rotational constants of the upper electronic state of the $E-B$ doublet photoluminescence series using only line intensity measurements. Relative energy positions of the electronic states have been obtained by perturbation considerations and by measuring the temperature dependent changes of relative intensities of photoluminescence lines belonging to different electronic transitions. These experiments suggest that there is an electronic state X', which is lower in energy than the X state. A potential energy diagram for Bi_2 is derived including the re-evaluated published spectroscopic data of Bi_2.

INTRODUCTION

Laser-excited photoluminescence of Bi_2[1] revealed the existence of several previously unknown electronic systems. In some cases the photoluminescence consists of long v'' progressions extending over the Franck–Condon distribution including both maxima. Doublet photoluminescence series are observed when using different Ar^+ laser lines for excitation. Strong photoluminescence is due to different vibrational–rotational transitions of the $A-X$ system. Transitions involving the lower part of the A state ($v'<22$) exhibit strong vibrational and rotational relaxation whereas higher vibrational levels show no relaxation within the Bi_2 vapor pressure range 0.1–10 torr. Relative populations of vibrational levels v' of the A state, obtained from white light photoluminescence, are equal from low v' to near $v'=20$ but between $v'=20$ and $v'=23$ the populations decrease by a factor of 10.

In addition to discrete line-photoluminescence, continuum spectra which arise from an unbound upper state are observed with Ar^+ laser excitation and with white light excitation.

In most laser-excited photoluminescence studies,[2] the laser excites one or more different vibrational–rotational transitions within one electronic system. However, in the experiments with Bi_2 several Ar^+ laser lines simultaneously excite transitions of more than one electronic system. This simultaneous excitation makes possible a determination of the relative energy position, $V(r)$, of the involved lower electronic states with respect to the X state by measuring the temperature dependence of the photoluminescence spectrum excited by the laser line.

From the results of both laser-excited photoluminescence and the data of previous studies[3–5] (both given in Table I) we have derived a set of suggested potential curves of Bi_2 (Sec. IV). The potential curves for the different electronic states have been constructed by the Rydberg–Klein–Rees[6] method. Calculated Franck–Condon factors based on these RKR potential curves are used to decide whether some of the spectroscopic assignments are correct or not. Considerations based on laser photoluminescence data and Franck–Condon factors lead to a change of the electronic term value T_e of the earlier[3,5] observed states O, G, and D.

From comparison of Franck–Condon factors with measured line intensities of photoluminescence series, extending over long v'' progressions including both Franck–Condon maxima, an additional measure for the accuracy of molecular constants and more information about the upper electronic states is obtained. This has been done for the $v'=19-v''=4$ transition of the $A-X$ system excited by the 514.5 nm Ar^+ laser (Fig. 1), giving a more accurate value for the rotational constant α_e of the X state. From the unique intensity distribution of the $E-B$ photoluminescence excited by the 488.0 nm Ar^+ laser, vibrational and rotational constants for the upper electronic state are derived.

The homonuclear diatomic molecules of the Group V elements are summarized in Sec. V with respect to their lowest excited states in an electronic term value T_e diagram. Owing to increasing spin–orbit interaction of the heavier elements, the electronic states of Bi_2 are best described in Hund's case (c). Because of lack of sufficient rotational structure in most observed electronic states of Bi_2 there has been made no attempt to systematically classify or to relabel the electronic states.

II. INTENSITIES IN ELECTRONIC TRANSITIONS OF Bi_2

The emission intensity for a vibrational–rotational line in an electronic transition is given by[7]

$$I(v'J';\ v''J'') = \frac{64\pi^4}{3}\, c\nu^4 [S_{J'J''} \times N_{v'J'}/(2J'+1)] \times [\langle \psi_{v'J'} | R_e(r) | \psi_{v''J''} \rangle]^2 \quad (1)$$

where $S_{J'J''}$ is the rotational line strength, $N_{v'J'}$ is the population of the initial state, ν is the frequency of the emitted line in wavenumbers, and ψ_{vJ} is the vibrational wavefunction including $v-J$ coupling characterizing the

TABLE I. Electronic states and molecular constants of Bi_2.

State	T_e[a]	ω_e	$\omega_e x_e$	$\omega_e y_e$	B_e	α_e	D_v	Transition	References
$X'(O_g^+)$	0	154.29	0.42		0.0218[b]	6.5×10^{-5}[c]		$K\rightarrow X'$	d, 1, 20
	0	±0.45	±0.05						
$X(O_g^-)$	1500	172.98	0.385	-6.3×10^{-4}	0.022806	5.5×10^{-5}	1.50×10^{-9}	$A\longleftrightarrow X$	d, 3, 4, 5, 20
	±800	±0.2	±0.005	$\pm1\times10^{-4}$	$\pm4\times10^{-6}$	$\pm5\times10^{-7}$	$\pm7\times10^{-11}$		
$B(O)$	6500	127.05	0.29	-1×10^{-3}	0.01790[b]	4.6×10^{-5}		$E\rightarrow B$	d, 1
	±1000	±0.1	±0.01	$\pm2\times10^{-4}$		$\pm1\times10^{-6}$			
$A'(O)$	9500	141.23	0.37	-1.9×10^{-3}	0.0199[b]	5.6×10^{-5}[c]		$L\rightarrow A'$	d, 1
	±2000	±0.35	±0.04	$\pm2\times10^{-4}$					
$A(O_u^-)$	19239.3	132.56	0.319		0.01968	5.3×10^{-5}	1.71×10^{-9}	$A\longleftrightarrow X$	d, 1, 3, 4, 5
		±0.13	±0.005		$\pm2\times10^{-5}$	$\pm2\times10^{-6}$	$\pm8\times10^{-11}$		
$G(O_u^-)$	21500	105.68	0.63		0.01490[b]	1.4×10^{-4}		$N\rightarrow G$	d, 1
	±200	±0.25	±0.03			$\pm5\times10^{-5}$		$G\rightarrow X$	5
O	23500	Continuous absorption and emission, repulsive state						$O\leftarrow X$	d, 1, 3
K	24000	Upper state of laser transition						$K\rightarrow X'$	d, 1
J	x	103.2	2.45					$P\rightarrow J$	22
E	27936.6	63.5	8.5		0.014250	1.5×10^{-4}		$E\rightarrow B$	d
		±1.2	±0.8		$\pm1\times10^{-5}$	$\pm1\times10^{-5}$			
D	28000	129	9.7					$D\rightarrow X'$	3
M	33500	Continuous absorption, repulsive state						$M\leftarrow X$	3
L	31500	Upper state of laser transition						$L\rightarrow A'$	d, 1
H	34091	Only one v' progression observed						$H\rightarrow A$	5
I	34716.9	156.4	6.1					$I\rightarrow A$	5
C	37957	157	4.6					$C\leftarrow X'$	3
N	42100	Upper state of laser transition						$N\rightarrow G$	d, 1
P	x+15746.3	94.7	5.2					$P\rightarrow J$	22
F	46000	Only partially analyzed						$F\leftarrow X$	3

[a]All constants are given in cm^{-1}. For a definition of T_e, ω_e, $\omega_e x_e$, ... see Eqs. (1)–(5) in Ref. 1.
[b]These B_e values are estimated using the r_e obtained from $r_e^2\times\omega_e=$ const.
[c]These α_e values are calculated using the Pekeris relation.[13]
[d]This paper.

(v, J) state. $R_e(r)$ is the electronic transition moment $\langle\psi_e'|M_e|\psi_e''\rangle$, in which ψ_e' and ψ_e'' are electronic wavefunctions and M_e is the part of the dipole moment depending only on the electrons. Owing to the difficulty of obtaining values of $R_e(r)$ for a many-electron molecule, the usual approximation is to replace $R_e(r)$ by $\bar{R}_e$, which is an average electronic transition moment in a small range of r assuming that $R_e(r)$ will be a slowly varying function in this range. The square of the remaining overlap integral $Q(v'J', v''J'') = |\langle\psi_{v'J'}|\psi_{v''J''}\rangle|^2$ is known as the Franck–Condon factor. For the evaluation of these overlap integrals the wavefunctions $\psi_{v'J'}$ and $\psi_{v''J''}$ must be known. The first step is to construct potential curves for the upper and lower electronic states.

Potential curves for the X and A states of Bi_2 have been constructed from the spectroscopic constants given in Table I using the Rydberg–Klein–Rees (RKR) method.[6] This method does not assume any analytic form for the potential. The turning points r_+ and r_- of the classical motion of the molecule are determined for a vibrational level of energy U from the expression

$$r_\pm(U) = (f/g + f^2)^{1/2} \pm f\,, \tag{2}$$

where f and g are given by

$$f(U) = \frac{h}{2\pi(2\mu)^{1/2}} \int_0^{I'} [U - E(I,\kappa)]^{-1/2} dI\,, \tag{3}$$

and

$$g(U) = \frac{h}{2\pi(2\mu)^{1/2}} \int_0^{I'} \frac{\partial E}{\partial \kappa} [U - E(I,\kappa)]^{-1/2} dI\,. \tag{4}$$

The energy function $E(I, \kappa)$ of the molecule depends upon the radial and angular momentum action variables $I = h(v+\frac{1}{2})$ and $\kappa = J(J+1)h^2/8\pi^2\mu$, where μ is the reduced mass of the molecule. In order to construct the potential function $V(r)$ for the nonrotating ($J=0$) molecule, Eqs. (3) and (4) have to be evaluated for $\kappa = 0$.

Potential energies and turning points for the X and A states are tabulated in Tables II and III. The calculations based on the constants given in Table I are carried out up to the highest observed vibrational levels, $v' = 30$ and $v'' = 50$.

The potential function $V(r)$ used in our calculations is

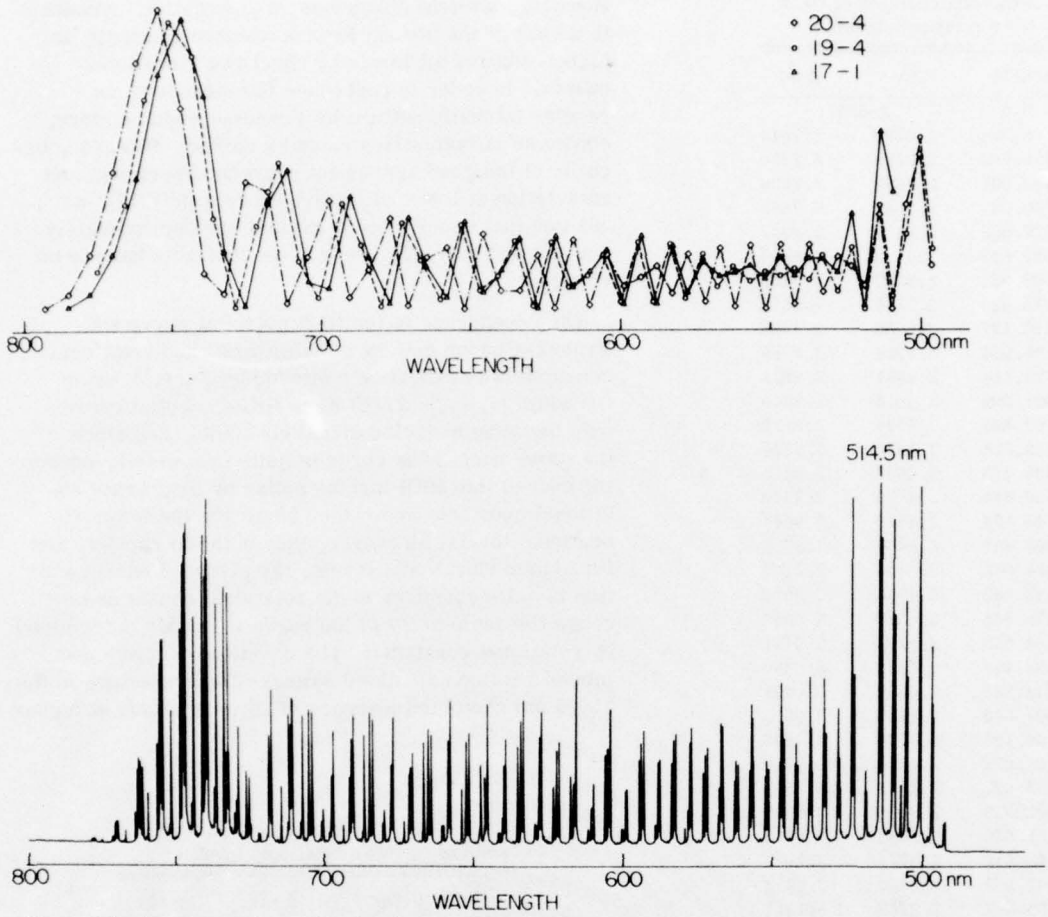

FIG. 1. The lower part shows the photoluminescence spectrum of Bi_2 excited by the 514.5 nm Ar^+ laser line. This spectrum extends over the whole Franck–Condon distribution including both maxima; it is not corrected for instrumental response. The upper part shows calculated Franck–Condon factors for three vibrational–rotational transitions excited in the A–X system.

obtained by connecting the turning points with a smooth curve. To estimate the potential outside the region covered by spectroscopic data, repulsive and attractive segments are smoothly connected with the turning point data and assumed to have the form $V_{rep} = a/r^{12} + c$ and $V_{att} = a'/r^b + d$. The constants a, a', b are determined from the last two pairs of RKR turning points and c and d are given by the experiment.

The centrifugal distortion of the potential $V(r)$ owing to rotation is taken into account by adding the rotational contribution to give the effective radial potential $U(r, J)$

$$U(r, J) = V(r) + [J(J+1)h^2/8\pi^2\mu r^2] \quad (5)$$

Once the potential $U(r, J)$ is constructed, wavefunctions ψ_{vJ} appropriate to this potential are obtained by numerically solving the radial Schrödinger equation[8] for each vibration–rotation level. The eigenfunctions so obtained will then be used to evaluate the overlap integrals.

Photoluminescence of the A–X system

Franck–Condon factors for the A–X system of Bi_2 have been calculated[9] from rotationless ($J = 0$) potentials. However, comparing measured intensities of photoluminescence series with intensities calculated according to Eq. (1) one has to use Franck–Condon factors calculated from $U(r, J)$ potentials with correct J values.[10] If vibration–rotation interaction is neglected, calculated intensities are in error by about ±10% for $J = 30$, ±20% for $J = 100$, and ±50% for $J = 300$. Moreover, the error does not show a systematic trend but varies irregularly from line to line and depends upon the vibrational level. Relative intensity measurements for the A–X system of Bi_2 (not corrected for instrumental response and ν^4 dependency) are given in the lower part of Fig. 1. Photoluminescence excited by the 514.5 nm Ar^+ laser consists[1] of four doublet series 21–5 ($J = 120$), 20–4 ($J = 170$), 19–4 ($J = 10$ and 20) and 17–1 ($J = 270$). Vibrational progressions from $v'' = 0$ to $v'' = 49$ cover the whole Franck–Condon distribution including both maxima. Calculated Franck–Condon distributions for three transitions are shown in the upper part of Fig. 1. The Franck–Condon factors are calculated from $U(r, J)$ potentials using the J values and molecular constants obtained from laser photoluminescence data[1] (Table I).

From Eq. (1) it is seen that the photoluminescence intensity mainly depends upon the frequency ν and the Franck–Condon factor. While the frequency ν varies

TABLE II. Potential energies of the X state of Bi_2 ($J=0$ rotational level).

$v+\frac{1}{2}$	$U(cm^{-1})$	$r_-(Å)$	$r_+(Å)$
0	0.0	2.6597	
0.5	86.394	2.6179	2.7044
1.5	258.602	2.5890	2.7390
2.5	430.034	2.5698	2.7639
3.5	600.687	2.5547	2.7848
4.5	770.556	2.5419	2.8033
5.5	939.639	2.5308	2.8203
6.5	1107.931	2.5207	2.8361
7.5	1275.428	2.5116	2.8510
8.5	1442.127	2.5032	2.8653
9.5	1608.024	2.4954	2.8789
10.5	1773.114	2.4881	2.8921
11.5	1937.396	2.4813	2.9049
12.5	2100.863	2.4748	2.9173
13.5	2263.514	2.4686	2.9295
14.5	2425.343	2.4627	2.9413
15.5	2586.348	2.4570	2.9529
16.5	2746.524	2.4516	2.9644
17.5	2905.867	2.4464	2.9756
18.5	3064.375	2.4414	2.9867
19.5	3222.042	2.4366	2.9976
20.5	3378.866	2.4319	3.0084
21.5	3534.843	2.4274	3.0191
22.5	3689.968	2.4229	3.0296
23.5	3844.238	2.4187	3.0401
24.5	3997.649	2.4146	3.0505
25.5	4150.198	2.4105	3.0608
26.5	4301.879	2.4066	3.0710
27.5	4452.692	2.4028	3.0812
28.5	4602.629	2.3989	3.0913
29.5	4751.690	2.3953	3.1013
30.5	4899.869	2.3917	3.1112
31.5	5047.163	2.3882	3.1212
32.5	5193.567	2.3847	3.1311
33.5	5339.079	2.3813	3.1410
34.5	5483.694	2.3779	3.1508
35.3	5627.408	2.3747	3.1606
36.5	5770.219	2.3715	3.1704
37.5	5912.121	2.3683	3.1802
38.5	6053.112	2.3652	3.1899
39.5	6193.187	2.3621	3.1997
40.5	6332.343	2.3591	3.2094
41.5	6470.576	2.3561	3.2192
42.5	6607.881	2.3531	3.2289
43.5	6744.257	2.3502	3.2386
44.5	6879.697	2.3473	3.2483
45.5	7014.200	2.3445	3.2580
46.5	7147.761	2.3416	3.2677
47.5	7280.375	2.3388	3.2775
48.5	7412.040	2.3361	3.2873
49.5	7542.753	2.3333	3.2970
50.5	7672.508	2.3306	3.3068

slowly and monotonically in the range of the observed photoluminescence, Franck–Condon factors vary irregularly from line to line of the progression (Fig. 1). Because the Franck–Condon factors predominantly control the intensity distribution of a photoluminescence series, comparison with measured intensities (Fig. 1) provides an additional check on the assignment and accuracy of molecular constants. Comparison of calculated Franck–Condon factors and measured intensities shows agreement up to $v'' \sim 10$ in each series. However, a slight disagreement at higher v'' results in a shift of the second Franck–Condon maximum to higher vibrational levels by about two vibrational quanta. In order to reproduce the measured nonregular intensity pattern by Franck–Condon factors, constants of both states could be varied. However, because of the good agreement between experiment and calculation at lower vibrational levels ($v'' < 10$), we assume that upper state constants are approximately correct and that only lower state constants have to be changed.

The dependence of the RKR potential curve and Franck–Condon factors on vibrational and rotational constants was extensively studied by Zare.[10] Since the width $(r_+ - r_-) = 2f(U)$ of an RKR-potential curve only depends upon vibrational constants, and since the lower part of the curve is quite symmetric, errors introduced into RKR turning points by inaccurate rotational constants are rather small for the lower vibrational levels. However, they build up rapidly, and for higher vibrational levels, the potential energy function is quite sensitive to the rotational constants because the asymmetry of the curve is mainly determined by rotational constants. The deviation of measured intensities and calculated Franck–Condon factors in the 514.5 nm photoluminescence of Bi_2 starts only at higher

TABLE III. Potential energies of the A state of Bi_2 ($J=0$ rotational level).

$v+\frac{1}{2}$	$U(cm^{-1})$	$r_-(Å)$	$r_+(Å)$
0	0.0	2.8632	
0.5	66.200	2.8155	2.9143
1.5	198.122	2.7826	2.9541
2.5	329.406	2.7609	2.9827
3.5	460.052	2.7438	3.0067
4.5	590.060	2.7294	3.0281
5.5	719.430	2.7167	3.0477
6.5	848.162	2.7055	3.0659
7.5	976.256	2.6952	3.0833
8.5	1103.712	2.6858	3.0997
9.5	1230.530	2.6770	3.1156
10.5	1356.710	2.6688	3.1309
11.5	1482.252	2.6611	3.1457
12.5	1607.156	2.6539	3.1601
13.5	1731.422	2.6470	3.1742
14.5	1855.050	2.6404	3.1880
15.5	1978.040	2.6342	3.2015
16.5	2100.392	2.6282	3.2148
17.5	2222.106	2.6224	3.2278
18.5	2343.182	2.6169	3.2407
19.5	2463.620	2.6115	3.2534
20.5	2583.420	2.6064	3.2660
21.5	2702.582	2.6014	3.2784
22.5	2821.106	2.5966	3.2907
23.5	2938.992	2.5919	3.3028
24.5	3056.240	2.5874	3.3149
25.5	3172.850	2.5830	3.3268
26.5	3288.822	2.5787	3.3387
27.5	3404.156	2.5745	3.3505
28.5	3518.852	2.5705	3.3622
29.5	3632.910	2.5665	3.3739
30.5	3746.330	2.5626	3.3855

vibrational levels ($v'' > 10$). Therefore it is reasonable to assume that in a first approximation only rotational constants have to be changed. According to the relation for B_v ($B_v = B_e - \alpha_e(v+\frac{1}{2}) + \gamma_e(v+\frac{1}{2})^2 + \dots$), the B_v value mainly depends on α_e and γ_e. A change of B_e seems unreasonable as long as the lower part ($v'' < 10$) of the progression is well reproduced by the calculation. The constant $\alpha_e = 5\times10^{-5}$ cm^{-1} is derived from laser photoluminescence data[1] and γ_e can be estimated either according to Dunham[11] from the B_e and ω_e values as 1×10^{-8} cm^{-1} or from the curve $\Delta\nu_{rot} = f(v'')$ of photoluminescence data, both methods give the same order of magnitude. From the α_e and γ_e values, it can be seen that even at $v'' = 50$ the corrective influence of γ_e on B_v is less than 0.1%, whereas the required change of $\Delta v \sim 2$ (Franck–Condon maximum shifted by about 2 vibrational quanta) leads to a change of $B_{v=50}$ of approximately 4%. Thus, keeping in mind that the vibrational constants ω_e and $\omega_e x_e$ are accurate to ~1% only a change of α_e will accomplish the necessary shift of the second Franck–Condon maximum without changing the agreement of experiment and calculation for $v'' < 10$. Therefore, the value of α_e was varied in increments of 5×10^{-6} from 3×10^{-5} cm^{-1} to 6.5×10^{-5} cm^{-1} without changing other parameters. The value of $\alpha_e = 5.5\times10^{-5}$ cm^{-1} produced the best agreement between the calculated intensity distribution and observed photoluminescence and is believed to be the most accurate α_e value for the X state of Bi_2. Comparison of observed and calculated relative intensity distributions of the $v' = 19 \rightarrow v'' = 4$ transition of the $A-X$ system is shown in Fig. 2. Intensities of the photoluminescence series are calculated according to Eq. (1) and normalized to the observed intensity of the $v' = 19 \rightarrow v'' = 27$ transition. Observed line intensities are accurate to 10% when corrected for instrumental response and ν^4 dependency. Agreement is good and seems to confirm the assignment as well as the set of spectroscopic constants used. Following the procedure described above, one achieves more accurate molecular constants (in this case α_e) by using the information contained in observed intensities. However, it should be kept in mind that the ability to give the correct vibrational overlap matrix is a necessary but not sufficient condition on a set of spectroscopic constants.[12]

Intensity measurements of transitions from a given v' level to several v'' levels allow a determination of relative Franck–Condon factors [Eq. (1)]. But, if intensity measurements are available for transitions to all v'' levels of the lower state, absolute Franck–Condon factors may be obtained instead of relative ones. With the 514.5 nm photoluminescence (Fig. 1) we observed transitions from v' to all possible v'' levels. That means the sum of the related Franck–Condon factors $\sum_{v''} Q_{v'v''}$ should be unity. For the example of the 19–4 excitation, this sum over the observed transitions ($v'' = 0$–49) is 0.986; therefore absolute rather than relative Franck–Condon factors have been obtained.

Photoluminescence of the E-B system

The $E-B$ doublet photoluminescence series with $\omega_e'' = 127.05$ cm^{-1} excited by the 488.0 nm Ar$^+$ laser con-

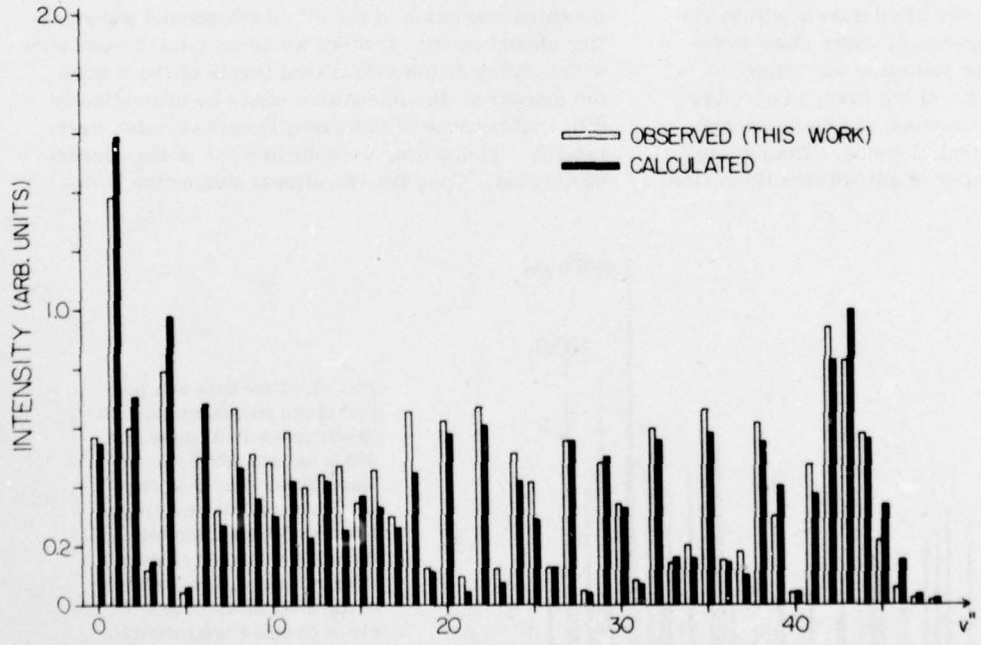

FIG. 2. Comparison of observed and calculated relative intensities (normalized to 19–27 transition) of the doublet photoluminescence series resulting from the 19–4 transition of the $A-X$ system excited by the 514.5 nm Ar$^+$ laser. The measured intensities are corrected for instrumental response. The calculated intensities reflect a specific α_e which is obtained by the best overall agreement of experiment and calculation.

sists of 39 vibrational–rotational transitions which form a unique intensity pattern. Figure 3 shows the measured intensity distribution (not corrected for instrumental response and ν^4 dependency) of the photoluminescence covering the complete Franck–Condon distribution where the line positions, extending from 465 to 585 nm are indicated by dots. Additional lines belong to different electronic transitions excited by the 488.0 nm laser. In this case both Franck–Condon maxima are close together in energy and not as well separated as in the 514.5 nm photoluminescence (Fig. 1). The lower electronic state B is well characterized by the position and number of the observed photoluminescence lines which result in molecular constants[1] given in Table I. If there were several photoluminescence series with the same ω_e excited by the laser line, the upper electronic state constants could be derived from spectroscopic analysis by standard procedures. But the accuracy of these constants would depend strongly upon the number of excited transitions. However, the photoluminescence indicated by dots in Fig. 3 consists only of one v'' progression. Although there is only one transition excited, we have succeeded in deriving the upper state constants by a method (to be described) utilizing only the intensity data. Information contained in intensity data is usually overlooked or used only in connection with Franck–Condon factors to confirm an assignment.

Emission intensities of vibrational–rotational lines are given by Eq. (1) and after correction for the ν^4 term and for instrumental response, intensities are proportional to the square of the overlap integral of the lower and upper state wavefunctions. Corrected measured intensities therefore reflect these wavefunctions. Knowing the lower state wavefunctions (as determined by photoluminescence) upper state wavefunctions are derived in the following way using intensity data. Turning points of the lower state vibrational levels are plotted in a graph to give the shape of the lower electronic potential curve. Taking into account the measured number of anti-Stokes lines, the corrected intensity of the photoluminescence line belonging to the highest energy is correlated with the $v''=0$ level. A line which reflects the intensity is placed at the internuclear separation of the $v''=0$ turning point r_+. The corrected intensity of the photoluminescence line of the second highest energy is correlated with the $v''=1$ level and the corresponding line is placed at r_+ of $v''=1$. In the same way all measured photoluminescence lines are connected with the r_+ turning points of corresponding vibrational levels v''. The envelope of all these lines gives in a first approximation the upper state vibrational wavefunction. The assumption that the heights of the last maximum at large r of the lower state vibrational wavefunctions are the same is, of course, not correct, but would only slightly change the shape and maxima of the upper vibrational state wavefunction. Actual calculations of the vibrational wavefunction show a 10% monotonic variation of heights between $v''=7$ and 30. Therefore, the wavefunction of the lower state can be taken out of the overlap integral $|\langle\psi_{v'}|\psi_{v''}\rangle|^2$ with the envelope now representing the probability density distribution of the upper wavefunction $|\psi_{v'}|^2$. The upper vibrational wavefunction of the $\omega_e''=127.05\ \mathrm{cm}^{-1}$ photoluminescence constructed as described above is shown in Fig. 4. The envelope suggests that $v'=1$ is the upper vibrational level. In principle the $v'=2$ level also could be a solution with the third maximum of the wavefunction not being measured. However, the intensity at the low energy side of the second peak, corresponding to large internuclear separations, decreases more slowly than on the high energy side before approaching zero. Even with sensitivity increased by a factor of 100 we did not detect any photoluminescence of the $E-B$ system at longer wavelengths where transitions due to the third maximum of the $v''=2$ vibrational wavefunction should occur. If there would be a third maximum with overlap of low vibrational levels of the B state, the measured line intensities would be dramatically different because of favorable Franck–Condon overlapping. Therefore, we believe $v'=1$ is the correct numbering. Once the vibrational numbering is de-

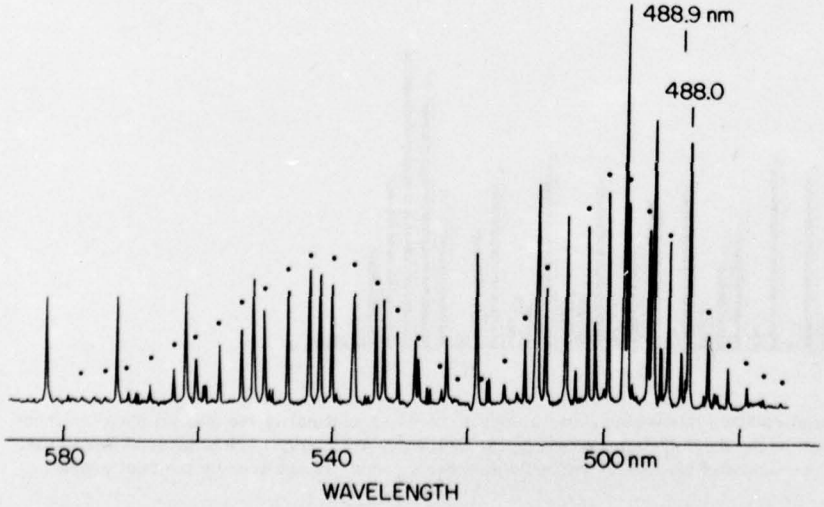

FIG. 3. Fast scan of a portion of the photoluminescence spectrum excited by the 488.0 nm and 488.9 nm Ar^+ laser lines. The $E-B$ doublet series covers the whole Franck–Condon distribution including both very close lying maxima. The position of the $E-B$ photoluminescence doublets are indicated by dots.

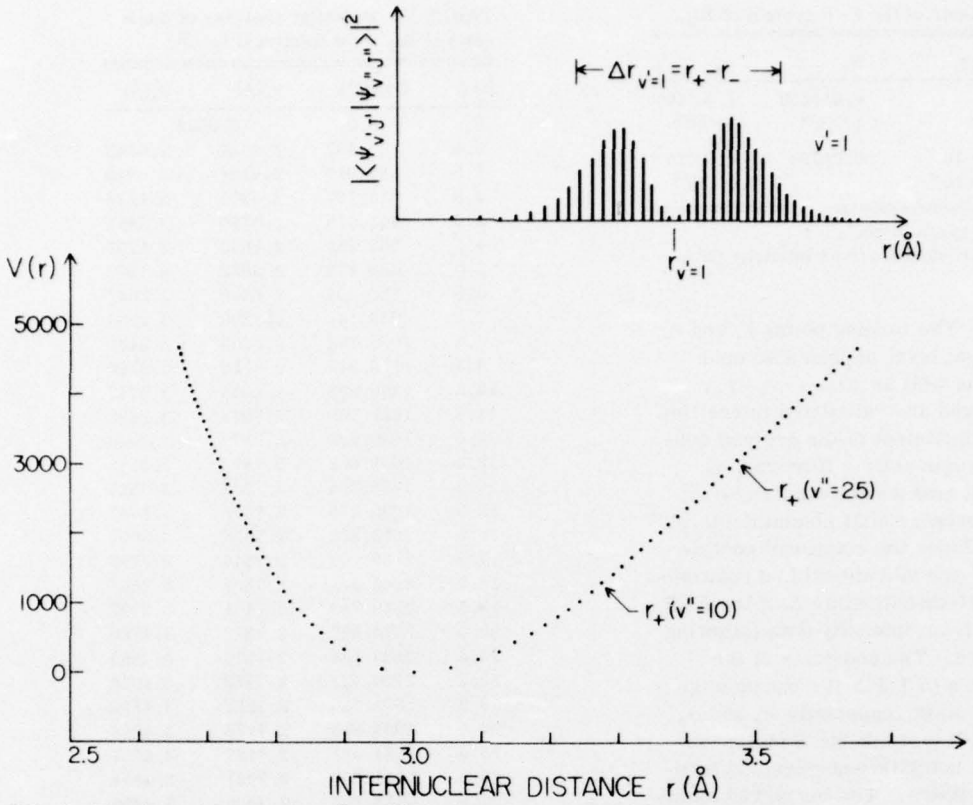

FIG. 4. Turning points r_+ and r_- of an RKR potential curve of the B state are used in connection with intensity data of the $E-B$ doublet photoluminescence series to construct the upper wavefunction $\psi_{v'J'}$ of the transition. The position of the lines are given by the turning point r_+ of the lower vibrational level involved and the length of the lines reflects the Franck–Condon factors as obtained by correcting the experimental data for instrumental response and for the ν^4 dependency.

termined, the values of $\Delta r(v'=1) = r_+ - r_-$ and eventually $r_{v'=1}$, may be derived. The amplitude of the classical vibrational motion $\Delta r = r_+ - r_-$ is obtained from the intersection of the potential energy curve with the corresponding energy level, since the turning points are the positions at which the total energy is entirely potential energy. However, the quantum-mechanical probability density $|\psi_v|^2$ still has a large value at these turning points. This value $|\psi_v|^2_{r_+}$ can be estimated for the $v'=1$ vibrational level using ω_e obtained from[13] $r_e^2 \times \omega_e \approx$ const and $r_{v'=1}$ in a harmonic oscillator approximation. The ratio between the maximum of $|\psi_{v'=1}|^2$ and the value for $|\psi_{v'=1}|^2_{r_+}$ at the turning point r_+ is then used to determine the location of the turning points r_+ and r_- of the derived probability density distribution for the $v'=1$ level given in Fig. 4. The turning points obtained in this way are $r_+ = 3.530$ Å and $r_- = 3.235$ Å and in good agreement with calculated turning points (Table VI) from the best fit of experiment and calculation. In the first step of an iteration procedure $r_{v'=1}$ may be taken as r_e of the upper electronic state. Using the empirical relation[13] $r_e^2 \times \omega_e \approx$ const, an approximate ω_e' may be obtained. On the other hand, an approximate value of ω_e' also may be obtained from a graph of $2f = \eta(U)$, where f is given by Eq. (2) and U is the energy of the vibrational level, using the fact that the difference $\Delta r = r_+ - r_-$ of the RKR turning points only depend upon the vibrational constants and for $v'=1$ mainly upon ω_e'. Knowing the constants ω_e' and B_e', one may find from a Morse potential a value for $\omega_e' x_e'$ which satisfies the given $\Delta r_{v'=1}$, using the relation $D_e = \omega_e^2 / 4\omega_e x_e$. From the Perkeris relation[13]

$$\alpha_e = \frac{6\sqrt{\omega_e x_e \times B_e^3}}{\omega_e} - \frac{6B_e^2}{\omega_e} ,$$

an approximate value for α_e' is obtained and with this value a more accurate B_e' follows (the approximation $r_{v'=1} \sim r_e$ no longer being used) and consequently more accurate ω_e' and $\omega_e' x_e'$ are derived. The α_e' value also may be improved by using the more accurate values for B_e', ω_e' and $\omega_e' x_e'$. Comparison of calculated and measured overlap integrals, provides an additional test for the constants. For instance, if the separation of the calculated maxima is too large, vibrational constants, especially ω_e', do not have correct values; if the separation agrees but the maxima do not occur at the correct vibrational levels, the constant B_e' has to be changed; and if the calculated and measured distributions disagree only in shape, a simultaneous change of α_e' and B_e' is necessary.

In cases of transitions with $J \neq 0$, the additional energy $F_{v'} = B_e \times J'(J'+1)$ has to be taken into account as well as the rotational distortion Eq. (5). For the $E-B$ photoluminescence, the rotational number $J' = 105$ is known from the measured doublet separation of the series and the B_e' value is approximately the

TABLE IV. Molecular constants of the $E-B$ system of Bi_2.

State	ω_e[a]	$\omega_e x_e$	$\omega_e y_e$	B_e	α_e
E[b]	63.5 ±1.2	8.5 ±0.8		0.014250 $\pm 1\times10^{-5}$	1.5×10^{-4} $\pm 1\times10^{-5}$
B	127.05 ±0.1	0.29 ±0.01	1×10^{-3} $\pm 2\times10^{-4}$	0.01790	4.6×10^{-5} $\pm 1\times10^{-6}$

[a]All molecular constants are given in cm^{-1}.
[b]The constants of this state are derived from intensity data.

same as in the $J=0$ case. The turning points r_+ and r_- of the vibrational–rotational level depend also upon the rotational number J' as well as $\Delta r_{v',J'} = r_+ - r_-$. The comparison of measured and calculated intensities again provides the final adjustment of the derived constants for the upper electronic state. However, it should be kept in mind that now the wavefunctions ψ_{vJ} are obtained using the effective radial potential $U(r, J)$ given by Eq. (5) which includes the rotational contribution. Given in Table IV are vibrational and rotational constants of the upper electronic state E of the $E-B$ doublet series as derived from intensity data following the method described above. The constants of the lower state B also are given in Table IV, because the derived constants of the E state, especially B_e and α_e, are strongly correlated with those of the B state. In Table V and VI we present potential energies and turning points for the E and B states. The measured intensity data (closed lines) and line intensities calculated according to Eq. (1) (open lines) are shown in Fig. 5. Agreement is good and the deviation is less than 5% (except for $v''=29$, 30 and 31), which is the experimentally determined uncertainty in line intensities of the $E-B$ photoluminescence. Uncertainties in derived constants are established by the variation of these constants not leading to changes of more than 5% of line intensities. Deviations of measured line intensities for $v''=29$, 30, and 31 are due to a perturbation of the lower electronic state B. The most strongly perturbed level is $v''=29$, which is in agreement with perturbations observed in the position of photoluminescence lines (Fig. 7 in Ref. 1) resulting in a shift of level 29 by -6 cm^{-1}, 30 by $+2.1$ cm^{-1}, and 31 by $+1.2$ cm^{-1}.

The procedure used in deriving the upper state vibrational wavefunction by connecting line intensities with lower state vibrational turning points r_+ is somewhat arbitrary. We could also have connected the intensities with the r_- turning points. Doing this and following the procedure described above we obtained a completely different set of vibrational and rotational constants. However, the calculated intensities do not match the measured line intensities better than ±30% for any set of constants. Also, we could not reproduce experimental measurements by connecting one maximum with r_+ turning points and the other one with r_- turning points of the lower state levels. A systematic variation of the constants found for the E state giving different calculated intensity distributions was carried out but showed much less agreement between experiment and calculation (Fig. 5) than achieved with the set of constants given in Table IV. Therefore, we believe the set of constants given for the E state in Table IV best describes the upper state of the $E-B$ photoluminescence.

TABLE V. Potential energies of the B state of Bi_2 ($J=0$ rotational level).

$v+\frac{1}{2}$	$U(cm^{-1})$	r_-(Å)	r_+(Å)
0	0.0	3.0022	
0.5	63.452	2.9534	3.0543
1.5	189.919	2.9198	3.0949
2.5	315.797	2.8975	3.1240
3.5	441.079	2.8799	3.1485
4.5	565.761	2.8652	3.1702
5.5	689.836	2.8522	3.1902
6.5	813.298	2.8406	3.2087
7.5	936.141	2.8300	3.2263
8.5	1058.358	2.8203	3.2431
9.5	1179.945	2.8113	3.2592
10.5	1300.895	2.8028	3.2747
11.5	1421.202	2.7949	3.2898
12.5	1540.859	2.7874	3.3045
13.5	1659.862	2.7802	3.3188
14.5	1778.204	2.7734	3.3329
15.5	1895.879	2.7668	3.3467
16.5	2012.880	2.7606	3.3602
17.5	2129.203	2.7546	3.3736
18.5	2244.841	2.7488	3.3867
19.5	2359.788	2.7431	3.3997
20.5	2474.037	2.7377	3.4126
21.5	2587.584	2.7324	3.4253
22.5	2700.422	2.7273	3.4379
23.5	2812.545	2.7223	3.4504
24.5	2923.946	2.7175	3.4628
25.5	3034.621	2.7127	3.4751
26.5	3144.563	2.7081	3.4874
27.5	3253.765	2.7036	3.4996
28.5	3362.223	2.6992	3.5117
29.5	3469.930	2.6948	3.5238
30.5	3576.879	2.6906	3.5359
31.5	3683.067	2.6864	3.5479
32.5	3788.484	2.6823	3.5599
33.5	3893.127	2.6783	3.5718
34.5	3996.989	2.6743	3.5838
35.5	4100.064	2.6703	3.5957
36.5	4202.345	2.6665	3.6077
37.5	4303.828	2.6627	3.6196
38.5	4404.506	2.6589	3.6315
39.5	4504.373	2.6551	3.6435
40.5	4603.422	2.6514	3.6554

III. TEMPERATURE DEPENDENCE

The excitation of two electronic states by one laser line provides a possibility for determining the relative energy positions of the lower electronic states involved. The measured intensity of the $K-i$ emission

TABLE VI. Potential energies of the E state of Bi_2 ($J=0$ rotational level).

$v+\frac{1}{2}$	$U(cm^{-1})$	r_-(Å)	r_+(Å)
0	0.0	3.3648	
0.5	29.625	3.2959	3.4472
1.5	76.125	3.2346	3.5382
2.5	105.625	3.1612	3.6492
3.5	118.125	2.9701	3.9226

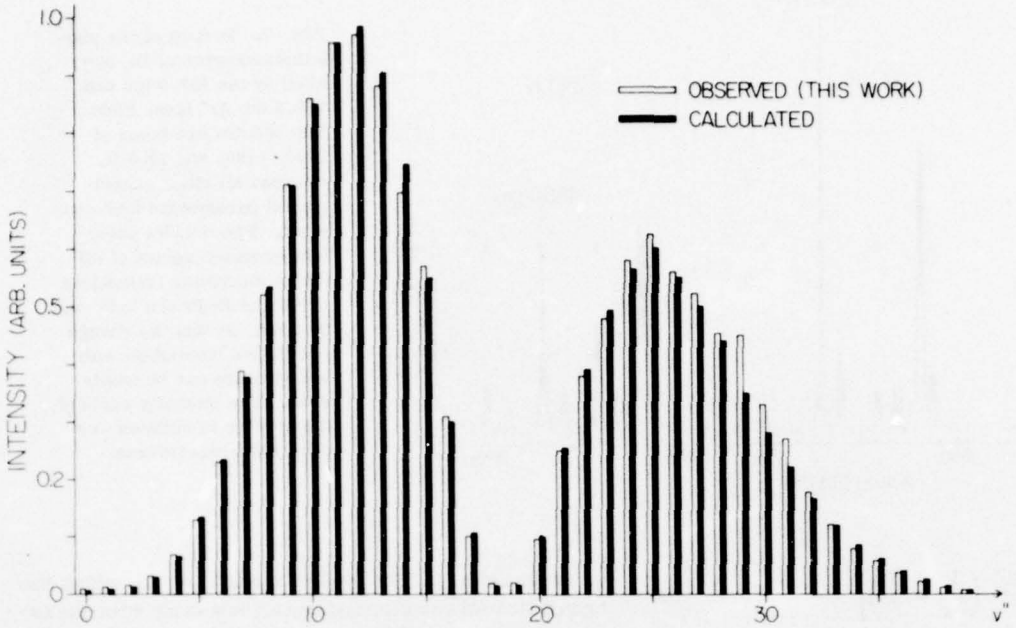

FIG. 5. Comparison of observed and calculated relative intensities (normalized to 1–11 transition) of the $E-B$ doublet photoluminescence series. The experimentally obtained intensity data are used (Sec. II) to derive the vibrational and rotational constants of the upper state E. Calculations of intensities are based on an RKR potential curve obtained from the derived constants. Agreement between experiment and calculation is within 5% (except for perturbed levels $v''=29$, 30, and 31).

may be represented by

$$I(K, i) \propto \frac{N_K(1/\tau_0)}{1/\tau_0 + 1/\tau_{nr} + \sigma P_{Bi_2}(T) + \sigma^* P_{Bi}(T)} \quad , \tag{6}$$

where τ_0 is the spontaneous lifetime of state K, τ_{nr} is its nonradiative lifetime, σ and σ^* are quenching cross sections for Bi_2–Bi_2 and Bi_2–Bi collisions and P_{Bi_2} and P_{Bi} are temperature dependent pressures of Bi_2 and Bi respectively. The number of Bi_2 molecules (per second) in the upper state K is given by

$$N_K \propto N_i(T) \times Q_{Ki} \times I_{laser} \, , \tag{7}$$

in the case of exciting the upper level κ by a laser line from a single lower level i, where $N_i(T)$ is the number of molecules in state i, Q_{Ki} is the Einstein coefficient for the transition, and I_{laser} is the incident light intensity.

The number of Bi_2 molecules in a given state i is connected with temperature T according to

$$N_i(T) = \frac{N_0(T) \times g_i e^{-E_i/kT}}{\sum_j g_j e^{-E_j/kT}} \quad , \tag{8}$$

where $N_0(T)$ is the total number of Bi_2 molecules and g_i and g_j are degeneracy factors.

The measured intensity of photoluminescence following laser excitation therefore depends upon the temperature T and reflects the population of the lower level i. Taking intensity ratios it can be easily seen that $N_0(T)$, which decreases with increasing temperature when keeping the pressure constant, has no influence on the ratios. Only the part $[\sigma P_{Bi_2}(T) + \sigma^* P_{Bi}(T)]$ of the denominator has an influence on the intensity ratios, because $(1/\tau_0 + 1/\tau_{nr})$ depends only on the structure of the molecule. A semilogarithmic plot of relative intensities of photoluminescence lines against $1/T$, the reciprocal of the temperature (measured in the heat pipe) gives a straight line, which indicates that the electronic states are in equilibrium. Vibrational levels also should be in equilibrium. Therefore, a change of temperature results in a change of relative populations. Measuring the relative change of photoluminescence intensities with temperature yields the relative energy positions of the vibrational–rotational levels of lower electronic states.

An example of such a temperature dependence measurement is illustrated in Fig. 6. This portion of the photoluminescence spectrum of Bi_2 excited by the 488.0 and 488.9 nm Ar^+ laser lines is measured several times in the heat pipe under the same experimental conditions. The only change is an increase in temperature which is monitored by a thermocouple attached to the outside wall. The experimental set up used for these measurements is described in the preceding paper.[1] Figure 6 shows how the intensities of the doublet photoluminescence belonging to the $A-X$ and $E-B$ systems are changed with increasing temperature. From the analysis of the white light photoluminescence and of a thermal emission spectrum of the $A-X$ system of Bi_2, the gas temperature of the system is known to agree within 10% with the measured wall temperature. Assuming that quenching and other collision induced effects do not greatly change the intensity ratios in a given temperature interval, the difference in energy between two vibrational–rotational levels of different electronic states may be represented by

$$\left[\frac{I_a(v'J', v''J'')}{I_b(v'J', v''J'')}\right]_{T_0} \left[\frac{I_a(v'J', v''J'')}{I_b(v'J', v''J'')}\right]^{-1}_{T_1}$$

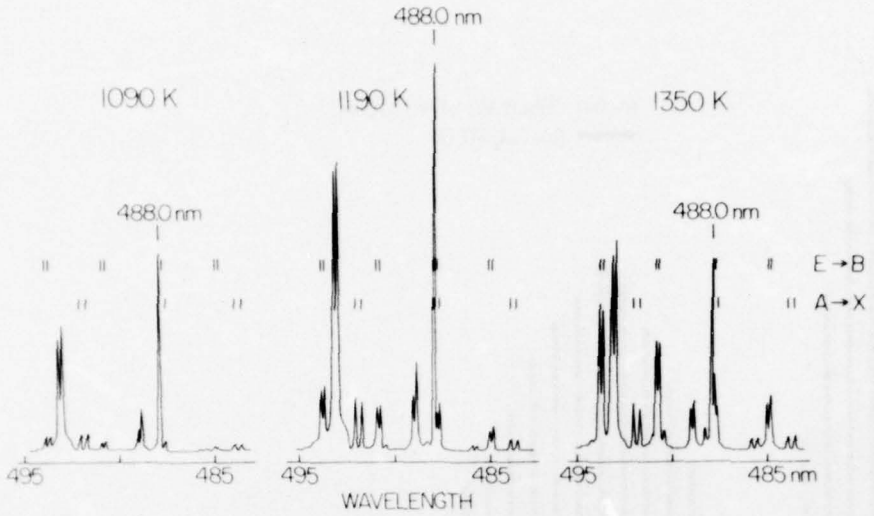

FIG. 6. Portion of the photoluminescence of Bi_2 excited by the 488.0 nm and 488.9 nm Ar^+ laser lines. The spectra are taken at 1099, 1190, and 1350 K, whereas all other experimental parameters kept constant. Two doublet photoluminescence series of different electronic transitions ($A-X$ and $E-B$) are indicated by lines, so that the change of relative intensities with temperature can be easily seen. The intensity scale of the spectra is different for different temperatures.

$$= \exp\left[-\frac{(E_a - E_b)}{k}\left(\frac{1}{T_0} - \frac{1}{T_1}\right)\right] , \qquad (9)$$

where $I(v'J', v''J'')$ is the intensity of a given line, T_0 and T_1 are the temperatures in °K of the system, E_a and E_b are the energies of the two vibrational–rotational levels of the electronic states a and b. From a semilogarithmic plot of $(I_a/I_b)_{T_0}/(I_a/I_b)_{T_1}$ versus $(1/T_0 - 1/T_1)$ the value $\Delta E = E_a - E_b$ can be obtained. Such a semilogarithmic plot in a case where the photoluminescence intensity of the $A-X$ system is compared with that of the $E-B$ system is shown in Fig. 7 where the error bars represent maximum deviations. The energy difference between the B state and the X state derived from such a plot properly normalized is $\Delta E = 5000\ cm^{-1} \pm 20\%$. The accuracy of the value ΔE may be increased by taking different pairs of doublets into account. However, the achievable accuracy is limited by the assumption that quenching and other collision induced effects are of minor importance while taking relative intensity data. The accuracy may be somewhat improved by knowing the number of Bi_2 molecules in a given state N_i as a function of pressure. From pressure dependence measurements we know that the $E-B$ intensity does not change very much with pressure, but the $A-X$ intensity does depend strongly on pressure.

Therefore, we have to correct in a first approximation only the $A-X$ intensity according to the changing density of Bi_2. The temperature T_0 is correlated to the Bi_2 vapor pressure maintained in the heat pipe according to $P_{Bi_2} = f(T)$. T_1 is a higher temperature, therefore $T_0/T_1 = \alpha$ is the correction factor for each ratio taken at T_0 and T_1.

The values obtained for the energy difference between the bottom of the X and B state potential curves is given in Table I. The uncertainty for this electronic term value T_e is mainly determined by errors introduced through temperature measurements and by errors connected with the measured intensity ratios. Electronic term values T_e obtained for the X' and A' state obtained by temperature dependence measurements are also given in Table I. The earlier work[3–5] on Bi_2 which has been done in absorption and emission was based on the assumption that X is the ground state and A the first excited state of Bi_2. Laser photoluminescence experiments[1] clearly show that these assumptions are not valid. We also find that the electronic state X' is 1500 $cm^{-1} \pm 800$ cm^{-1} lower in energy than the X state originally considered as the ground state of Bi_2.

IV. POTENTIAL CURVE DIAGRAM OF Bi_2

All the known information about the bismuth diatomic molecule is summarized in the potential curve diagram of Fig. 8, based on results of earlier work[3–5] on Bi_2 as well as on laser photoluminescence.[1] The po-

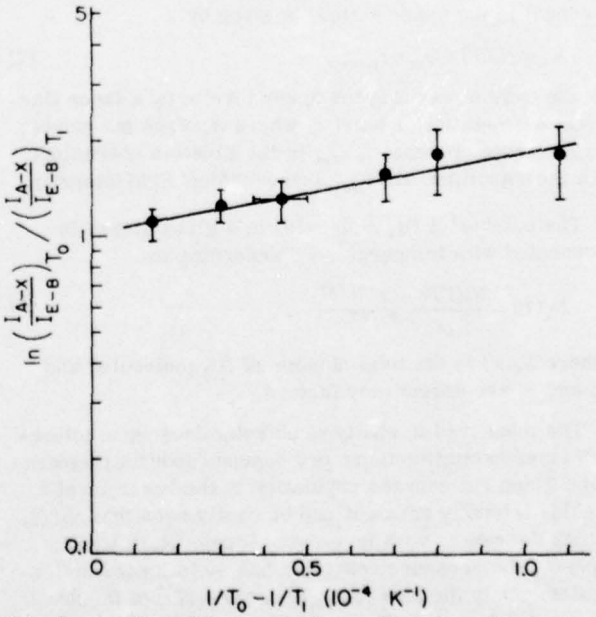

FIG. 7. Semilogarithmic plot of intensity ratios, obtained by temperature dependence measurements, from which the energetic position of an electronic state can be derived.

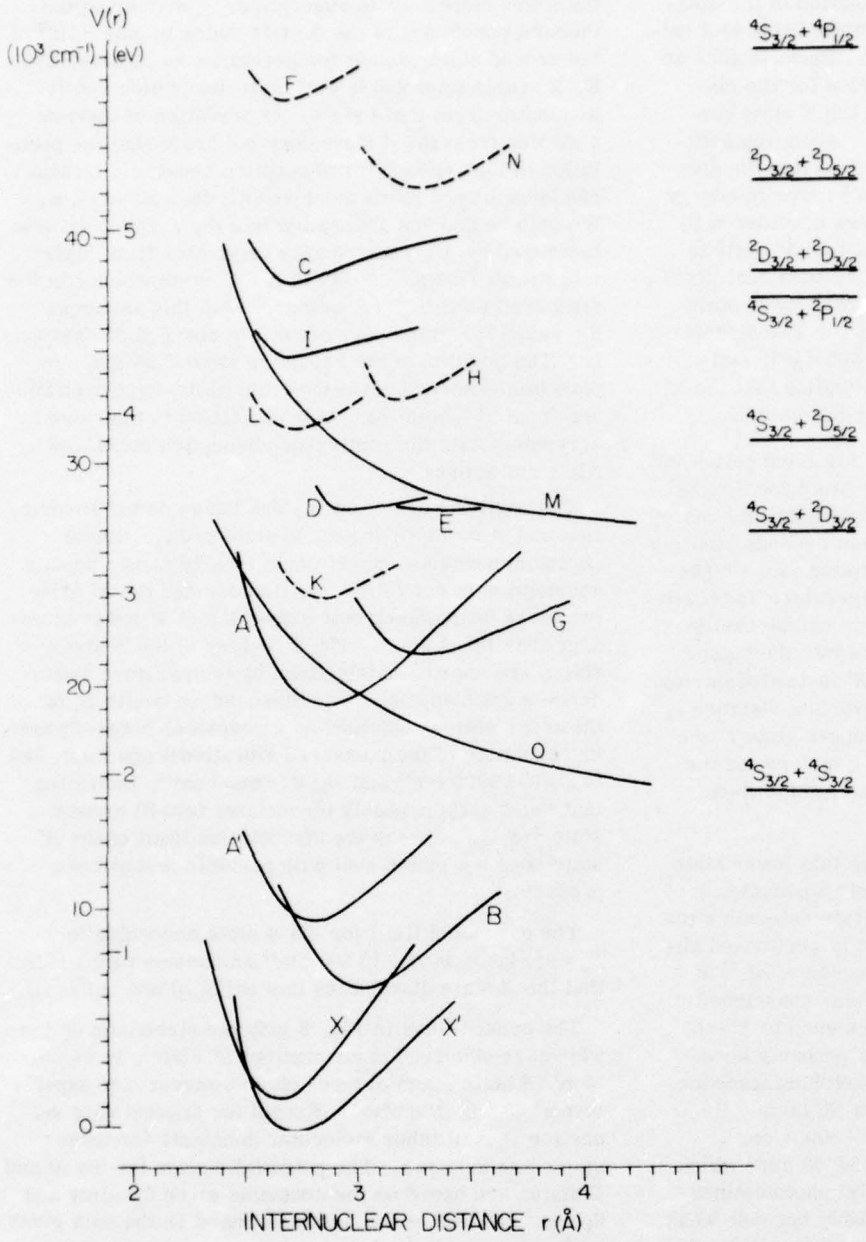

FIG. 8. Potential curve diagram of the diatomic bismuth molecule. The potential curves for the bound electronic states are calculated RKR potential curves (solid line) based on the molecular constants (Table I). Potential curves indicated by broken lines are only characterized by an approximate value for electronic energy T_e. Potential curves for the repulsive states are constructed using the available data. The equilibrium internuclear distances r_e, if not given by experimental data, are estimated from $r_e^2 \times \omega_e \approx \text{const.}$[13]

tential curves for the bound electronic states are calculated RKR potential curves (solid lines in Fig. 8) based on the molecular constants given in Table I. Potential curves indicated by broken lines are characterized by an approximate value for T_e. Potential curves for repulsive states are constructed using available data.[1,3] Energy positions of lower electronic states are obtained from temperature dependence measurements. For the higher electronic states D, G, and O, the value of T_e had to be changed by reanalyzing earlier data[3,5] in the light of laser photoluminescence information. Equilibrium internuclear distances r_e for most electronic states are estimated according to the empirical relation $r_e^2 \times \omega_e \approx \text{const.}$ This relation between r_e and ω_e holds fairly well for the different electronic states of the same homonuclear molecule.[13,14]

From rotational analysis of partially resolved bands as carried out by Åslund *et al.*,[4] rotational constants are known for the $A-X$ system and therefore r_e values may be estimated for the other electronic states.

Energy levels of the atomic states of Bi are taken from Ref. 15. Combinations of different Bi states are used as possible dissociation limits according to their energies and are given on the right-hand side of Fig. 8. The dissociation energy of Bi_2 is not very well known. Gaydon[16] gives a value of $D_0 = 1.85$ eV ± 0.1 for the X state whereas Rosen[17] gives $D_0 = 16500 \pm 500$ cm^{-1} (2.05 eV) for Bi_2. Recent mass-spectrometric work done by different groups[18] suggests $D_e = 15\,500$ cm^{-1} (1.92 eV) as the most likely value for the dissociation energy of Bi_2.

A graphical Birge–Sponer extrapolation of the measured vibrational spacings of the X state leads to a value of $D_e = 17500\ cm^{-1}$ for the X state. Because such an extrapolation usually gives a high value for the dissociation energy, it is believed that the X state dissociates into Bi ground state atoms. From temperature dependence measurements, we find that the electronic state X' is $1500\ cm^{-1} \pm 800\ cm^{-1}$ lower in energy than the X state which earlier workers considered to be the ground state. We believe that this X' state is more likely the ground state of Bi_2. Vibrational perturbations seen in the X state and in this lower state are further support for this conclusion. The dissociation energy of the X' state is $D_e = 14\,500\ cm^{-1}$, estimated according to $D_e = \omega_e^2/4\omega_e x_e$ indicating that the X' state also dissociates into Bi ground state atoms.

Within the framework of two very low lying states in Bi_2, an experimental observation of Almy and Sparks[3] can now be well understood. They found that the energy range of absorption in the A–X system depends strongly on temperature, whereas, the absorption into a higher state C is almost independent of temperature and much more intense. An explanation for this can be easily given by assuming that the absorption into the higher state C starts from the lower state X' instead of starting from the X state. Because the equilibrium distance r_e of the lower state X' and that of the upper state C are almost the same, the Franck–Condon factors for the C–X' system are more favorable than for the A–X system.

Almy and Sparks[3] did not recognize this lower state because the diffuse band heads in their absorption measurements did not allow an accurate determination of vibrational spacings. More recently performed absorption measurements by Topouzkhanian *et al.*[19] at low temperatures (1070 K) contain many unassigned band heads. Some of them can be assigned to $X' \rightarrow C$ absorption. This lower state X' has probably been observed earlier by Parys[20] in the photoluminescence of Bi vapor excited with the light of a Hg lamp. He photographed doublet series with $\omega_e'' = 309.1\ cm^{-1}$, which is about twice as big as $\omega_e'' = 154.29\ cm^{-1}$ which we obtained from laser excited doublet photoluminescence. Parys obtained this ω_e'' probably because weak Franck–Condon factors prevented the observation of every second transition. He found a difference in energy between the electronic states involved as $23\,092\ cm^{-1}$, close to the approximate value $T_e = 24\,000\ cm^{-1}$ derived from laser photoluminescence data. It is significant that Parys observed the $\omega_e'' = 309.1\ cm^{-1}$ photoluminescence series at temperatures as low as 770 K, whereas the $\omega_e'' = 173.2\ cm^{-1}$ photoluminescence was observed by him only at 1070 K and higher temperatures.

Another part of the absorption measurements by Almy and Sparks[3] also must be revised in the light of the laser photoluminescence experiments. Almy and Sparks claim that they measured discrete absorption from the A state into the D state and continuous absorption from A into a repulsive state O. From the close agreement of the vibrational spacings of their lower state with that of the A state it was concluded that the A state must be the lower state seen in absorption. Considering the thermal population of the A state which is only $\sim 10^{-9}$ of the ground state even at temperatures as high as 1270 K, it seems improbable that their absorption really originates from the A state. Observation of thermal emission from the A state does not prove that the population is high enough for absorption because emission can be observed much more readily than absorption. We believe that the absorption into the D and O state as measured by Almy and Sparks originates from higher vibrational levels ($v'' \sim 20$) of the X' state which fits the measured vibrational spacings. With this assumption the value T_e of the upper state D is changed dramatically. The position of the repulsive state O as given by photoluminescence resulting from white-light excitation and from 514.5 nm Ar^+ laser excitation is then also in agreement with the continuous absorption measured by Almy and Sparks.

The earlier work[3–5] on Bi_2 was based on the assumption that A is the first excited state of Bi_2. Laser photoluminescence experiments clearly show that this assumption is not valid. We find besides the X' state two more bound electronic states B and A' lower in energy than the A state. The T_e values of the B and A' states are approximately given by temperature dependence measurements. The dissociation limits D_e of these two states, obtained by a graphical Birge–Sponer extrapolation of the measured vibrational spacings, led to $D_e(B) = 9900\ cm^{-1}$ and $D_e(A') = 8900\ cm^{-1}$, indicating that the B state probably dissociates into Bi ground state atoms, whereas the dissociation limit of the A' state does not match well with possible dissociation products.

The estimated limit for the A state according to $D_e = \omega_e^2/4\omega_e x_e$ is $D_e = 13\,500\ cm^{-1}$ and seems to indicate that the A state dissociates into $Bi(^4S_{3/2})$ and $Bi(^2D_{5/2})$.

The broken lines in Fig. 8 indicate electronic states which are observed in absorption[3] (F state), in emission[5] (H state), and in laser photoluminescence experiments[1] (K, L, N states). Except for approximate values for T_e, all other molecular constants for these states are unknown. The potential curves for the M and C states are based on the constants given by Almy and Sparks[3] and that of the I state is based on the data given by Reddy and Ali.[5]

The electronic state G was observed by Reddy and Ali[5] in emission. They claimed that the lower state of this emission is the A state, because of close agreement of measured vibrational spacings with those of the A state. The G state also is observed in laser photoluminescence experiments[1] as the lower state of a doublet series with molecular constants given in Table I. However, the laser photoluminescence data do not support the conclusion of Reddy and Ali that the A state is the lower state observed in emission and the subsequent value of T_e for the G state. A Franck–Condon factor analysis shows that there is no overlap between low vibrational levels of the A and G state where, according to Reddy and Ali, most of the transitions should take place. Moreover, the $\omega_e x_e = 0.6\ cm^{-1}$ value for the A state as given by Reddy and Ali[5] from their analysis

of the $G-A$ emission does not agree with the value $\omega_e x_e = 0.32$ cm^{-1} obtained by several other groups[1,3] and also by Reddy and Ali[5] analyzing different emission systems. The constants[5] given $\omega_e = 132.3$ cm^{-1} and $\omega_e x_e = 0.6$ cm^{-1} for the lower state of the $G-A$ emission system would rather fit high vibrational levels ($v'' = 50$) of the X state, which have considerable Franck–Condon overlap with low vibrational levels of the G state. The value for T_e obtained assuming that high vibrational levels of the X state would be the lower part in the G emission system is 21 060 cm^{-1}, which is close to the value $T_e = 21\,400$ cm^{-1} derived from laser photoluminescence data.

The energy position $T_e = 21\,400$ cm^{-1} of the G state is based on the strong perturbation of the A state, seen in white-light photoluminescence[1] and in several $A-X$ laser photoluminescence series.[1] The RKR potential curve for the G state is based on the photoluminescence data given in Table I.

The E state is observed as the upper state of the $E-B$ photoluminescence whose line intensities were used (Sec. II) to derive E state molecular constants. The potential curve of this very shallow electronic state ($v' = 0$, 1, 2, and 3 are bound levels) is given only for $v' = 0$ and 1.

V. DISCUSSION OF THE ELECTRONIC STATES OF Bi_2

For the determination of the character of the electronic states a rotational analysis of the observed bands has to be carried out. This has been done only for the $A-X$ system of Bi_2 by Åslund *et al.*[4] who identified the electronic state A as $^1\Sigma_u^+$ [or O_u^+ in the notation of Hund's case (c)] assuming that the X state is the ground state of Bi_2. The configuration of the ground state of Bi_2, in analogy with the ground state configuration of N_2, P_2, ..., may be written as $\cdots(\sigma_g 6s)^2(\sigma_u 6s)^2(\sigma_g 6p)^2(\Pi_u 6p)^4$ which can give rise to only one molecular state $^1\Sigma_g^+$, as in N_2 and P_2.[13] Because of the increasing spin–orbit interaction for the heavier elements of the Group V (the fine structure splitting $^2D_{3/2}-^2D_{5/2}$ in atomic bismuth is 4019 cm^{-1} whereas it is only 8 cm^{-1} in atomic nitrogen), a Hund's case (c) description of the electronic states of Bi_2 becomes more appropriate. The electronic states in case (a) and case (c) description are readily correlated.[13] The $^1\Sigma^+$ becomes O^+, the $^3\Sigma^+$ becomes O^- and 1 and the regular $^3\Pi$ state is split into O^+, O^-, 1, and 2. The ground state $^1\Sigma_g^+$ of Bi_2 therefore becomes O_g^+.

Rotational analysis of the $A-X$ system[4] shows that $^1\Sigma-^1\Sigma$ is the transition involved. Because of the X state being the lowest energy state observed by Åslund *et al.*,[4] they assumed $^1\Sigma_g^+$ as the X state and consequently $^1\Sigma_u^+$ (O_u^+) as that of the A state. However, spectroscopic data and temperature dependence measurements of laser photoluminescence of Bi_2[1] as well as the experiments carried out by Parys[20] show that there is an electronic state X' lower in energy that the X state.

The doublet series observed in laser photoluminescence[1] and by Parys[20] suggest that the X' state has an O-type symmetry. Therefore we believe O_g^+ is the appropriate description of the X' state, since it is probably the ground state of Bi_2. If, however, the photoluminescence series with $\omega_e'' = 309.1$ cm^{-1} observed by Parys[20] belongs to an electronic state other than the X' state, it might be possible that this would be the ground state of Bi_2. Therefore, all the symmetry considerations and assignments should be considered preliminary.

The rotational analysis[4] and the doublet photoluminescence of the $A-X$ system show that there are O-type states involved. The fact that there are no transitions observed between the A state and the lower X' state is believed to be due either to the gerade character of the A state or to the $+\leftrightarrow-$ rule, because the selection rule $\Delta\Omega = 0, \pm 1$ and the Franck–Condon factors are favorable. If the A state has ungerade character, the X state must have gerade character, because of the $g \rightleftharpoons u$ restriction. The weak interaction between the X and the X' states, indicated by the small displacement of vibrational levels in both states, suggest that these two electronic states do not have different character. Therefore we believe $X(O_g^-)$ is the most appropriate description in Hund's case (c), because the interaction with the $X'(O_g^+)$ state would be stronger if X had O_g^+ symmetry. The symmetry of the A state is very probably O_u^-, which could be one of the components of $^3\Pi_g$. The dissociation energies $D_e(X') = 14\,500$ cm^{-1} and $D_e(X) = 17\,500$ cm^{-1}, obtained from Birge–Sponer extrapolations of the vibrational levels, indicate that the X' and X state dissociate into Bi atoms in the $^4S_{3/2}$ ground state. The possible molecular states arising from two ^4S atomic states are $^1\Sigma_g^+$, $^3\Sigma_u^+$, $^5\Sigma_g^+$ and $^7\Sigma_u^+$ which give in Hund's case (c) description $O_g^+(2)$; $O_u^-(2)$; $1_u(2)$; 1_g; 2_g; 2_u; and 3_u. The $^1\Sigma_g^+$ (O_g^+) state arises from the ground state configuration as described above. The $^3\Sigma_u^+$ becomes O_u^- and 1_u probably arises from the configuration $\cdots(\sigma_g 6s)^2(\sigma_u 6s)^2(\sigma_g 6p)^2(\Pi_u 6p)^3(\Pi_g 6s)$. The $^5\Sigma_g^+$ state belongs to a configuration of a higher excited state. However in Hund's case (c) description, the $^5\Sigma_g^+$ splits into O_g^+, 1_g, and 2_g, but because of the strong spin–orbit interaction in the heavy Bi_2 the O_g^+ state could be located at low energies. The components of the $^7\Sigma_u^+$ state are believed to lie at higher energies. Assuming that there is in Bi_2, even at strong spin–orbit interaction, still a correlation between the molecular states and the atomic states of the dissociation products, the X state best described having O_g^- symmetry could originate from $^3\Pi_g$ which probably arises from the configuration $\cdots(\sigma_g 6s)^2(\sigma_u 6s)^2(\sigma_g 6p)(\Pi_u 6p)^4(\Pi_g 6p)$. This result agrees with the known order of excited states[13,17] in N_2 and P_2 as the highest elements in the Group V. The first excited states in N_2 are $A^3\Sigma_u^+$ and $B^3\Pi_g$, while this order is changed in P_2 with $^3\Pi_g$ and than $^3\Sigma_u^+$ being the first excited states. A comparison of observed electronic term values T_e of the low-lying excited electronic states of the Group V diatomic molecules is given in Fig. 9, where straight line segments connect states believed to have the same symmetry. The energy of the electronic states T_e and the symmetry designation are taken from Ref. 13, 17, and 21. This comparison seems to indicate that the $^3\Pi_g$ molecular state is the first excited state of the Group V diatomic

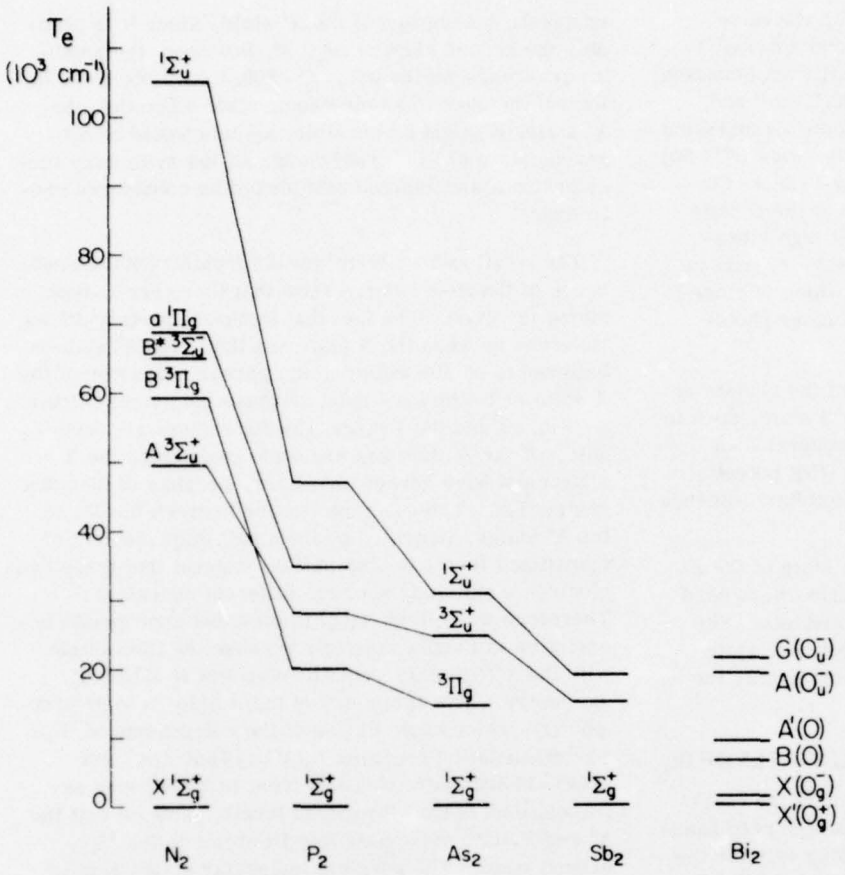

FIG. 9. Comparison of observed electronic term values, T_e, for the low-lying excited electronic states of the Group V diatomic molecules. Straight line segments connect states believed to have the same symmetry.

molecules (except N_2).

The character of the *B* state is most probably of *O* symmetry, because of the doublet series observed in laser photoluminescence.[1] However, it cannot be ruled out that the *B* state could have 1 symmetry with the *Q* component not being observed due to its weakness. The extrapolated dissociation energy $D_e = 9900\ \text{cm}^{-1}$ indicates that the *B* state dissociates into ground state Bi atoms. However, there is too little information available to decide upon the configuration from which this *B* state originates.

The *A'* state is the lower electronic state of a doublet series observed in laser photoluminescence,[1] therefore probably having *O*-type symmetry. The extrapolated dissociation energy $D_e = 8900\ \text{cm}^{-1}$ does not match closely with possible dissociation limits, but it might be correlated with $\text{Bi}(^4S_{3/2}) + \text{Bi}(^4S_{3/2})$. It is again not clear from which configuration this *A'* state arises.

The *A* state which is the upper electronic state of the *A–X* system has been observed in absorption,[3,4] emission[3,5] and laser photoluminescence.[1] A rotational analysis[4] and the arguements given above identify the *A* state as state as being of O_u^- symmetry. The estimated dissociation energy $D_e = 13\,500\ \text{cm}^{-1}$ closely agrees with the $\text{Bi}(^4S_{3/2}) + \text{Bi}(^2D_{5/2})$ dissociation limit. This dissociation scheme for the $A(O_u^-)$ state also was suggested by Almy and Sparks.[3]

Because of the strong interaction of the *G* and *A* states, observed in white-light photoluminescence[1] as well as in laser photoluminescence,[1] we believe the symmetry of the *G* state is the same as for the *A* state: O_u^-. The interaction between O_u^+ and O_u^- would be much smaller.[13] The *G* state is the lower electronic state of a doublet series observed in laser photoluminescence.[1] This also supports the designation O_u^- for the *G* state. A reanalysis of the emission observed by Reddy and Ali,[5] which involves the *G* state as the upper state, leads to the conclusion that this emission goes to high vibrational levels ($v'' = 50$) of the $X\ (O_g^-)$ state rather than to the *A* state, which agrees with the assumed O_u^- symmetry for the *G* state. From the estimated dissociation energy ($D_e = 4500\ \text{cm}^{-1}$) it seems likely that the *G* state dissociates into $\text{Bi}(^4S_{3/2})$ and $\text{Bi}(^2D_{3/2})$. Because the mainfold of molecular states correlated with $^4S_{3/2} + {}^2D_{3/2}$ is so large, no attempt has been made to ascribe the $G(O_u^-)$ state to a specific configuration.

The electronic state *E* is the upper state of the *E–B* doublet photoluminescence whose intensity pattern was used to establish the molecular constants of the *E* state. (Sec. II). The symmetry of the *E* state could either be 0 or 1, because a doublet photoluminescence series may arise from 0–0 and from 1–0 transitions,[13] the lower state *B* being of 0 symmetry. But the available data allow no determination of the character of this state.

Almy and Sparks[3] observed the electronic state *D* in

absorption ($D \leftarrow A$) as a strongly predissociated state. However, a reanalysis of these data in the light of the photoluminescence data seems to indicate that Almy's absorption into the D state originates from higher vibrational ($v'' \sim 20$) levels of the $X'(O_g^+)$ state. The repulsive state M, observed by Almy and Sparks in absorption, could be the state causing the predissociation of the D state. The available data do not allow any speculation about the character of the D state.

The electronic states K, L, and N are upper states of different electronic systems excited by the Ar^+ laser where doublet photoluminescence series occur and therefore having either 0 or 1 symmetry. Because the states C, F and H, I are observed in connection with states of 0 symmetry in absorption and emission, we believe these states have either 0 or 1 symmetry. Owing to the lack of rotational structure in most electronic transitions observed in Bi_2 there has been made no attempt to systematically classify and relabel the electronic states. There has been reported an unknown electronic system of Bi_2 by Singh *et al.*[22] They investigated the spectrum of BiCl by dissociating $BiCl_3$ in a discharge and observed in addition to the A–X system of BiCl about twenty new bands in the region 620–650 nm. The bands have been fitted into a Deslandre's table, the lower and upper state vibrational frequencies being $\omega_e'' = 103.2\ cm^{-1}$, $\omega_e' = 94.7\ cm^{-1}$, $\omega_e''x_e'' = 2.45\ cm^{-1}$ and $\omega_e'x_e' = 5.2\ cm^{-1}$ with $\nu_{00} = 15\,746.34$. Singh *et al.*[22] believe that the bismuth diatomic molecule is the emitter of these bands, because of the absence of any chlorine isotope effect and because of the vibrational frequencies for both the states are of the order of 100 cm^{-1} whereas bismuth halides and oxide correspond to much higher frequencies. However, the available data do not allow any determination of the energy position $V(r)$ of the lower electronic state and of the symmetry of states involved.

VI. ACKNOWLEDGMENTS

We want to thank Dr. Katsumi Sakurai for his continued interest and many helpful suggestions. Discussions with and critical comments from Dr. Brian G. Wicke have been of great value. One of us (Dr. G. Gerber) would like to thank the Deutsche Forschungsgemeinschaft for a fellowship.

*Work supported in part by Office of Naval Research, Contract No. N00014-69-A-0200-8013.

†Present address: Fakultät für Physik, Universtiy of Freiburg D 78 Freiburg, West Germany.

[1]G. Gerber, K. Sakurai, and H. P. Broida, J. Chem. Phys. **64**, xxxx (1976), preceding paper.

[2]W. Demtröder, M. McClintock, and R. N. Zare, J. Chem. Phys. **51**, 5495 (1969). K. Sakurai, S. E. Johnson, and H. P. Broida, J. Chem Phys. **52**, 1625 (1970).

[3]G. M. Almy, F. M. Sparks, Phys. Rev. **44**, 365 (1933). G. M. Almy, J. Phys. Chem. **41**, 47 (1937).

[4]N. Åslund, R. F. Barrow, W. G. Richards, and D. N. Travis, Ark. Phys. 30, 171 (1965).

[5]S. P. Reddy, M. K. Ali, J. Mol. Spectrosc. **35**, 285 (1970).

[6]R. Rydberg, Ann. Physik **73**, 376 (1931). O. Klein, Z. Physik **76**, 226 (1932). A. L. G. Rees, Proc. Phys. Soc. A **59**, 998 (1947).

[7]R. W. Nicholls and A. L. Stewart, "Allowed Transitions" in *Atomic and Molecular Processes*, edited by D. R. Bates (Academic, New York, 1962), Chap. 2.

[8]J. W. Cooley, Math. Compu. **15**, 363 (1961).

[9]B. G. Wicke, University of California, Santa Barbara (private communication). The authors wish to thank B. G. Wicke for making these programs available to us.

[10]R. N. Zare, J. Chem. Phys. **40**, 1934 (1964); R. N. Zare, University of California Radiation Laboratory Report UCRL-10925, 1963.

[11]J. L. Dunham, *Phys. Rev.* **41**, 721 (1932).

[12]J. I. Steinfeld, R. N. Zare, L. Jones, M. Lesk, and W. Klemperer, J. Chem. Phys. **42**, 25 (1965).

[13]G. Herzberg, *Spectra of Diatomic Molecules* (Van Nostrand, Princeton, 1950).

[14]R. T. Birge, Phys. Rev. **25**, 240 (1925). R. Mecke, Z. Phys. **32**, 823 (1925).

[15]C. E. Moore, Natl. Bur. Stand. (U.S.) Circ. **467** (1949).

[16]A. G. Gaydon, *Dissociation Energies and Spectra of Diatomic Molecules* (Chapman and Hall, London, 1968).

[17]B. Rosen, *Spectroscopic Data Relative to Diatomic Molecules, International Tables of Selected Constants* (Pergamon, New York, 1970).

[18]F. J. Kohl, O. M. Ury, and K. D. Carlson, J. Chem. Phys. **47**, 2667 (1967); A. K. Fischer, *ibid.* **45**, 375 (1966); R. F. Porter and C. W. Spencer, *ibid.* **32**, 943 (1960).

[19]A. Topouzkhanian, A. M. Sibai, and J. d'Incan, Z. Naturforsch. Teil A **29**, 426 (1974).

[20]J. Parys, Z. Physik **71**, 807 (1931); Acta. Phys. Pol. **1**, 93 (1932).

[21]J. Sfeila, P. Perdigon, F. Martin, and B. Femelat, J. Mol. Spectrosc. **42**, 239 (1972).

[22]J. Singh, K. P. R. Nair, and D. K. Rai, Spectrosc. Lett. **4**, 313 (1971).

CHEMICALLY REACTING BISMUTH AND NITROUS OXIDE IN A HEAT PIPE OVEN*

Katsumi SAKURAI and H.P. BROIDA
Department of Physics and Quantum Institute, University of California, Santa Barbara, California 93106, USA

Received 29 September 1975
Revised manuscript received 11 November 1975

The chemical reactions between bismuth and oxidants in a heat pipe oven are described. Strong chemiluminescence ($A\,^2\Pi_{1/2} \rightarrow X\,^2\Pi_{1/2}$) was observed in the reaction with N_2O and the vibrational temperature of the $A\,^2\Pi_{1/2}$ state was measured to be 3150 ± 300 K.

A recent preliminary study of the reaction of Ba and N_2O in a heat pipe oven has demonstrated the utility of such ovens for studies of chemical reactions between metals and oxidants. We have tested two different heat pipe configurations with chemical reactions of Bi and Bi_2 with oxidants.

One heat pipe consisted of a simple cross-shaped stainless steel pipe with a stainless steel wick in a 5 cm diameter [1] stainless tube. The other heat pipe was more complicated. Its shape was a double cross, consisting of 5 cm diameter stainless steel tubes, eight sets of 250 W heater elements, and additional cooling systems. Temperatures of the heat pipe oven were indicated by an alumel–chromel thermocouple attached directly to the outside surface of the oven (fig. 1). When the heat pipe is working properly, the temperature inside the heat pipe is in equilibrium at a pressure determined by Ar buffer gas pressure. Vapor pressures then are measured by a pressure gauge, and temperatures are obtained from vapor pressure versus temperature tables. 12.5 mm diameter quartz tubing was used to introduce microwave discharge products into the center of the metal vapor region, and 3 mm stainless steel tubing was used to introduce other reactants.

Laser induced photoluminescence of Bi_2 molecules [2] was used to determine the distribution of metal vapor along the pipe. Metal vapor existed only in the middle heating zone, and a very sharp boundary was observed between the metal and buffer gas

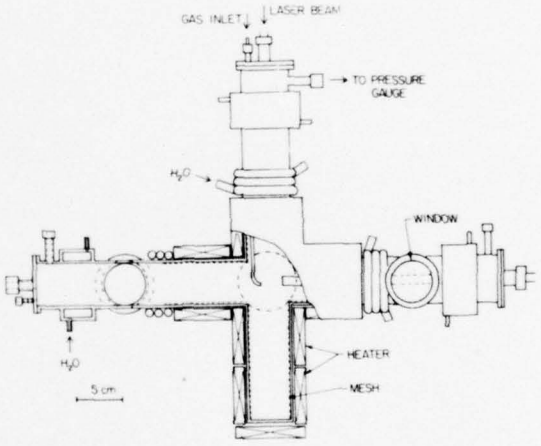

Fig. 1. Heat pipe oven.

zones. About 4 cm outside the sharp boundary, particles of bismuth were observed. The metallic particle region was about 4 cm long when the Bi_2 vapor region was 15 cm. Scattered light from these particles was completely plane polarized, indicating particle sizes much smaller than the wavelength of light [3]. Even when the buffer gas pressure was higher than the equilibrium vapor pressure and heat pipe action was not complete, there was a separation of the metal zone from the buffer gas zone. We believe that operation in this steady-state condition, without equilibrium heat pipe action but with a separation of the metal rich zone from the buffer gas zone, will be very useful for chemical reaction studies as well as for spectroscopic measurements.

* Work supported in part by Office of Naval Research, Contract No. N00014-69-A-0200-8013.

We have tried chemical reactions between bismuth and several oxidants such as O_2, discharged O_2, N_2O, and NO_2. During the chemical reaction, laser photoluminescence was used to detect changes in the concentration of Bi_2 as well as reactant products in the reaction zone. Oxidants were introduced into the middle of the heat pipe oven. No visible chemiluminescence was observed in the reaction with O_2 or NO_2, but the laser induced photoluminescence showed that Bi_2 was totally consumed. In the reaction between discharged oxygen and bismuth, a faint yellow glow was observed in the reaction zone. It is so faint that spectra has not been obtained because the background radiation from the hot walls is so large. The shape of the flame was confined in a small cone, indicating that the reaction is fast.

Above 1300 K, the thermally excited $A \rightarrow X$ transition of Bi_2 also was observed. The vibrational distribution of the thermally excited $A\,^1\Sigma_g^+$ state was

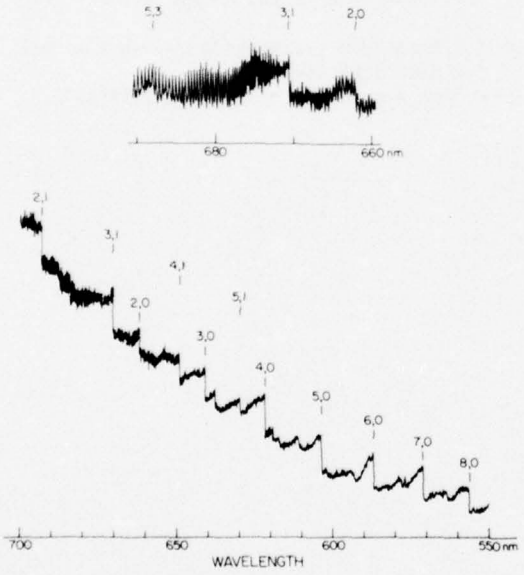

Fig. 2. BiO ($A\,^2\Pi_{1/2} \rightarrow X\,^2\Pi_{1/2}$) chemiluminescence spectra from the reaction of bismuth and N_2O in a heat pipe oven at a temperature near 1050 K estimated from the vibrational distribution of Bi_2 in the A state (see text), and a pressure of 7 torr. Thermal radiation from the walls is very strong at longer wavelengths. The lower spectrum was taken at 0.2 nm resolution, while the upper one was 0.075 nm. No correction has been made for the wavelength response of the GaAs photomultiplier.

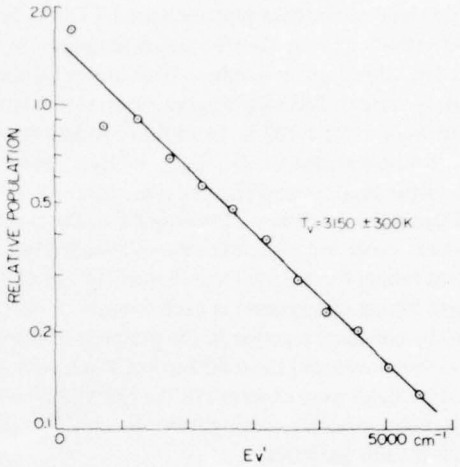

Fig. 3. Vibrational population distribution in the $A\,^2\Pi_{1/2}$ state of BiO produced from the reaction of bismuth and N_2O. Vibrational populations (v') were obtained by averaging over the observed v'' progression. Franck–Condon factors were calculated by the RKR method using molecular constants obtained by Barrow et al. [4]. The total pressure was 7 torr and the temperature reading of the thermocouple outside the oven was 1350 K.

determined by the measured intensity distribution and calculated Franck–Condon factors [4]. The vibrational temperature was found to be 1050 ± 150 K. This temperature, as expected, was somewhat lower than that measured by the outside thermocouple (1320 K). Total pressure was 7 torr.

Relatively strong chemiluminescence also has been observed in the reaction with N_2O at a buffer pressure of 7 torr. The shape of the flame was round, and the flame spread within the oven indicating a slow reaction. During the reaction, slow pumping was needed to maintain a constant pressure. Flow rates of N_2O and buffer Ar gas were estimated to be 10^{18}–10^{19} molecules/s. The N_2O flow was less than one third of the total flow.

In the reaction with N_2O the chemiluminescence produced the $A\,^2\Pi_{1/2} \rightarrow X_1\,^2\Pi_{1/2}$ system of BiO (fig. 2) with the $v'' = 0$ progression observable from $v' = 2$ to 10 and the $v'' = 1$ progression from $v' = 1$ to 5. The vibrational intensity distribution is slightly different from spectra obtained previously by microwave discharges [4,5]. A rotational temperature of 1200 ± 150 K was estimated from the rotational intensity distributions when the temperature of the

outside wall of the heat pipe measured 1320 K, in good agreement with the vibrational temperature of Bi_2. The vibrational population distribution of the $A\,^2\Pi_{1/2}$ state of BiO (fig. 3) gave a vibrational temperature of 3150 ± 300 K. In addition to BiO emission, strong emission of the $^2D_{3/2} \rightarrow {}^4S_{3/2}$ transition of the Bi atom at 875.5 nm was observed.

During the reaction of discharged O_2, the stainless steel mesh and gas inlets were oxidized. Even the quartz tubing for the inlet was "eaten" (1 cm of quartz tubing disappeared in each 5 hours of operation) by chemical reaction in the presence of bismuth. At excess pressures (15 to 30 torr) of N_2O, soot-like small particles were observed in the chemiluminescent region, possibly coming from the oxidation of small metallic particles.

In the reaction of Ba and N_2O [1], metal is supplied by evaporation, while oxidant is supplied from outside the metal vapor region. Metal oxides and other reactant products condense or are trapped in the pipe and pressure remains constant. Unfortunately, the bismuth and oxidant reaction does not fit this mode of operation; it is necessary to remove excess oxidant and products to maintain a stable pressure. By pumping, a steady-state condition is established. In this pumping mode, quantitative studies of chemical reaction rates and photon yield will be difficult. Moreover, in the present system, both oxidant and the metal inlet tube are heated to the oven temperature. Thus, a large fraction of reacting oxidant molecules were vibrationally excited, since kT is nearly 1000 cm^{-1}, and some oxidant may be decomposed before entering the reaction zone. Another difficulty of the present system is the strong background thermal emission from the walls and from the metal vapor itself.

References

[1] M.M. Hessel, R.E. Drullinger and H.P. Broida, J. Appl. Phys. 46 (1975) 2317;
D.J. Eckstrom, S.A. Edelstein and S.W. Benson, Stanford Research Institute Report.
[2] G. Gerber, K. Sakurai and H.P. Broida, J. Chem. Phys. (1975), submitted for publication.
[3] D.M. Mann and H.P. Broida, J. Appl. Phys. 44 (1973) 4950.
[4] R.F. Barrow, J.M. Gissane and D. Richards, Proc. Roy. Soc. A300 (1967) 469.
[5] O. Scari, Acta. Phys. Acad. Sci. Hung. 6 (1955) 73.

Journal of Crystal Growth 33 (1976) 353–355

OBSERVATION OF HOMOGENEOUSLY NUCLEATED FINE PARTICLES OF PbI_2 BY ELECTRON MICROSCOPY AND LIGHT SCATTERING *

J.D. EVERSOLE, K. SAKURAI and H.P. BROIDA
Department of Physics and Quantum Institute, University of California at Santa Barbara, Santa Barbara, California 93106, USA

Received 15 October 1975

Homogeneous nucleation of PbI_2 particles with diameters less than 10 nm has been observed in N_2 gas by white light scattering. The relative intensity of the scattered light has been measured as a function of wavelength. Particle sizes and shapes have been determined by electron microscopy.

Size effects of elementary excitations in solids are expected when crystalline sizes become extremely small, i.e., less than a few nm. Some earlier experiments have been made with homogeneously nucleated metallic particles [1–4]. This report describes preliminary studies on very fine crystals of PbI_2.

Homogeneous nucleation of PbI_2 crystals was obtained in flowing N_2 at pressures from 0.1–2 kPa (0.75–15 torr). Vapor from reagent grade PbI_2 in an alumina crucible heated to about 600 K was entrained by the N_2 flow. Since the N_2 gas was in contact with room temperature walls, the vapor was cooled and PbI_2 particle nucleation occurred when the supersaturation ratio was sufficiently large. This method of particle nucleation and the apparatus have been described for the work with pure metals [3–5].

Samples of "floating" particles were collected on standard microscope grids exposed to the gas flow downstream from the region where particles were formed. Electron microscope pictures of these particles show individual particles with diameters less than 8 nm. Fig. 1 shows examples of individual particles. Shapes are not well defined but the sizes are quite uniform, between 10 and 30 nm. Occasionally, under conditions of low pressure, particle samples reveal a faint hexagonal outline on which smaller par-

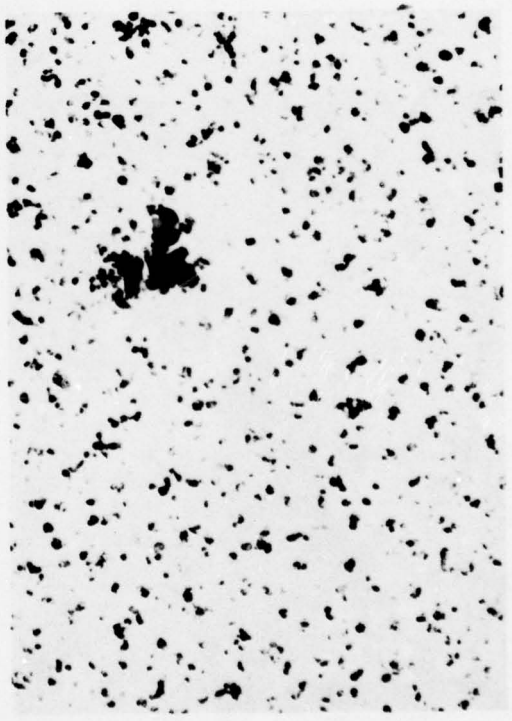

Fig. 1. Example of individual "floating" PbI_2 particles with irregular shapes but a sharp size distribution centered around 20 nm diameter (20,000 × plus photographic enlargement).

* Work supported in part by National Science Foundation Grant NSF-MPS74-22174 and Office of Naval Research Contract No. N00014-69-8013.

ticles can be seen. It is possible that the hexagonal shape is an artifact of the collection process rather than an indication of a "floating" particle. It is generally difficult to determine to what extent growth and movement take place on the grid surface rather than in the vapor phase.

Unlike pure metals [4], PbI_2 particles tend to clump or coagulate into long chains and lacey networks as shown in fig. 2. Higher magnification than fig. 2 indicates that these chains consist of small particles linked together. Presumably the chains are formed on the deposition grids. Electron diffraction photographs of these samples show a ring pattern which have the same diameter as diffraction patterns obtained from bulk material, indicating that the small particles have the same crystal structure.

Light scattering from "floating" particles was observed at right angles to the flow direction and to a xenon-arc white light source. The scattered light from fine particles appeared blue or bluish grey; larger par-

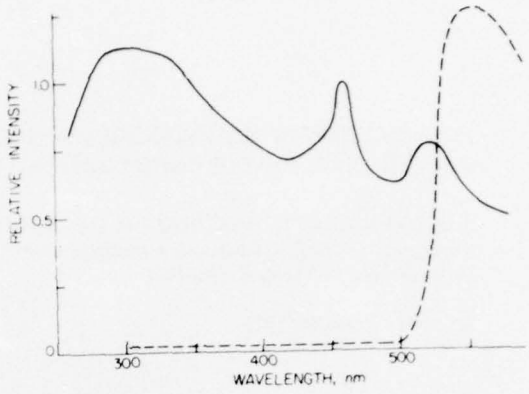

Fig. 3. Light scattering at 90° to the incident light from fine particles at a pressure near 1/3 kPa (2.5 torr) compared to scattering from bulk material collected on the chamber walls. The relative intensity has been corrected for instrument response and light source characteristics.

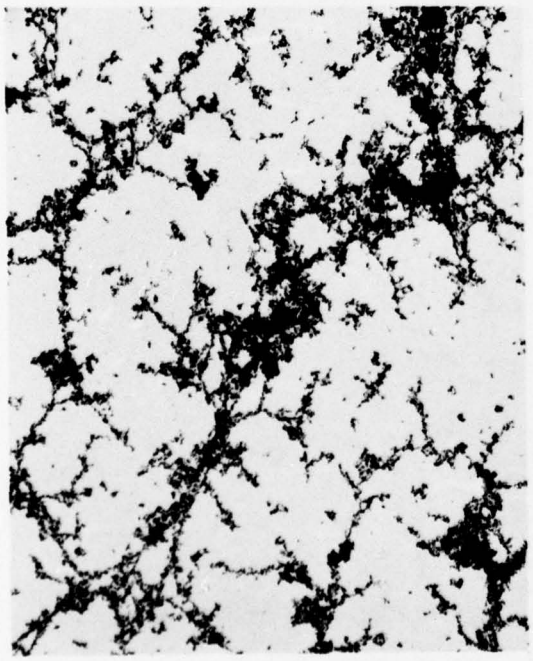

Fig. 2. Lacey networks and long chains are formed by smaller particles as seen at low magnification (5000 × plus photographic enlargement).

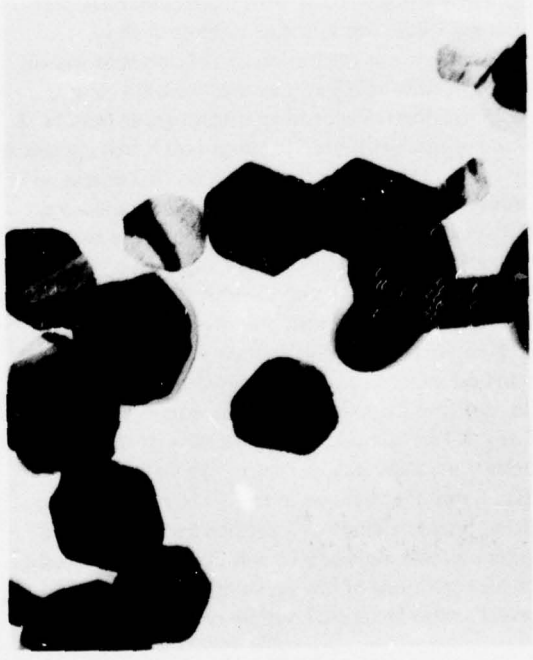

Fig. 4. An example of hexagonal platelets collected from the chamber walls. These hexagons are approximately 130 nm on a side (40,000 × plus photographic enlargement).

ticles trapped outside the flowing gas caused a wide variety of colored patterns. The blue light was totally plane-polarized indicating that the maximum particle size was less than the wavelength of light. With increasing N_2 gas pressure the intensity of scattered light increased but it is not known if the increase is caused by greater numbers or greater size of the particles.

A 3/4 monochromator with 1 nm resolution was used to measure the relative spectral scattering at 90° to the incident light. Neither phosphorescence nor photoluminescence were detected; only elastic scattering at the incident wavelength was observed. Fig. 3 shows the relative scattering from "floating" particles and, for comparison, from material collected on the walls. Small shifts in peak heights and positions were noted under different conditions but no consistent pattern was found. We were not able to associate any of observed structure to known absorption or photoluminescence of PbI_2.

Deposits of PbI_2, 1–4 mm thick, covered most of the interior of the vacuum chamber in 1 to 4 h of operation. This "wall material" was most likely formed from "floating" particles but might have some component of single molecule accretion. Its color was similar to that of bulk PbI_2, but its density was considerably less, appearing to be a finely divided powder. The thickness of the wall material decreased in a period of several days after exposing to atmosphere conditions. Low magnification photographs obtained with a scanning electron microscope suggest that macroscopically the wall material is spongy. Higher magnification photographs of the wall material obtained with transmission electron microscopy shows clearly defined hexagonal platelets with diameters as small as 40 nm (fig. 4). Electron diffraction patterns of this material are consistent with X-ray diffraction patterns of which showed peaks corresponding to the (001) and (110) planes of bulk PbI_2 crystals.

References

[1] K.A. Kimoto and I. Nishida, Japan. J. Appl. Phys. 6 (1967) 1047.

[2] K. Komoto, Y. Kamiya, M. Nonoyama and R. Uyeda, Japan. J. Appl. Phys. 2 (1963) 702.

[3] D.M. Mann and H.P. Broida, J. Appl. Phys. 44 (1973) 4950.

[4] J.D. Eversole and H.P. Broida, J. Appl. Phys. 45 (1974) 596.

[5] J.B. West, R.S. Bradford Jr., J.D. Eversole and C.R. Jones, Rev. Sci. Instr. 46 (1975) 164.

CHEMILUMINESCENCE OF CaH AND AlH IN THE REACTION OF THE METAL ATOMS AND FORMALDEHYDE*

K. SAKURAI, A. ADAMS and H.P. BROIDA
Quantum Institute and Physics Department, University of California, Santa Barbara, Santa Barbara, California 93106, USA

Received 17 December 1975

Chemiluminescence from the reaction of calcium and aluminum with various hydrogen containing compounds in a flowing gas system and in a heat pipe oven are described. Red chemiluminescence of CaH was observed in the reaction of calcium, and weak chemiluminescence of AlH was seen in the reaction of aluminum with formaldehyde (H_2CO). It is proposed that a reaction between metal atoms and formaldehyde may be used as a source of diatomic metallic hydrides.

Diatomic metallic oxides and halides have been well studied in various types of reactions [1,2]. Although metallic hydrides are very important in the study of stellar atmospheres, very few sources of metallic hydrides with high spectral purity have been studied in detail in the laboratory. Both flow systems [3] and heat pipe ovens [4] have proved to be useful for the study of reactions of some metal vapors with a variety of gaseous chemicals. This report describes the production of diatomic metallic hydrides in these sources.

The flow system [3] consisted of 10 cm diameter stainless steel tubing in the shape of a double cross. A heatable alumina crucible for the calcium, along with an argon (carrier gas) inlet was placed in the bottom section of the tubing. Through one of the horizontal arms of the double cross, a stainless steel, heatable reactant gas inlet was positioned over the center of the crucible. The remaining four arms were used for pumping and observation. Carrier gas pressures were between 0.4 and 15 torr. The inlet nozzle of H_2CO gas was heated to 1300 K by a tungsten heater.

The heat pipe oven [4] was a simple, horizontally oriented, cross-shaped stainless steel pipe of 5 cm diameter containing a wick of stainless steel wire mesh. Argon was introduced as a buffer gas to produce a well-defined region of metallic vapor in the heated part of the cross. Reactive gases were introduced into the metal vapor region via either stainless steel, quartz or alumina (Al_2O_3) tubing. Usual operating pressures were between 1 and 10 torr and temperatures between 1080 and 1300 K. Background thermal radiation from the heat pipe was relatively large.

Table 1 lists several metallic-hydride binding energies and some dissociation reactions of hydrogen containing compounds which we tried. Formaldehyde is the simplest, weakly bonded hydrogen compound that we used. Paraformaldehyde, heated to 110°C was pyrolyzed as the source of formaldehyde.

Table 1
Dissociation energy of hydrogen bond

Reaction	Endothermic energy (eV)
$CaH \rightarrow Ca + H$	2.40
$AlH \rightarrow Al + H$	2.90
$H_2CO \rightarrow H + HCO$	3.25
$HCO \rightarrow H + CO$	1.21
$H_2 \rightarrow H + H$	4.47
$NH_3 \rightarrow NH + H$	4.59
$NH_2 \rightarrow NH + H$	3.85
$NH \rightarrow N + H$	3.67
$H_2O_2 \rightarrow H + HO_2$	3.83

* Work supported in part by Office of Naval Research, Contract No. N00014-69-A-0200-8013.

H_2, discharged H_2 ("active hydrogen") and formaldehyde were used as reactant gases in the heat pipe. As expected, (table 1), no chemiluminescence appeared with either H_2 or discharged H_2. The addition of formaldehyde to the calcium vapor in the heat pipe produced red chemiluminescence with emission mainly from CaH and CaO [5,6]. Weak CaOH emission was observed. The observed CaH emission systems were $A\,^2\Pi-X\,^2\Sigma$ (692 nm), $B\,^2\Pi-X\,^2\Sigma$ (639 nm) and $E\,^2\Pi-X\,^2\Sigma$ (490 nm) with intensity ratios of approximately 1000:100:5.

CaO emission was observed from the $A\,^1\Sigma-X\,^1\Sigma$ system in the near infrared between 700 and 920 nm. In addition strong band systems were seen in the orange (580–650 nm) and green (540–580 nm). These bands have been attributed to CaO, but it appears that the emitter is a polyatomic oxide, such as Ca_2O_2 and partly CaOH [7]. We cannot positively identify all of the orange band systems, but relative strengths of various parts of the bands are dependent on the concentrations of Ca and H_2CO and on the temperature.

In the flow system NH_3, H_2O_2 and H_2CO were tried. There was no chemiluminescence from the reaction of NH_3 with Ca. Only CaO and CaOH were observed in the reaction of H_2O_2 with Ca. With heated formaldehyde (1200–1300 K), CaH and CaO again were observed. Only the $A\,^2\Pi-X\,^2\Sigma$ and $B\,^2\Pi-X\,^2\Sigma$ systems of CaH were observed. The spectrum was similar to that obtained in the heat pipe oven, except that there was an interesting temperature effect (see fig. 1). At low temperatures of the crucible and reactant gas inlet, no CaO $A\,^1\Sigma-X\,^1\Sigma$ emission was observed and the strength of the main CaH system, $A\,^2\Pi-X\,^2\Sigma$, near 692 nm, was weak in relation to the complex orange system of calcium oxide around 625 nm. At high temperatures, red and infrared bands of the A–X system of CaO became prominent and the strength of CaH $A\,^2\Pi-X\,^2\Sigma$ system increased in relation to the orange system.

To test the generality of the reaction, aluminum with heated formaldehyde was tried in the flow system. The $A\,^1\Sigma-X\,^1\Sigma$ system of AlH, but no emission from AlO, was observed.

We would like to propose a possible mechanism of chemiluminescence between metal atoms and H_2CO. As shown in table 1, reaction between Ca and ground state H_2CO does not occur since the reaction

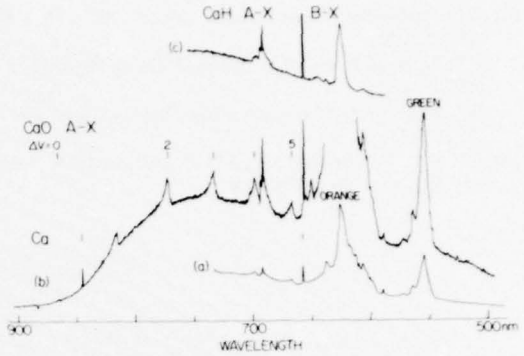

Fig. 1. CaH chemiluminescence in a flow system. The top spectrum was taken at relatively low nozzle temperature of H_2CO. Note the lack of CaO $A\,^1\Sigma-X\,^1\Sigma$ emission and the relative weakness of the CaH system in relation to the complex orange band systems. The middle and bottom spectra were taken at high nozzle temperature and higher density of Ca atoms. Relatively strong CaO $A\,^1\Sigma-X\,^1\Sigma$ was observed. The band shape of orange band is quite different from that at low temperature. Most part of continuum is due to thermal background emission from heater.

is about 0.85 eV endothermic. When stretching vibrations of CH bond are excited thermally to have energy greater than 0.85 eV ($v \geqslant 6$), the reaction becomes exothermic. H_2CO molecules heated to 1300 K have an average energy near 0.1 eV. At this temperature, an order of 10^{-5} of the H_2CO molecules have enough energy (0.85 eV) for the reaction with Ca. H_2CO molecules excited vibrationally in high CH stretch modes possibly initiate the reaction. The reaction between metal and HCO produced from the reaction between the metal and H_2CO, or possibly produced from thermal decomposition, may be responsible for visible chemiluminescence since the reaction is more energetically favorable (about 1.2 eV).

We want to thank Dr. G. Taieb for his continued interest and early assistance in obtaining spectra.

References

[1] C.J. Hsu, W.D. Krugh, H.B. Palmer, R.H. Obenhauf and C.F. Aten, J. Mol. Spectry. 43 (1974) 273;
R.J. Dagdigian, H.W. Cruse and R. Zare, J. Chem. Phys. 62 (1975) M4;
J. West and H.P. Broida, J. Chem. Phys. 62 (1974) 2566;
D.J. Eckstrom, S.A. Edelsten and S.W. Benson, J. Chem. Phys. 60 (1974) 2930.

[2] R.C. Oldenberg, J.C. Gole and R. Zare, J. Chem. Phys. 60 (1970) 4032;
R.S. Bradford Jr. and H.P. Broida, J. Chem. Phys. 62 (1975) 2060;
D.J. Wren and M. Menzinger, Chem. Phys. Letters 20 (1973) 471.
[3] J.B. West, R.S. Bradford Jr., J.D. Eversole and C.R. Jones, Rev. Sci. Instr. 46 (1975) 164.
[4] M.M. Hessel, R.E. Drullinger and H.P. Broida, J. Appl. Phys. 46 (1975) 2317.
[5] R.W.B. Pearse and A.G. Gaydon, The identification of molecular spectra (Wiley, New York, 1963).
[6] B. Rosen, Table Internationals Constantes Selectionés, 17 Données Spectroscopique Relatives on Molécules Diatomique (Pergamon Press, New York, 1970).
[7] B. deB. Darwent, Bond Dissociation Energies in Simple Molecules, NBS National Standard Reference Data, NSRDS-NBS-31 (1970).

Laser photoluminescence of calcium molecules*

Katsumi Sakurai† and H. P. Broida

Department of Physics and Quantum Institute, University of California, Santa Barbara, California 93106
(Received 12 March 1976)

Calcium diatomic molecules were produced in a heat-pipe oven at temperatures from 1000 to 1200 K. Photoluminescence of Ca_2 has been studied with various laser sources and with white light. Discrete, sharp line spectra are attributed to known bound states of Ca_2. A broad continuum emission with an oscillatory intensity distribution is associated with emission to the repulsive part of the lower state. A weak continuum emission to another repulsive state also has been observed. The observed strong emission from the atomic resonance lines at 422.7 and 657.3 nm probably is caused by dissociation of excited Ca_2 molecules. The laser-excited photoluminescence experiments suggest that the ground state of Ca_2 is repulsive and that the lowest observed bound state of Ca_2 correlates with the ^1P atomic state.

I. INTRODUCTION

Recently, homonuclear diatomic molecules of group IIa in the periodic table of elements, Be_2,[1] Mg_2,[2,3] and Ca_2,[4,5] have been observed by absorption spectroscopy in the gas phase[2,4] and in solid matrices at low temperature.[1,3,5] From simple orbital theory, these molecules are considered to be van der Waals molecules in the ground electronic state since the molecular electron configuration has an equal number of bonding and antibonding electrons.[6,7] No regular chemical bond would be expected and, except for the van der Waals interaction, the ground state would be repulsive.

We have studied photoluminescence of Ca_2 excited by several laser lines between 458 and 660 nm at temperatures from 1000 to 1200 K. Photoluminescence spectra show discrete emission identified as the previously reported $A\,^1\Sigma_u^+ - X\,^1\Sigma_g^+$ transition,[4] overlapping oscillatory continuum emission identified as transitions to the repulsive part of the lower state, the atomic calcium resonance lines at 422.7 and 657.3 nm, and other Ca atomic lines. These observations strongly support the view that ground state atoms do not form stable diatomic molecules and that bound molecules are formed only in electronically excited states.

II. EXPERIMENTAL

Calcium vapor was produced in a heat-pipe oven[8] using a horizontally oriented, cross-shaped stainless steel pipe of 5 cm diameter containing a stainless steel wick.[9,10] Argon, or at times helium, was introduced at pressures from 1 to 10 torr as a buffer gas. A well-defined region of metal vapor was observed by laser photoluminescence in the heated section of the cross. Most experiments were carried out with the buffer gas pressure exceeding the Ca vapor pressure at the given oven temperature. Under these conditions there was a mixture of Ca vapor and buffer gas in the observation region. Partial pressures of Ca were determined by measured oven temperatures.

Temperature was monitored by a chromel–alumel thermocouple attached to the outside wall of the heated cross. The thermocouple reading was calibrated at the melting point of calcium inside the cross; agreement was within the experimental error of ± 3 K. An additional estimate of the difference between thermocouple readings and gas temperatures inside the oven was obtained from measurements of vibrational temperatures of CaCl, a trace impurity. Thermally excited CaCl emission of the $A\,^2\Pi_{1/2} - X\,^2\Sigma^+$ and $B\,^2\Sigma^+ - X\,^2\Sigma^+$ systems gave vibrational population temperatures agreeing with the thermocouple temperatures to ± 30 K.

It should be noted that when the oven was operated in the normal mode for a heat-pipe oven with buffer gas pressure equal to the calcium pressure,[8] solid calcium crystals grew rapidly from the walls at the hot-cold transition region. This crystalline deposit formed a solid, thin (~1 mm) diaphragm completely closing the optical paths in less than an hour.

Various lines of an Ar^+ laser (Table I) were used to excite photoluminescence. In addition, some exploratory experiments used a cw tunable rhodamine B dye laser pumped by all lines of a 4 W Ar^+ laser; the width

TABLE I. Photoluminescence of molecular calcium (Ca_2) excited by Ar^+ laser line.[a]

Laser wavelength (nm)	Main transitions: Excited v'	v''	Normalized integrated intensities of emission: Molecular[b] Continuum	Discrete	Atomic[c] 422.7 nm	657.3 nm
528.7	7,4,2	2,1	650	200		0.4
514.5	4,3	2,0	550	200	100	0.3
501.7	7	0	200	100	400	1.0
496.5	11,10	3,5	650	300	500	1.2
488.0	12	1	650	350	600	1.3
476.5	16,17	0,2	850	400	1 900	1.6
472.7	18	1	450	350	3 500	1.6
465.8	22	2	150		8 500	
457.9	29	3	100	100	13 000	2.2
454.5	Very weak				17 000	

[a] A blank indicates that the emission was so weak that measurements of quantitative data were not made.

[b] Integrated intensity was estimated from the spectral area without correcting for instrumental response. The lack of resolution caused some uncertainty in separating continuum from discrete spectra. Data were taken with lock-in detection. Intensities are normalized to unit power excitation. The accuracy of measurement is ± 50%.

[c] Integrated intensities of the self-reversed line at 422.7 nm were estimated as follows. Peak height intensity was determined by measuring the intensity distribution at the tail of the Lorentzian line shape, $I\alpha(\Delta\omega)^{-2}$, and by extrapolating to the assumed linewidth of 0.1 cm^{-1}; integration was over the entire observed emission.

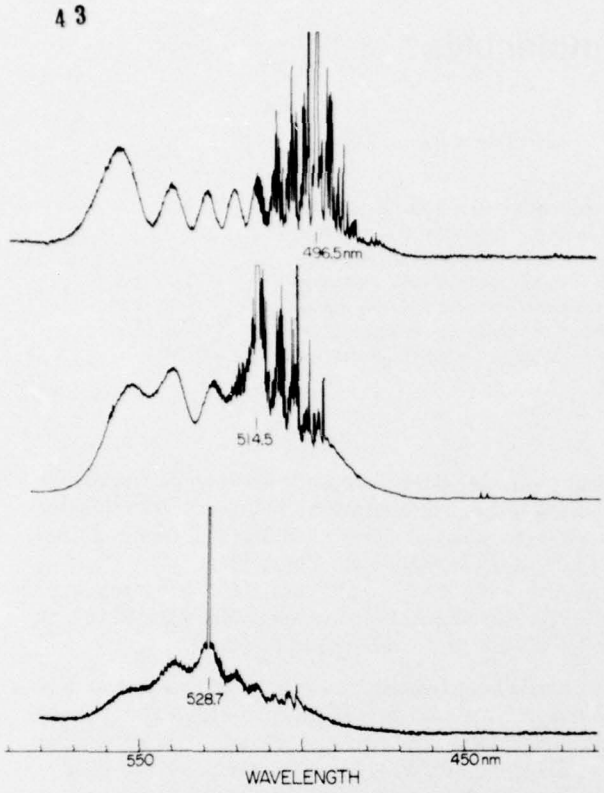

FIG. 1. Laser photoluminescence spectra of Ca_2 with 0.1 nm resolution. Laser power was 0.52, 3.3, and 1.2 W at 528.7, 514.5, and 496.5 nm, respectively. In addition to the discrete and continuum emission from Ca_2, Ca atomic emission can be seen at 560, 445, 430, and 423 nm. Above 540 nm, there is some small background radiation from the heat pipe. The oven temperature was about 1070 K, corresponding to an equilibrium Ca vapor pressure of 0.67 torr; the Ar pressure was 3 torr.

at half-maximum intensity of this laser was 0.05 nm. Photoluminescence also was obtained with continuum emission between 250–1000 nm from a 150 W xenon arc lamp. A tungsten lamp was used for absorption measurement. Emission and absorption spectra from 400 to 800 nm were recorded using a $\frac{3}{4}$ m grating monochromator with photoelectric detection. Phase-sensitive detection with a lock-in amplifier was used to measure weak photoluminescence obscured at longer wavelengths by strong thermal radiation from the oven walls.

III. OBSERVATIONS

A. Molecular emission

Photoluminescence spectra of Ca_2 (Figs. 1–3) excited by laser lines are not like the usually observed photoluminescence spectra of diatomic molecules.[9,10,12–15] In addition to the usual discrete, sharp line emission, there is broad continuum emission with an oscillatory intensity distribution (Table II). No small scale structure was observed in the continuum emission even with a resolution of 0.02 nm. Near the laser excitation lines, the discrete spectra are very complicated but become progressively simpler in appearance at both longer and shorter wavelengths (Fig. 3). Discrete spectra end abruptly at wavelengths longer than the excitation line and cover approximately ± 500 cm^{-1}. Complete rotational assignments of these lines was not possible because of the complexity, the lack of resolution, and the very small rotational constants of Ca_2.[4] Tentative vibrational assignments are included in Table I.

The oscillatory, continuum spectra show a regular change of pattern with decrease of the excitation wavelength. With decreasing excitation wavelength, or increasing energy, of the laser excitation, the last observed continuum maxima shift to longer wavelength, and the number of oscillatory peaks increases. Also, the continuum emission at wavelengths shorter than the excitation wavelength extends to 420 nm and gets relatively weaker with decreasing excitation wavelength (Figs. 2 and 4). The line to continuum intensity ratios and the general appearance of the spectra were unchanged with pressure variations of Ar buffer gas from 1 to 10 torr and with oven temperatures from 1000 to 1200 K (i.e., partial pressures of Ca from 0.1 to 5 torr). Integrated intensities of the discrete line emission are comparable with the total intensities of the continuum emission (Table I). Intensities of both dis-

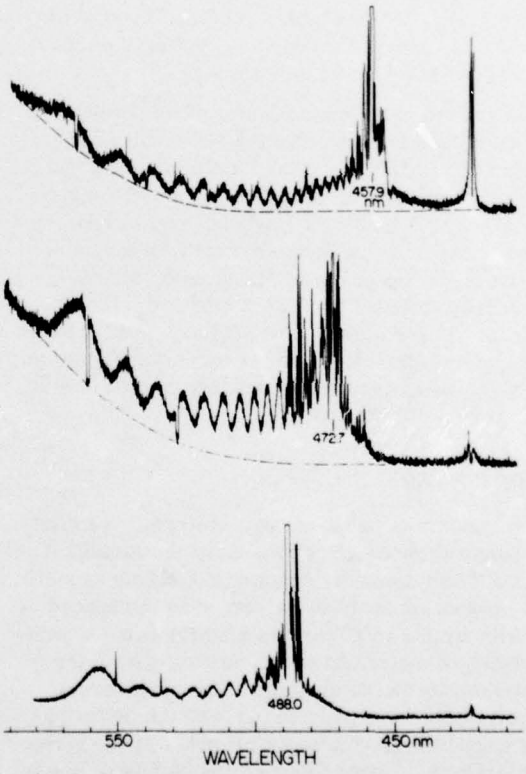

FIG. 2. Laser photoluminescence spectra of Ca_2 with 0.1 nm resolution for 488.0 nm excitation and 0.2 nm for 472.7 and 457.9 nm. Laser power was 2.2, 0.15, and 0.57 W at 488.0, 472.7, and 457.9 nm, respectively. The resonance line of Ca at 422.7 nm is self-reversed and its normalized intensities rapidly increased with excitation laser energy. Dotted lines show the approximate intensities of the background thermal radiation for the heat pipe. The temperature of oven was about 1080 K, corresponding to an equilibrium Ca vapor pressure of 0.79 torr; the Ar pressure was 3 torr.

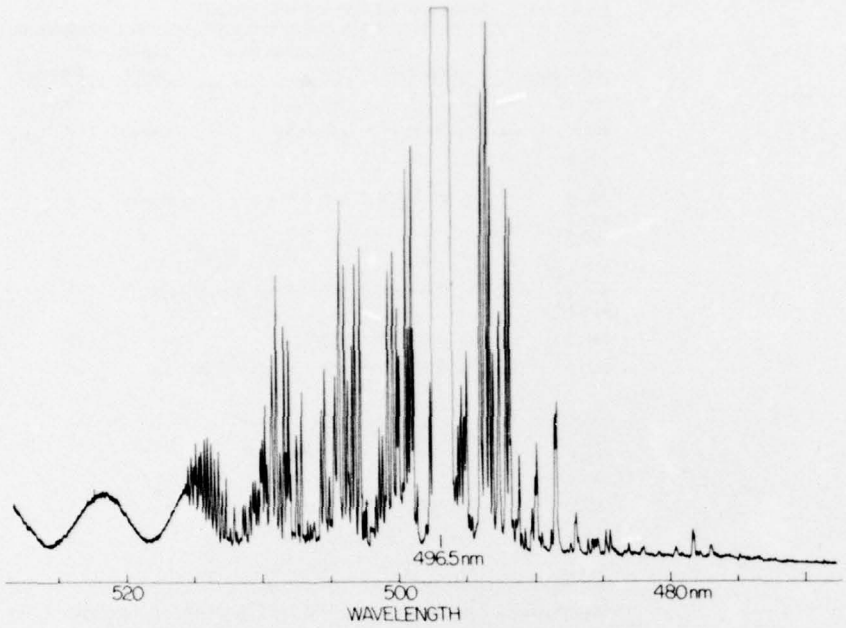

Fig. 3. High resolution spectra (0.036 nm) of the photoluminescence of Ca_2 excited by the 496.5 nm laser line. The underlying continuum begins near 470 nm.

crete and continuum emission increase linearly with increasing laser power from 0 to 3 W.

With white light excitation, only the impurity CaCl gave molecular emission. No absorption or photoluminescence of Ca_2 was detected with temperatures as high as 1300 K. Excitation spectra, with broad band detection over the entire visible region obtained by tuning the dye laser from 610 to 670 nm, showed some radiation at all laser wavelengths in addition to strong peaks due to impurities of CaCl, CaBr, and CaI. With the laser set at 657.3 nm, a complex discrete spectrum with peak separations similar to Ca_2 vibrational spacings was observed. Similar discrete spectra also were observed about 1 nm on either side of 657.3 nm.

Other methods for producing Ca_2 emission were tried. In one case a low current discharge (20 mA) was produced in the Ca vapor in the oven. In addition to many lines of atomic Ca, there was very strong emission of the $A-X$ and $B-X$ systems of CaH, but no Ca_2 radiation. In another experiment in a flow system[16] and using laser excitation, no Ca_2 photoluminescence was observed even though a high density of Ca vapor was entrained in relatively low temperature Ar gas.

B. Atomic emission

In addition to discrete and continuum emission from molecular Ca_2, several atomic transitions were observed (Table III). The allowed resonance $4s^2\,{}^1S-4p\,{}^1P$ atomic Ca transition at 422.7 nm was very strong and usually appeared with a large amount of self-reversal (Figs. 1, 2, and 4). White light excitation also showed strong 422.7 nm emission. The self-reversed line was asymmetric[17] with the long wavelength maximum of greater intensity than the short wavelength one. In addition, the long wavelength tail from the resonance line spreads into the molecular continuum emission as

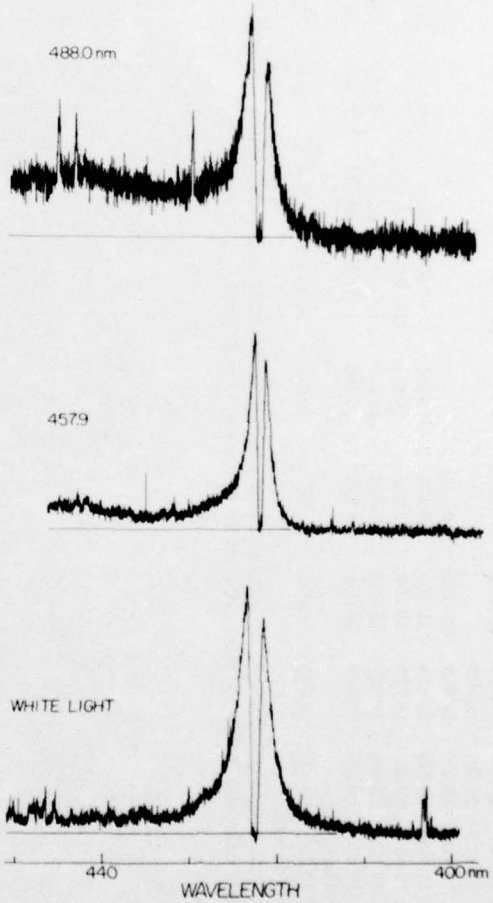

FIG. 4. Photoluminescence spectra near the resonance line of Ca at 422.7 nm. (a) 488.0 nm laser excitation, (b) 457.9 nm laser excitation, and (c) excitation by white light from a xenon arc lamp.

TABLE II. Wavenumbers of observed continuum maxima.[a]

Excitation (nm)	Wavenumbers of peaks (cm^{-1})																
528.7	18145	18520	18905	(19230)	(19685)												
514.5	18085	18500	18940														
501.7	18025	18550	18940	(19305)	(19550)												
496.5	17930	18520	18850	19175	19435	(19645)	(19840)	(20000)	(20161)	(20280)							
488.0	17950	18450	18775	19100	19380	19610	(19820)	(20000)									
476.5	17825	18280	18690	19030	19320	19570	19820	20020	20200	20365	(20510)	(20680)					
472.7	17775	18280	18650	19011	19280	19530	19760	19980	20180	20345	(20490)	(20640)	(20745)	(20875)			
465.8	Too weak																
457.9	17615	18200	18615	18970	19260	19525	19775	20015	20175	20425	20590	20750	20915	21045	21160	21293	(21385)
454.5	Too weak																

[a]Parentheses ( ) indicate that continuum and discrete spectra are overlapped.

TABLE III. Observed atomic Ca transitions.

Atomic emission (nm)	Assignment	Excitation laser (nm)	Laser power	Intensity[a]
344.8[b]	?	488.0, 514.5	c	1
422.7	$4s^2\,{}^1S-4p\,{}^1P^0$	All lines	Linear	10^4
428.3				
428.9				
430.2	$4p\,{}^3P^0-4p^2\,{}^3P$	488.0, 514.5	Square	1
430.7				
431.8				
442.5				
443.5	$4p\,{}^3P^0-4d\,{}^3D$	488.0, 514.5, 496.5	Square	1
445.6				
535.0	$3d\,{}^1D-4p'\,{}^1F^0$	488.0	c	10
551.3	$4p\,{}^1P^0-6s\,{}^1S$	488.0	c	10
558.1				
558.8				
559.8	$3d\,{}^3D-4p'\,{}^3D^0$	488.0, 514.5	c	1
560.1				
560.2				
585.7	$4p\,{}^1P^0-4p^2\,{}^1D$	488.0, 514.5, 496.5	c	5
657.3	$4s^2\,{}^1S-4p\,{}^3P^0$	All lines	c	10
732.6	$4p\,{}^1P^0-4d\,{}^1D$	488.0, 514.5	c	1

[a]Approximate intensities excited by 1.5 W 488.0 nm laser line.
[b]J. A. Anderson, Astrophys. J. **59**, 76 (1924).
[c]Appears only with high power; no measurement of power dependence.

readily seen in the 457.9 nm excitation (Figs. 2 and 4). The partly forbidden resonance transition $4s^2\,{}^1S-4p\,{}^3P$ of Ca at 657.3 nm also was observed with thermal excitation as well as with laser and with white light excitation. With changing pressures of Ar or Ca, the intensities of the atomic resonance transitions relative to the molecular intensities remained the same.

Effects of laser power and laser wavelength on the resonance line emission are illustrated in Figs. 5 and 6. Line intensities at 422.7 and 657.3 nm increased linearly with increasing laser power for all laser lines, indicating that both upper levels are produced by single photon processes. However, the intensities of the two lines had a very different dependence on the excitation

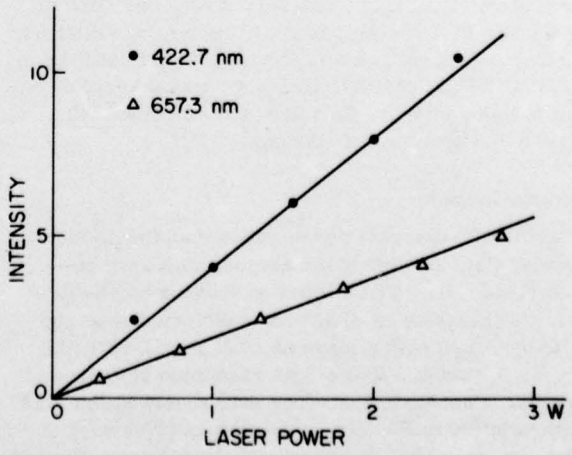

FIG. 5. Intensity dependence on laser power of the resonance atomic lines.

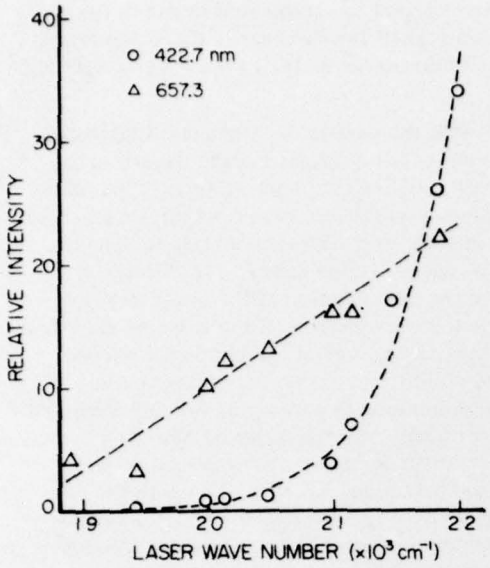

FIG. 6. Intensity dependence on laser energy of the resonance atomic lines. The dotted line for 422.7 nm is calculated from $\beta' \exp - [(\nu_0 - \nu_1)/\alpha']$.

wavelength, suggesting that different mechanisms populate the ^1P and ^3P atomic states. The 657.3 nm line showed a linear increase with decreasing excitation wavelength (Fig. 6), while the 422.7 nm line increases exponentially with decreasing wavelength.

Several other atomic Ca lines were observed (Table III), usually at high laser power. Some lines, but not all, showed a square dependence on laser power. At 460.7 nm, the Sr resonance line was observed and its intensity increased with decreasing excitation wavelength.

Both 422.7 and 657.3 nm photoluminescence were observed when the dye laser was tuned to 657.3 nm. An excitation spectrum near 657.3 nm, while using 422.7 nm detection, peaked at 657.3 nm but showed an asymmetric profile with a sharp cutoff at shorter wavelengths and a longer tail on the long wavelength side; the width was about 0.1 nm. In contrast, a symmetric shape was observed for 657.3 nm detection.

In the white light photoluminescence spectra, weak emission also was seen from the 612.2 and 616.2 nm lines ($^3P_{2,1}$–$^3S_1$) of Ca and from lines of impurities of Sr, Ba, Na, and Li.

IV. ANALYSIS

A. Radiation to bound states

Figure 7 is a proposed set of simplified potential curves of Ca_2 to fit the observed photoluminescence. Curves A and B are drawn using constants given by Balfour and Whitlock[4] but assuming that their lower state correlates to ^1S and ^3P atoms rather than to two ^1S atoms.

Since the laser induced photoluminescence falls in the same spectral region as the observed absorption spectrum,[4] and since the observed vibrational spacing of the anti-Stokes components is the same, we have assumed that the bound states in emission are the same as those observed in absorption. However, there are several observations that are incompatible with the lower state of these transitions being the ground electronic state—there is extensive continuum emission to the short wavelength side of the excitation line; there is strong emission of the resonance Ca lines at 422.7 and 657.3 nm, and the temperature dependence of the photoluminescence indicates that the lower state is at least 12000 cm^{-1} above the ground state.

Discrete spectra observed in the laser photoluminescence occur as a result of absorption from the A state to the upper B state with re-emission to various vibrational levels of the bound part of the A state. Laser excited photoluminescence from closely spaced rotational and vibrational levels of molecules such as Ca_2, Rb_2,[9] and Bi_2[10] is very complicated. Vibrational assignments of Ca_2 excited by the various laser lines (Table I) were made using known rotational and vibrational constants[4] and calculated Franck–Condon factors. The calculated Franck–Condon factors are strongly dependent on the assumed rotational levels of the molecules. Obviously, the exact assignment is difficult because of the overlapping of many lines due to the close molecular spacing and the lack of sufficient spectral resolution.

The binding energy of ~1000 cm^{-1} is the same magnitude as the thermal energy in the heat-pipe oven with a temperature of 1100–1200 K. Therefore, thermal energy is sufficient to excite all vibration–rotation levels of the lower state with $J \approx 80$ as the most populated rotational level. Since the binding energy is so

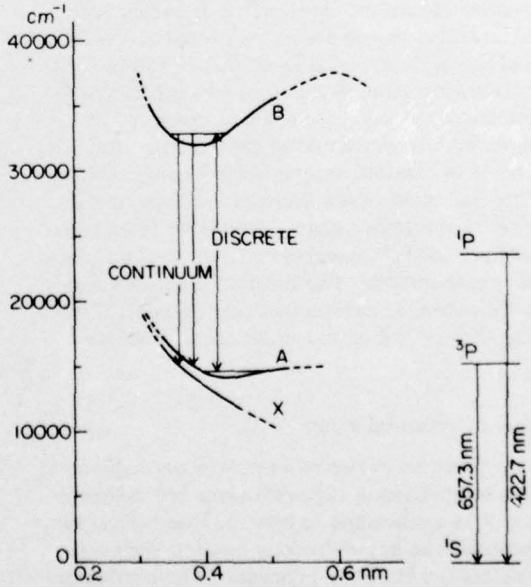

FIG. 7. Suggested potential curves of the Ca_2 molecule. Solid curves for the ground states are calculated from Balfour and Whitlock's[4] constants. The repulsive curve is drawn from estimates derived from the continuum emission.

47

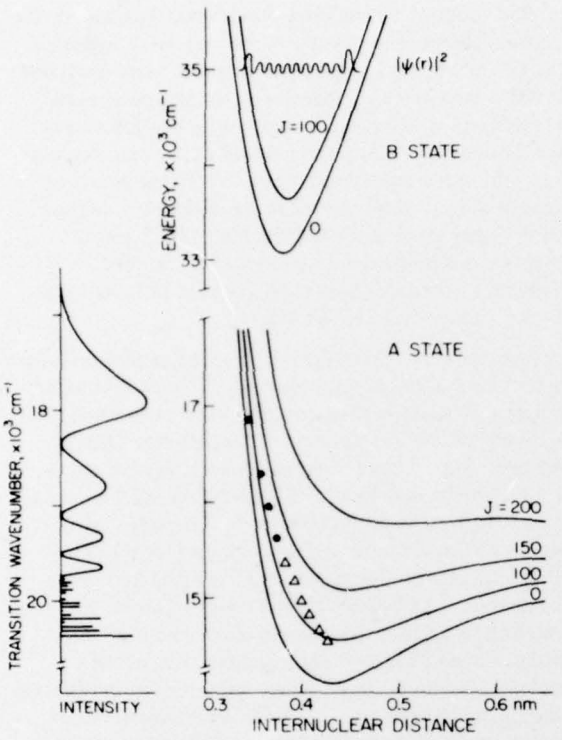

FIG. 8. Calculated potential curves for the A and B states for several rotational levels. The square of the wavefunction for $v' = 10$, $J' = 100$ is shown for the B state. On the left is the calculated intensity distribution to the lower A state from $v' = 10$, $J' = 100$ of the B state. Turning points estimated from measured photoluminescence emission excited by the 496.5 nm laser are indicated by circles and triangles. Circles are obtained from the oscillatory continuum peaks, while triangles are determined from the discrete emission.

small, predissociation by rotation[18] will easily occur. There are no bound levels above rotational levels of $J \approx 200$, and the highest bound level for $J = 150$ is $v = 2$. It is this predissociation which accounts for the relative simplicity of the discrete spectra observed at larger wavelength intervals from the exciting line. If a high J' level is excited, only a few v'' progressions are possible and most of the emission will be to the unbound part of the lower state. Emission from low J' levels will have long v'' progressions as well as more anti-Stokes components. The relative positions and shapes of the potential curves are very important for quantitative understanding of the discrete intensity patterns.

B. Radiation to unbound states

Since there was no observed pressure dependence of the relative intensities of the continuum and discrete emissions, it is reasonable to assume that both transitions come from the same directly excited states and not from an energy transfer process. The oscillatory continuum spectra are assumed to be caused by emission to the unbound portion of the lower potential curves,[19-21] while the discrete spectra are due to transitions to the bound portion of the lower state (Fig. 7). Most of the intensity of the continuum is due to the transition from high J' levels because there are fewer possible bound vibrational states in the lower electronic state.

We suggest that the oscillatory intensity distribution of the continuum is the reflection of the square of the wavefunction $|\psi_{v'}(r)|^2$ of the upper state B. The intensity of emission of a transition from a vibrational level v' of the bound state to the repulsive state is proportional to the Franck–Condon factor, $|\int \psi_{v'}(r)\psi_R(r)dr|^2$, where $\psi_R(r)$ is the wavefunction of the lower unbound state.[18] Since the wavefunction of the unbound state has a relatively large amplitude at the turning point, we assume for simplicity that the contribution to the Franck–Condon integral is only at the turning point and thus the intensity depends primarily on $|\psi_{v'}(r)|^2$, i.e., only vertical transitions are possible owing to the Franck–Condon principle. Intensity peaks in the continuum occur at those frequencies for which Franck–Condon factors give maxima. The emission frequency, ν, is given by

$$h\nu = E(v') - V(r_t), \tag{1}$$

where $E(v')$ is the energy of the upper state vibrational level and $V(r_t)$ is the energy of the turning point r_t of the repulsive lower state.

Figure 8 shows calculated potential curves, calculated intensity distributions of continuum and discrete emissions and observed turning points of the potential curve. The bound potential curves of the upper and lower states were calculated by the RKR method[22] using constants[4] of the $^1\Sigma_g^+$ and $^1\Sigma_u^+$ states. For the lower A state, the repulsive section was obtained by smoothly connecting the left side of the RKR potential curve to $Ar^{-12} + C$. The effective potential curves for different J values were obtained by the addition of the rotational energy to the rotationless potential.[18]

The intensity distribution of the continuum emission from the $v' = 10$, $J' = 100$ level is illustrated on the left side of Fig. 8. This distribution was calculated from the product $\nu^3|\psi_{v'}(r)|^2$, using Eq. (1) and $|\psi_{v'}(r)|^2$ obtained from numerical integration of the Schrödinger equation. Intensities of discrete lines due to transitions to the bound A state were calculated from $\nu^3 Q_{v'v''}$, where $Q_{v'v''}$ is the Franck–Condon factor. The scale factor between the continuum and discrete emission is arbitrarily set. Above $v'' = 16$, predissociation by rotation takes place for $J'' = 100$ and there are no discrete spectra.

The lower state potential curve obtained from observed intensity maxima of the continuum emission excited by the 496.5 nm is shown by black circles. The small difference between the slope of the measured potential and the calculated potential probably is due to the simplifying assumptions that only a single $v' = 10$, $J' = 85$ level was excited and the only contribution to the Franck–Condon factor was at the turning point. Moreover, we can not exclude the possibility that an r^{-12} potential is too steep in this region and that the measured potential is more nearly the correct one. It will be possible to obtain true potentials from the intensity dis-

tribution of a single v' excitation and the self-consistent potentials with complete numerical integration of Franck–Condon factors between the bound and unbound states.

Excitations to high v' levels are expected to show a simple oscillatory continuum because the positions of the amplitude maxima of the wavefunctions from neighboring vibrational levels are very close to each other. In contrast, however, excitation to several low v' levels would produce a more complex structure caused by the large displacements of intensity maxima from various v' levels. The continuum emission excited by 514.5 nm (Fig. 1) shows the superposition of emission from at least $v' = 3$ and 4. Similar, but less clearly, observed continuum emission has been observed in the transition from the $B\,^1\Sigma_u^+$ state of H_2[23] and a fluctuating continuum has been observed in the He_2 spectrum near 60 nm.[24]

Another repulsive state is needed to account for the continuum emission observed (Figs. 1, 2) at shorter wavelengths than the excitation line and underlying the discrete emission. The energy of photons in the anti-Stokes continuum is as much as twice the depth of the potential well of the A state. Moreover, the intensity distributions of these anti-Stokes continua have little structure and decrease monotonically with decreasing wavelength; the very weak continuum extends to at least 420 nm. These observations fit a potential curve X (Fig. 7) correlating with two ground state ^1S Ca atoms. Since there is no preference on J' for transitions from the B state to the repulsive curve X, the continuum intensity is a sum of transitions from all v', J' levels and the oscillations are smoothed. This smoothing is similar to the intensity distribution observed in the H_2 continuum.[25] The continuum emission to the X state extends to both sides of the laser excitation, and therefore, part of the continuum underlying the oscillatory structure at long wavelengths can be due to this continuum.

Another method was used to estimate the energy of the lower state of the molecular emission by studying the photoluminescence intensity as a function of oven temperature T.[10,11] If quenching is neglected, the luminescence intensity of laser induced photoluminescence is proportional to the number of molecules in the lower state. The population of molecules N at any energy E is determined by the Boltzmann distribution $N \propto N_0 e^{-E/kT}$ in terms of the number of Ca atoms N_0. $N_0 = A e^{-B/kT}$, where the constants A and B are obtained from temperature and pressure curves.[26] It is assumed that the Ca vapor pressure is the equilibrium vapor pressure. The intensity of luminescence I is

$$I \propto A e^{-(B+E)/kT}. \tag{2}$$

The temperature dependence of the molecular luminescence has been measured at constant buffer gas pressure and at excess gas pressure. The energy E of the lower A state was found to be $12\,000 \pm 2000$ cm^{-1}. This number is a lower limit to the energy of the A state since quenching in the B state has been neglected. Nevertheless, this measured value fits well with the energy of Ca(^3P) at 15 200 cm^{-1}.

C. Atomic emission

The linear excitation power dependence of the intensities of atomic Ca from the ^3P and ^1P states indicates that the excitation process is due to a single photon. However, the different dependencies on excitation energy (Fig. 6) show that there are at least two separate mechanisms for populating the upper electronic states. The potential curves (Fig. 7) suggest that ^3P atoms are formed as a result of the dissociation of Ca_2 from transitions to the repulsive part of curve A. Excited state ^1P atoms could be formed as a result of Ca_2 in the B state tunneling through the potential hump at large internuclear distances.

Since higher energy laser lines can reach higher energy states in curve B, the tunneling probability will increase rapidly as the potential maximum is reached. An approximation to the intensities of the 422.7 nm line with various excitation wavelengths can be calculated by assuming that the transmission probability T through the potential hump $V(x)$ is[27]

$$T \approx \exp -2\int_{x_1}^{x_2} \frac{2m}{\hbar^2} V(x) - E^{1/2} dx, \tag{3}$$

where x_1 and x_2 are the entrance and exit points to the potential barrier and E is the energy to which a molecule is excited by the laser. If an inverted parabolic barrier is chosen for simplicity T can be integrated. The probability for dissociation of Ca_2 in the B state by tunneling is approximately

$$T \propto \exp -\left(\frac{\epsilon_0 - \epsilon_{v'}}{\alpha}\right). \tag{4}$$

α is a parameter related to the curvature of the parabola and the normalization factors. ϵ_0 is the barrier height measured from bottom of the potential B, and $\epsilon_{v'}$ is the vibrational energy of the laser excited level. Although we do not know whether the repulsive potential curve to the right of the barrier correlates directly to the ^1P state or to some other atomic state (Fig. 7), the relative intensity of 422.7 nm is assumed to be proportional to the number of dissociated molecules. In this case, then, the dependence of intensity on the laser frequency ν_l is derived as

$$I = \beta' \exp -\left(\frac{\nu_0 - \nu_l}{\alpha'}\right), \tag{5}$$

where ν_0 is barrier height from the v'' lower state, and β' is a proportionality constant. The calculated laser frequency dependence of 422.7 nm line intensity shown as the dotted curve (Fig. 6) used the constants $\nu_0 = 22.5 \times 10^3$ cm^{-1}, $\alpha' = 494$, and $\beta' = 104$. Since the barrier height measured from the lower state is 22.5×10^3 cm^{-1}, ϵ_0 the barrier height measured from bottom of the potential B is about 3.5×10^3 cm^{-1}. An estimate of the position of the potential maximum was found to be 0.55 nm by extrapolation of the right side of potential B. This calculated transmission fits reasonably well with the excitation dependence of the resonance line (Fig. 6, Table I).

The linear dependence of the 657.3 nm line on excitation energy can be qualitatively understood because

49

with increasing laser energy a larger fraction of the Ca_2 transitions go to the repulsive part of the lower A state. Thus the intensity of the 657.3 nm line will depend upon the overlap of the bound B state with the repulsive part of the A state. Shorter laser wavelengths excite higher vibrational levels of the B state, resulting in a greater overlap with the repulsive part of the A state.

In addition to the resonance radiations, many atomic emission lines were observed (Table III). Transitions due to triplet–triplet transitions such as $4p\,^3P$–$4p^2\,^3P^0$ (428.3–431.8 nm) and $4p\,^3P^0$–$4d\,^3D$ (442.5–445.6 nm) and many lines initiated from complex terms with two excited electrons have been observed. Most observed emission starts from levels with energy 4.6 ~ 5.15 eV, which is very close to twice the laser energy.

V. DISCUSSION

Potential curves A and B (Fig. 7), derived from absorption measurements,[4] are very consistent with the discrete molecular spectra and the oscillatory continuum spectra that were observed in laser photoluminescence. However, there is an unresolved discrepancy because the absorption studies[4] concluded by assigning the lower state as a van der Waals bound $^1\Sigma_g^+$ ground state, correlating with the two $Ca(^1S)$ atoms. This assignment of the ground electronic state is supported by the possible observation of Ca_2 at low temperature in a Kr matrix.[5]

While much of the molecular photoluminescence does not contradict the previous assignment, there are several observations of the present experiments which cannot be explained by the assumption that the lowest bound state is the ground electronic state: (1) the continuum emission on the short wavelength side of the excitation laser wavelength, (2) the strong emission from both the 422.7 and 657.3 nm atomic lines, (3) the pressure independence of the relative intensities of the atomic and molecular emissions, (4) the temperature dependence of all emission intensities indicating that the lowest state is at least 12000 cm^{-1} above the ^1S atomic state, and (5) no Ca_2 was observed in the room temperature flow systems at Ca densities comparable to those obtained in the higher temperature heat-pipe oven.

We are forced to conclude that the calcium dimer molecule Ca_2 is an eximer molecule like the rare gas diatomic molecules rather than a van der Waals molecule. The simple set of potential curves suggested in Fig. 7 best fit the main observations on Ca_2. There are, however, two major unresolved difficulties with this conclusion. First of all, the assignment from rotational analysis[4] of the lower A state as a $^1\Sigma$ state is incompatible with the ^3P atomic state. Second, while the observation of Ca_2 in a low temperature matrix is not a clear cut assignment, Be_2[1] and Mg_2[3] also have been identified in matrix isolation studies and tend to support the assignment of a bound ground state. Further studies by sensitive photoluminescence and absorption spectroscopy will be necessary to resolve these uncertainties.

ACKNOWLEDGMENT

We greatly appreciate discussions, assistance with analysis, and experimentation which Guy Taieb has given to us.

*Work supported in part by Office of Naval Research, Contract No. N00014-75-C-0829 and National Science Foundation Grant No. NSF-MPS-74-22174.

†Permanent Address: Pure and Applied Sciences, University of Tokyo, Tokyo, Japan.

[1] J. M. Brom, Jr., W. D. Hewett Jr., and W. Weltner, Jr., J. Chem. Phys. **62**, 3122 (1975).
[2] W. J. Balfour and A. E. Douglas, Can. J. Phys. **48**, 901 (1970).
[3] L. Brewer and J. L. Wang, J. Mol Spectrosc. **40**, 95 (1971).
[4] W. J. Balfour and R. F. Whitlock, Can. J. Phys. **53**, 472 (1975).
[5] J. E. Francis, Jr. and S. E. Webber, J. Chem. Phys. **56**, 5879 (1972).
[6] C. J. Ballhausen and H. B. Gray, *Molecular Orbital Theory* (Benjamin, New York, 1964).
[7] C. F. Bender and E. R. Davidson, J. Chem. Phys. **47**, 4972 (1967).
[8] C. R. Vidal and J. Cooper, J. Appl. Phys. **40**, 3370 (1968).
[9] J. M. Brom, Jr. and H. P. Broida, J. Chem. Phys. **61**, 982 (1974).
[10] G. Gerber, K. Sakurai, and H. P. Broida, J. Chem. Phys. **64**, 3410 (1976).
[11] J. I. Gersten, Phys. Rev. Lett. **31**, 73 (1973).
[12] W. Demtroder, M. McClintok, and R. N. Zare, J. Chem. Phys. **51**, 5495 (1969).
[13] K. Sakurai, S. E. Johnson, and H. P. Broida, J. Chem. Phys. **52**, 1625 (1970).
[14] R. N. Zare and P. J. D. Dagdigian, Science **185**, 739 (1974).
[15] W. Demtroder, Phys. Rep. **7**, 223 (1973).
[16] J. B. West, R. S. Bradford, Jr., J. D. Eversole, and C. R. Jones, Rev. Sci. Instrum. **46**, 164 (1975).
[17] M. Espenhain, H. J. Kusch, and W. Lochte-Holtegreven, Zeit. Phys. **61**, 77 (1965).
[18] G. Herzberg, *Molecular Spectra and Molecular Structure I. Spectra of Diatomic Molecules* (Van Nostrand Reinhold, New York, 1950), Chap. VII.
[19] E. U. Condon, Am. J. Phys. **15**, 365 (1947); originally, Phys. Rev. **32**, 858 (1928). Condon emphasizes that the "rippling fluctuation in intensity in the continuous spectrum accompanying dissociation" are diffraction bands. This "internal diffraction" is "an intramolecular manifestation of the wave nature of matter."
[20] D. L. Rousseau and P. F. Williams, Phys. Rev. Lett. **33**, 1368 (1974).
[21] J. Tellinghuisen, Phys. Rev. Lett. **34**, 1137 (1975).
[22] R. N. Zare, J. Chem. Phys. **40**, 1934 (1964).
[23] A. Dalgano, G. Herzberg, and T. L. Stephens, Astrophy. J. **162**, L49 (1970).
[24] Y. Tanaka and K. Yosnino, J. Chem. Phys. **39**, 3081 (1963).
[25] H. M. James and A. S. Coolidge, Phys. Rev. **55**, 184 (1939).
[26] A. N. Nesmeyanov, *Vapour Pressure Data for the Elements* (Elsevier, New York, 1963).
[27] E. Merzbacher *Quantum Mechanics* (Wiley, New York, 1961).

LIFETIME MEASUREMENT OF A SINGLE ROTATIONAL TRANSITION OF THE $B^3\Pi_u^+ \rightarrow X^1\Sigma_g$ TRANSITION OF IODINE*

K. SAKURAI**, G. TAIEB* and H.P. BROIDA
Physics Department and Quantum Institute, University of California, Santa Barbara, California 93106, USA

Received 11 March 1976

Lifetimes, self-quenching, and vibrational and rotational energy transfer cross sections of individual rotational levels in the $B^3\Pi_u^+$ state of I_2 were measured by observing the correlation between fluorescence photons and the pulsed excitation from 514.5 and 501.7 nm argon ion lasers. Lifetimes were measured with both vibrationally resolved (1.0 nm) and rotationally resolved detection (0.015 nm). The cross sections from Stern–Volmer plots were respectively, 76 and 89 $Å^2$ with 5% accuracy for single (43–2) band emission and the P(16) line emission in the same band. The difference in cross sections is interpreted as vibrational and rotational energy transfer from the originally excited level. Measured radiative lifetimes are consistent with previous measurements except that a 10% shorter lifetime was observed with single rotational line detection.

1. Introduction

In recent years, many measurements of lifetimes and self-quenching cross sections of levels in the $B^3\Pi_u^+$ state of iodine have been made by several different techniques [1–4]. Recently lifetimes have been measured [5,6] by observing the fluorescence decay following excitation by a narrow band tunable dye laser. These are the first measurements in which the excitation laser was sufficiently narrow to excite single vibrational and rotational transitions but the resolution of detection was not suitable for detailed analysis of complicated energy transfer processes.

Photon counting and photon correlation techniques have been used to measure the photon statistics of light and to study fluctuation phenomena at critical points [7]. Since a photon correlator can measure the correlation between isolated photons, this device makes possible very sensitive measurements of intensity decay from single rotational–vibrational transitions after laser excitation. Using both narrow band excitation and narrow band detection, it is possible to measure the rotational and vibrational energy transfer cross sections as well as quenching cross sections. Vibrational and rotational energy transfer cross sections and quenching cross sections for iodine have been extensively investigated by steady-state methods [8–10].

There has been little discussion of the influence of the spectral band widths of the detector on the measured lifetimes and quenching cross sections. The purpose of this paper is to call attention to the possible need of reanalysis of such measurements.

2. Experimental

A schematic diagram of the experimental set-up is shown in fig. 1. An excitation pulse was obtained by mechanically switching a laser beam with a fast rotating mirror (500 r.p.s.) driven by an air motor. A 0.5 mm hole was placed in the light path 4 m from the rotating mirror, giving rise and fall times of the light intensity of less than 50 ns. Output powers from an Ar^+ laser were 1 W at 514.5 nm and 0.2 W at 501.7 nm. The photoluminescence from iodine was measured with a 3/4 m grating monochromator. For steady-state

* Work supported in part by National Science Foundation Grant No. MPS-74-22174.
** Permanent address: Department of Pure and Applied Sciences, University of Tokyo, Tokyo, Japan.
* Permanent address: Laboratoire de Photophysique Moléculaire, Université de Paris Sud, Paris, France.

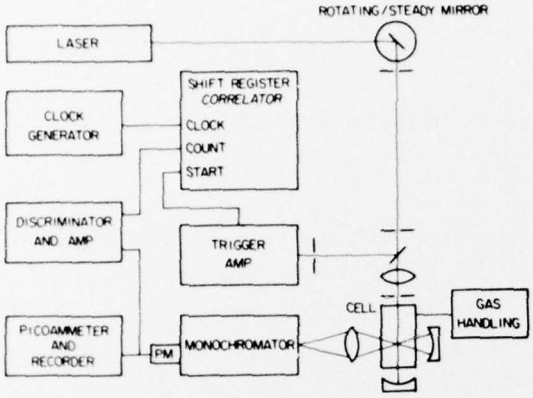

Fig. 1. Experimental arrangement.

spectral observations, both ordinary picoammeter and photon counting methods were used.

A 5 cm diameter pyrex cell with a flat window was connected to a high vacuum pumping station to control iodine pressure. The control and measurement of iodine pressure are important for successful lifetime measurements. In initial experiments, iodine pressure was controlled by maintaining the side arm of the cell at constant temperature by cooling with ice and various freezing mixtures. In later experiments, iodine pressure measured by a Pirani gauge which had been exposed to iodine for long periods and was calibrated at ice (0°C) and $CaCl_2$–ice mixture temperatures (−19.2°C). The most consistent data were obtained by the latter method.

A very high detection sensitivity is required to measure the luminescence decay of a single rotational transition. Such sensitivity can be achieved by using a photon correlation or delayed coincidence method. A photon correlator is a device which can measure the correlation of photons at two different times. The correlation between a δ-function excitation pulse and the emitted photons, $\langle N(t)\delta(t+\tau)\rangle$, is the time variation of the intensity of fluorescence, where $N(t)$ is the number of photoelectrons detected by photomultiplier. The circuitry of the photon correlator is similar to that first proposed by Jakeman and Pike [11]. The differences are that it uses fast Schottky shift registers as delay elements, has synchronizing circuits between the start and fluorescence photon pulses, and has a clock suitable for lifetime measurements. Laser pulses trigger the correlator to start counting photon pulses. Photomultiplier pulses due to photons are amplified, shaped and then fed to the count input of the correlator. The signal from the excitation pulse is delayed by the shift register and the coincidence between the delayed excitation pulse and fluorescence photon pulses is counted. The basic unit delay time, τ is determined by a synchronized clock (50 ns–5 ms). 8 channels for delay times are available by an 8 bits shift register. Photons emitted in time delay τ are counted by the counter 1, those in 2τ are counted by the counter 2 and so on.

Since there are dark counts due to thermal electrons from the photocathode and steady-state stray background photons, the actual counting distribution over every channel is an exponential decay plus a constant background due to accidental coincidences of background photoelectrons. Because measurements are taken only in brief time periods ($\lesssim$10 μs) after excitation of I_2, dark counts in this time are so small that they have little effect on the measurements. There was no need to correct for the piling-up of photons since the number of photons in a single excitation was less than 1 in usual experimental conditions. The major noise source is due to statistical fluctuations of the counted photons in each channel and thus the signal-to-noise ratio in each channel is proportional to the square-root of the number of photons in the channel.

3. Results and discussion

Two detection schemes were used to measure fluorescence intensity decay. First, a single vibrational transition (43–2) at 526 nm, which consisted of transitions from rotationally relaxed levels as well as the originally excited rotational level, was detected with a spectrometer slit width of 1 nm. Then, the single rotational transition $v' = 43, v'' = 1, J' = 15$ line from the level originally populated by the laser was detected with a spectrometer slit width of 0.015 nm. Typical decays observed in the correlator are shown in fig. 2 and are exponential for 3 orders of magnitude. At higher pressure, systematic deviations from the exponential were observed at later times; this non-exponential decay is due to back energy transfer from the levels populated by collisions. Decay times of I_2 at various pressures from 2 to 30 mtorr were measured and depopulation cross sections and radiative lifetimes were obtained by means of Stern–Volmer plots. Major errors are due to lack of accuracy

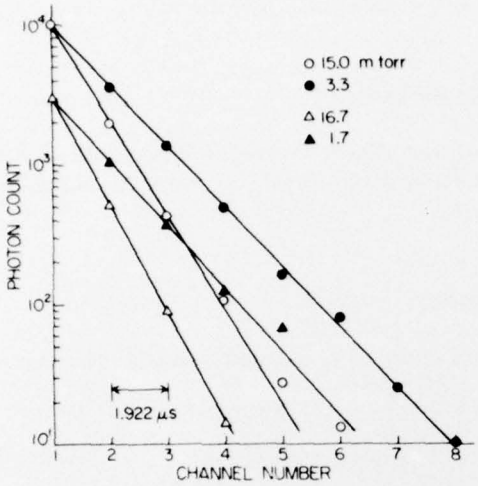

Fig. 2. Observed decay of fluorescence intensity. Circles represent single band detection (1 nm) and triangles represent single rotational line detection (0.015 nm). The delay time per channel is 1.922 μs.

in pressure measurements. The results are shown in table 1. For comparison with these measurements, table 1 also lists some measurements obtained with filtered detection of total emission at the same excitation wavelengths [5] and at nearby wavelengths [4].

The differences in measured cross sections (table 1) can be interpreted in terms of the several mechanisms of depopulation of an excited level. When a laser excites a single vibrational–rotational level (v'_0, J'_0) in an upper electronic state, molecules can collisionally relax to other rotational levels (v'_0, J') and to other vibrational–rotational levels (v', J') before emitting radiation. Also spontaneous predissociation can take place for I_2 even at zero pressure [12]. When all emission is detected with a filter, the cross section from the Stern–Volmer plot is due to the average electronic quenching of the upper state. If emission from the originally excited level and the rotationally relaxed levels is detected, the measured cross section is due to electronic quenching and to depopulation by the vibrational relaxation; molecules which have undergone vibrational relaxation do not emit radiation into this detection band width. Finally when only emission from the originally excited level is detected with high resolution as a single rotational line, the combined electronic, vibrational, and rotational depopulation cross section is measured.

With 514.5 nm excitation, the value [5] of 64 Å^2 is due to electronic quenching, 76 Å^2 to the electronic quenching plus depopulation by vibrational transfer, and 89 Å^2 due to the combined effects of electronic quenching, vibrational relaxation and depopulation by rotational energy transfer. From the differences between these measured values, the total effective cross sections for the vibrational and rotational depopulation are determined to be 12 and 13 Å^2 respectively.

It is important to note that these cross sections are for net depopulations which include both forward and backward processes by multiple collisions. Kurzel et

Table 1
Measured lifetimes and self-quenching cross sections of I_2

Excitation (nm)	Detection	Lifetime (μs)	Cross section (Å^2)
514.5 (Ar^+)	all emission (filter)[a]	2.28 ± 0.08	63.6 ± 0.8
	43–2 band (1 nm)[b]	2.13 ± 0.15	76 ± 4
	part of 42–2 band (0.2 nm)[b]	2.11 ± 0.05	81 ± 4
	R(16) line in 42–2 band (0.015 nm)[b]	1.82 ± 0.10	89 ± 4
501.7 (Ar^+)	all emission (filter)[a]	8.8 ± 0.2	75.1 ± 0.9
	62–5 band (1 nm)[b]	7.5 ± 1.0	83 ± 8
	part of 62–5 band (0.2 nm)[b]	5.4 ± 0.3, −1.0	110 ± 10
513.4 (dye)	all emission (filter)[c]	2.24 ± 0.21	60 ± 1
501.6 (dye)	all emission[c]	5.55 ± 1.41	68 ± 2

[a] Ref. [5]. [b] Present measurements. [c] Ref. [4].

al. [8] have measured the single process removal cross sections for vibration and for rotation to be 18.4 and 31.3 $Å^2$ respectively. The large difference (31.3 − 13 = 18 $Å^2$) in the rotational depopulation cross sections between the 2 sets of measurements indicates that multiple collisions are important in rotational relaxation. The somewhat smaller difference (18.4 − 12 = 6 $Å^2$) in the vibrational cross sections indicates that the backward process is less likely.

Although a simple model predicts the same radiative lifetime with any detection scheme, small deviations are observed which are larger than the experimental error in each measurement as shown in table 1. The narrow band detection tends to show slightly shorter lifetimes. A small deviation from linearity in the Stern–Volmer plot is observed at lower pressure (<5 mtorr) in band detection whereas a linear plot was obtained from the single line rotational detection. These small discrepancies possibly are due to different lifetimes and cross sections of various rotational and vibrational levels caused by predissociation [12].

4. Conclusion

It has been demonstrated that the spectral band width of the detector for fluorescence decay affects the measured depopulation cross sections and radiative lifetimes. Both single rotational line excitation and detection by a single rotational transition are essential to obtain true lifetimes and depopulation cross sections.

Acknowledgement

We would like to express our thanks to Dr. Robert S. Bradford Jr. for his help in constructing the photon-correlator.

References

[1] A. Chutijan, J.K. Link and L. Brewer, J. Chem. Phys. 46 (1967) 2666.
[2] K. Sakurai, G.A. Capelle and H.P. Broida, J. Chem. Phys. 54 (1971) 1220.
[3] K.C. Shotton and G.D. Chapman, J. Chem. Phys. 56 (1971) 1012.
[4] G.A. Capelle and H.P. Broida, J. Chem. Phys. 58 (1973) 4212.
[5] J.A. Paisner and R. Wallenstein, J. Chem. Phys. 61 (1974) 4212.
[6] M. Broyer, J. Vigué and J.C. Lehmann, J. Chem. Phys. 63 (1975) 5428.
[7] R. Glauber, ed., Quantum optics (Academic Press, New York, 1970).
[8] R.B. Kurzel and J.I. Steinfeld, J. Chem. Phys. 53 (1970) 3293.
[9] J.I. Steinfeld and A.N. Schweid, J. Chem. Phys. 53 (1970) 3304.
[10] R.B. Kurzel, J.I. Steinfeld, D.A. Hatzenbuhler and G.E. Leroi, J. Chem. Phys. 55 (1971) 4822.
[11] E. Jakeman and E.R. Pike, Nature 227 (1970) 242.
[12] J. Tellinghuisen, J. Chem. Phys. 57 (1972) 2397.

III. Publications

1. "Laser Photoluminescence of Bi_2"
   G. Gerber, K. Sakurai and H. P. Broida
   J. Chem. Phys. 64, 3410-22 (1976)

2. "Electronic States and Molecular Constants of Bi_2"
   G. Gerber and H. P. Broida
   J. Chem. Phys. 64, 3423-37 (1976).

3. "Chemically Reacting Bismuth and Nitrous Oxide in a Heat Pipe Oven"
   K. Sakurai and H. P. Broida
   Chem. Phys. Lett. 38, 234 (1976).

4. "Observation of Homogeneously Nucleated Fine Particles of PbI by Electron Microscopy and Light Scattering
   J. D. Eversole, K. Sakurai and H. P. Broida,
   J. Cryst. Growth, 33, 353-55 (1976).

5. Chemiluminescence of CaH and AlH in the Reaction of the Metal Atoms and Formaldehyde"
   K. Sakurai, A. Adams, and H. P. Broida
   Chem. Phys. Lett. 39, 442-4 (1976).

6. "Laser Photoluminescence of Calcium Molecules"
   K. Sakurai and H. P. Broida
   J. Chem. Phys. (tentative issue date 1 August 1976).

7. "Lifetime Measurement of a Single Rotational Transition of the $B^3\Pi_u^+ \rightarrow X^1\Sigma_g$ System of Iodine"
   K. Sakurai, G. Taieb and H. P. Broida
   Chem. Phys. Lett. (accepted for publication 1976).

IV. Talks

Nov 12 1975 "Laser Photoluminescence and Lifetime Measurements of Bi_2 and Electronic States and Molecular Constants of Bi_2"
G. Gerber, UCSB Molecular Spectroscopy Group Meeting

Oct 28 1975 "Lifetime Measurement of a Single Rotational Transition of I_2 of the $B^2\Pi_u^+ \rightarrow A^1\Sigma_g^+$ Transition"
K. Sakurai, 1975 Western Symposium on Laser Studies of Relaxation Porcesses, Hollywood

Jun 1975 "Laser Excited Photoluminescence of Bi_2"
G. Gerber, Molecular Spectroscopy Symposium, Columbus, Ohio

Jun 15 1976 "Laser Photoluminescence of Calcium Molecules"
G. Taieb, Molecular Spectroscopy Symposium, Columbus, Ohio

Jun 16 1976 "Neutral and Ionic Emission from Collisionally Excited Additives to an Helium Afterglow"
G. Taieb, Molecular Spectroscopy Symposium, Columbus, Ohio